A Genome-Wide Arrayed CRISPR Screen Reveals PLSCR1 as an Intrinsic Barrier to SARS-CoV-2 Entry

Authors

Jérémie Le Pen[1,*], Gabrielle Paniccia[1,*], Michael Bauer[1,#], H.-Heinrich Hoffmann[1,#], Volker Kinast[2,3,#], Marcela Moncada-Velez[4,#], Ana Pinharanda[5,#], Inna Ricardo-Lax[1,#], Ansgar F. Stenzel[1,6,#], Edwin A. Rosado-Olivieri[7,8,#], Alison W. Ashbrook[1], Kenneth H. Dinnon[1], William C. Doyle[1,9], Catherine A. Freije[1], Seon-Hui Hong[1], Danyel Lee[4,10,11], Tyler Lewy[1], Joseph M. Luna[1,12], Avery Peace[1], Carltin Schmidt[4,13], William M. Schneider[1], Roni Winkler[1], Chloe Larson[14], Timothy McGinn[14], Miriam-Rose Menezes[14], Lavoisier Ramos-Espiritu[14], Priyam Banerjee[15], John T. Poirier[16], Francisco J. Sànchez-Rivera[17,18], Qian Zhang[4], Jean-Laurent Casanova[4,10,11,19,20], Thomas S. Carroll[21], J. Fraser Glickman[14], Eleftherios Michailidis[1,22,§], Brandon Razooky[1,23,§], Margaret R. MacDonald[1,§], Charles M. Rice[1,§]

[*] Contributed equally to this work

[#] Contributed equally to this work

[§] Contributed equally to this work

Correspondence: Jérémie Le Pen: jlepen@rockefeller.edu; Charles M. Rice: ricec@rockefeller.edu

Affiliations:

1. Laboratory of Virology and Infectious Disease, The Rockefeller University, New York, NY, USA.

2. Department of Medical Microbiology and Virology, Carl von Ossietzky University Oldenburg, Oldenburg, Germany.
3. Department for Molecular and Medical Virology, Faculty of Medicine, Ruhr University Bochum, Bochum, Germany.
4. St Giles Laboratory of Human Genetics of Infectious Diseases, Rockefeller Branch, The Rockefeller University, New York, NY, USA.
5. Department of Biological Sciences, Columbia University, New York, NY 10027, USA.
6. Present address: Department of Infectious Diseases, Molecular Virology, Heidelberg University, Heidelberg, Germany.
7. Laboratory of Synthetic Embryology, The Rockefeller University, New York, NY, USA.
8. Present address: Department of Molecular Pathobiology, New York University.
9. Present address: Laboratory of Host-Pathogen Biology, The Rockefeller University, New York, NY, USA.
10. Laboratory of Human Genetics of Infectious Diseases, Necker Branch, INSERM U1163, Paris, France, EU.
11. University of Paris, Imagine Institute, Paris, France, EU.
12. Present address: Department of Biochemistry and Center for RNA Science and Therapeutics, Case Western Reserve University, Cleveland, OH, USA.
13. Present address: Medical Faculty, Heinrich Heine University Dusseldorf, Germany.
14. Fisher Drug Discovery Resource Center, The Rockefeller University, New York, NY, USA.
15. Bio-Imaging Resource Center, The Rockefeller University, New York, NY, USA.
16. Laura and Isaac Perlmutter Cancer Center, New York University Grossman School of Medicine, NYU Langone Health, New York, NY.
17. Department of Biology, Massachusetts Institute of Technology, Cambridge, 02142, Massachusetts, USA.
18. David H. Koch Institute for Integrative Cancer Research, Massachusetts Institute of Technology, Cambridge, 02142, Massachusetts, USA.
19. Department of Pediatrics, Necker Hospital for Sick Children, Paris, France, EU.
20. Howard Hughes Medical Institute, New York, NY, USA.

21. Bioinformatics Resource Center, The Rockefeller University, New York, NY, USA.
22. Present address: Laboratory of Biochemical Pharmacology, Department of Pediatrics, Emory University School of Medicine, Atlanta, GA, USA.
23. Present address: National Resilience, Inc., La Jolla, CA, USA.

Abstract

Interferons (IFNs) play a crucial role in the regulation and evolution of host-virus interactions. Here, we conducted a genome-wide arrayed CRISPR knockout screen in the presence and absence of IFN to identify human genes that influence SARS-CoV-2 infection. We then performed an integrated analysis of genes interacting with SARS-CoV-2, drawing from a selection of 67 large-scale studies, including our own. We identified 28 genes of high relevance in both human genetic studies of COVID-19 patients and functional genetic screens in cell culture, with many related to the IFN pathway. Among these was the IFN-stimulated gene *PLSCR1*. PLSCR1 did not require IFN induction to restrict SARS-CoV-2 and did not contribute to IFN signaling. Instead, PLSCR1 specifically restricted spike-mediated SARS-CoV-2 entry. The PLSCR1-mediated restriction was alleviated by TMPRSS2 over-expression, suggesting that PLSCR1 primarily restricts the endocytic entry route. In addition, recent SARS-CoV-2 variants have adapted to circumvent the PLSCR1 barrier via currently undetermined mechanisms. Finally, we discuss the association between PLSCR1 variants and severe COVID-19 cases reported in a recent GWAS.

Introduction

Viruses maintain a complex relationship with their host cells, co-opting host factors for their replication while being targeted by cellular defense mechanisms. Such cellular defenses include the interferon (IFN) pathway, where the infected cell senses foreign molecules and secretes IFN to trigger an antiviral state in neighboring cells.

Approximately 1-5% of critical COVID-19 patients have mutations that compromise the production of or response to type I IFNs, while an additional 15% possess autoantibodies that neutralize type I IFNs [1-7]. This highlights the essential role of type I IFN in the defense against the SARS-CoV-2 virus that caused the COVID-19 pandemic [8, 9]. Consequently, investigating IFN-

79 stimulated genes (ISGs) is crucial to our understanding of the remarkable antiviral systems that
80 evolved in nature. This knowledge could enhance our preparedness for future pandemics.

81 Several recent studies have identified ISGs restricting SARS-CoV-2. Most of these studies
82 involved gain-of-function genetic screens, over-expressing individual ISGs. The factors bone
83 marrow stromal cell antigen 2 (BST2), cholesterol 25-hydroxylase (CH25H), lymphocyte antigen 6
84 family member E (LY6E), 2'-5'-oligoadenylate synthetase 1 (OAS1), and receptor transporter
85 protein 4 (RTP4) were notably identified as SARS-CoV-2 antivirals in these studies [9-14]. One
86 advantage of the gain-of-function approach is that it circumvents potential genetic redundancies
87 between ISGs [15, 16]. However, this approach is biased towards ISGs that act autonomously
88 when over-expressed and does not mimic the cellular context of the IFN response, where
89 hundreds of genes and gene products are differentially regulated to establish an antiviral state.
90 To counter this limitation, two recent publications examined the effects of ISG loss of function in
91 IFN-treated cells. They conducted pooled CRISPR knockout (KO) screens in cells pre-treated with
92 IFN before SARS-CoV-2 infection [17, 18]. By sorting for cells with high SARS-CoV-2 viral load, they
93 identified SARS-CoV-2 restriction factors such as death domain associated protein (DAXX).

94 Here, we conducted a human whole-genome arrayed CRISPR KO screen to identify genes
95 that influence SARS-CoV-2 infection in cells with or without pretreatment with a low dose of IFN.
96 The arrayed approach, though logistically challenging, has advantages over the pooled format in
97 capturing both proviral and antiviral genes, genes affecting virus egress, and those coding for
98 secreted products that exert their impact on neighboring cells. It reliably captures genotype-
99 phenotype correlations while also unveiling the effects of single gene perturbation on cell growth
100 and death [19]. We then compiled a comprehensive list of genes interacting with SARS-CoV-2,
101 incorporating findings from our own screen as well as existing literature. This meta-analysis
102 revealed several host genes of interest, both previously described and novel. Notably, the ISG
103 product phospholipid scramblase 1 (PLSCR1) emerged as a prominent antiviral factor. PLSCR1 is
104 involved in several biological processes [20], including regulating the movement of phospholipids
105 between the two leaflets of a cell membrane (lipid scrambling) [21] and IFN signaling in the
106 context of virus infection [22]. Follow-up experiments revealed that PLSCR1 is a cell intrinsic factor
107 that restricts spike-mediated SARS-CoV-2 entry, independently of the IFN pathway, via currently

108 undetermined mechanisms. Our genetic screen data and meta-analysis provide a valuable
109 resource to broaden our understanding of coronavirus infection and innate immunity.
110 Furthermore, we extend the recent characterization of PLSCR1 as an antiviral against SARS-CoV-
111 2 impacting COVID-19 outcomes (**Fig. 1**)[18, 23, 24].

112 Results

113 A genome-wide arrayed CRISPR KO screen identifies known and novel factors influencing
114 SARS-CoV-2 infection.

115 While the liver is not the primary target organ of SARS-CoV-2 infection, human
116 hepatocellular carcinoma Huh-7.5 cells naturally express SARS-CoV-2 dependency factors,
117 including the receptor angiotensin converting enzyme 2 (ACE2), and proved unexpectedly useful
118 in SARS-CoV-2 research [18, 25-32]. Huh-7.5 cells do not produce IFN during SARS-CoV-2 infection,
119 but they do induce an antiviral state in response to IFN pretreatment (**Fig 2A-2C, Supp Tables 1-**
120 **4**), making them a convenient model to control the exposure of the cells to IFN.

121 Using these cells, we conducted a whole-genome arrayed CRISPR KO screen designed to
122 identify both SARS-CoV-2 proviral and antiviral genes, whose KO reduces or enhances SARS-CoV-
123 2 infection, respectively. In particular, we aimed to identify factors involved in the IFN response,
124 from IFN sensing to ISG induction, including effector ISGs that directly influence the virus life
125 cycle. With this arrayed approach performed in 384-well plates, the cells in each well received a
126 pool of four gRNAs targeting a single host gene. Each well was then either treated with 1 pM IFN-
127 α2a or left untreated before being infected with SARS-CoV-2, followed by SARS-CoV-2
128 nucleoprotein (N) immunofluorescence staining and high content microscopy (**Fig 2D**). This low
129 dose of IFN was chosen to mimic a cellular environment where IFN triggers an antiviral state
130 before infection. We anticipated that a saturating amount of IFN would lead to high ISG
131 transcription and functional redundancy between effectors, biasing hits towards factors in IFN
132 signaling. In contrast, a low dose of IFN, around the IC50, might enable identification of the
133 specific roles of individual effector ISGs.

134 Of the 16,790 screened genes, we selected 16,178 genes where KO did not lead to changes
135 in cellular fitness assessed by nuclei count (-2 ≤ z-score ≤ 2)(**Supp Fig 1A**). Of these, we selected

136 12,119 genes expressed in three cell lines relevant for SARS-CoV-2 research (A549, Calu-3, Huh-
137 7.5 cells) and human lung cells, the primary target cell type *in vivo*, for downstream analysis [33-
138 35]. We then binned the genes into two groups for data visualization, depending on whether they
139 were induced by IFN-α2a treatment in Huh-7.5 cells as determined by mRNA-seq (log 2 FC ≥ 2
140 and padj ≤ 0.05) (**Supp Fig 1B, Supp Tables 5-7**).

141 Our screen found known and previously unidentified host factors influencing SARS-CoV-2
142 infection (**Fig 2E**). As expected, positive regulators of IFN signaling, such as interferon-alpha/beta
143 receptor alpha chain 1 and 2 (IFNAR1,2) [36-38], interferon regulatory factor 9 (IRF9) [39, 40],
144 Janus kinase 1 (JAK1) [41], and signal transducer and activator of transcription 2 (STAT2) [42, 43]
145 were antiviral only in IFN pretreated cells. Known negative regulators of IFN signaling, such as
146 ISG15 ubiquitin-like modifier (ISG15) [44-46], suppressor of cytokine signaling 1 (SOCS1) [47], and
147 ubiquitin specific peptidase 18 (USP18) [48, 49] were proviral only in IFN pretreated cells.

148 The SARS-CoV-2 receptor ACE2 was confirmed as proviral with or without IFN
149 pretreatment. In our mRNA-seq analysis, IFN treatment was found to significantly upregulate
150 ACE2 mRNA levels (**Supp Fig. 1B**). Prior studies indicate that IFN induces transcription of a
151 truncated ACE2 isoform, rather than the full-length receptor for SARS-CoV-2 [50, 51].

152 The lysosomal cysteine protease cathepsin L (CTSL), required for SARS-CoV-2 spike protein
153 activation [52-54], was a proviral hit in our screens. In contrast, KO of the cell-surface
154 transmembrane serine protease 2 (TMPRSS2) did not influence infection, suggesting that SARS-
155 CoV-2 particles primarily enter Huh-7.5 cells through the endocytic pathway that does not depend
156 on TMPRSS2 (**Fig 1**) [55, 56].

157 The screen data likely contains false negatives. For example, STAT1 and tyrosine kinase 2
158 (TYK2) [57, 58] did not influence infection alongside other positive regulators of IFN signaling,
159 which we attribute to the fact that some gRNAs in the library may have not efficiently directed
160 Cas9 to cut at their respective target gene loci.

161 Collectively, the identification of known proviral and antiviral factors confirms the validity
162 of our screening method.

163 We performed a Gene Set Enrichment Analysis (GSEA) to identify cellular pathways
164 exhibiting proviral or antiviral properties in our screen. The full GSEA results, including the genes

165 driving each pathway enrichment (so-called *leading edge*), can be found in **Supp Table 8**. Some
166 top pathways ranked by adjusted p-value are summarized in **Fig 2F**. Notably pathways associated
167 with RNA pol II transcription and mRNA maturation, as well as pathways related to cellular
168 respiration, exhibited antiviral activity independent of IFN. Surprisingly, pathways associated with
169 RNA pol III transcription, in part driven by the genes RNA polymerase III subunit A (*POLR3A*) and
170 RNA polymerase III subunit B (*POLR3B*), were critical to the antiviral response mediated by IFN.
171 Conversely, factors involved in translation, such as eukaryotic translation initiation factor 3
172 subunits F and G (EIF3G and EIF3F), likely co-opted for producing viral proteins, were identified
173 as proviral. Similarly, factors regulating cholesterol homeostasis, likely crucial for SARS-CoV-2
174 entry [13, 59], were also identified as proviral. For instance, the gene sterol regulatory element
175 binding transcription factor 2 (*SREBF2*) was one of the top proviral genes (**Fig 2E**).
176 Our arrayed CRISPR KO screen results thus constitute a valuable resource for research on
177 coronavirus infection and innate immunity. These can be used to help characterize human genes
178 influencing SARS-CoV-2 infection and the IFN response.
179

180 The ISG PLSCR1 is associated with COVID-19 outcomes and exhibits antiviral effects 181 in functional SARS-CoV-2 genetic screens

182 To provide a thorough perspective on human genes that impact SARS-CoV-2 infection and
183 to place our arrayed CRISPR KO screen results within the context of existing research, we have
184 compiled a table that includes findings from a selection of 67 large-scale 'omic' studies related to
185 SARS-CoV-2. This compilation encompasses this study and 25 other functional genetic screens for
186 genes that influence SARS-CoV-2 infection [10-12, 14, 17, 18, 26, 29, 60-76], 24 human genetic
187 studies that correlate certain alleles with severe COVID-19 outcomes [4, 5, 7, 23, 24, 77-95], ten
188 publications detailing SARS-CoV-2 protein interactomes [96-105], six focusing on SARS-CoV-2 RNA
189 interactomes [106-111], and one that examines proteins with altered phosphorylation states in
190 SARS-CoV-2-infected cells [112] **(Supp Tables 9-10 for the full, and summary tables,
191 respectively)**. This table highlights the depth of research in publications addressing SARS-CoV-2
192 infection: genes reported in several independent large-scale studies are more credible candidates

193 for biological relevance (**Supp Fig 2**). As expected, genes associated with the IFN pathway, such
194 as *IFNAR2*, *OAS1*, and *ZC3HAV1/ZAP*, frequently emerged as significant in SARS-CoV-2 studies.
195 We focused on 28 genes identified in both human genetic studies of COVID-19 patients
196 and in functional genetic screens in cell culture, including our own (**Fig 3**). These genes are likely
197 to have significant physiological relevance and to be well-suited for mechanistic studies in cell
198 culture. Among these, the ISG *PLSCR1* stood out, being identified as one of the most potent
199 antiviral genes in our screen (**Fig 2E**). *PLSCR1* variants have been linked to severe COVID-19 in a
200 recent GWAS (listed in **Table 1**)[23, 24]. This was attributed to a role of PLSCR1 in regulating the
201 IFN response in COVID-19 patients [24]. Indeed, a pioneering study showed that PLSCR1
202 potentiates the transcriptional response to IFN-β treatment in human ovarian carcinoma Hey1B
203 cells [22]. However, PLSCR1 surprisingly appeared as a potent SARS-CoV-2 antiviral even in the
204 absence of IFN in our screens, suggesting a cell intrinsic, IFN-independent function. In other
205 words, baseline levels of PLSCR1 may be sufficient to restrict SARS-CoV-2, and IFN pretreatment
206 could simply enhance this effect by elevating cellular PLSCR1 levels.
207

208 ## Intrinsic PLSCR1 restricts SARS-CoV-2 independently of the IFN pathway.

209 To better characterize the function of PLSCR1 during SARS-CoV-2 infection, we generated
210 and validated by western blot (WB) PLSCR1 KO bulk Huh-7.5 and A549-ACE2 lines (**Supp Fig 3A**).
211 As observed in the arrayed screen (**Supp Fig 1A**), PLSCR1 KO cells were viable (**Supp Fig 3B**).
212 PLSCR1 depletion increased susceptibility to SARS-CoV-2 independently of IFN pretreatment (**Fig**
213 **4A**). Cell treatment with a JAK-STAT inhibitor, which effectively abrogated IFN signaling, confirmed
214 that intrinsic PLSCR1 limits SARS-CoV-2 infection independently of the IFN signaling pathway (**Fig**
215 **4A**). SARS-CoV-2 susceptibility of PLSCR1 KO cells was reversed by the ectopic expression of
216 PLSCR1 (**Fig 4B, Supp Fig 3C**). Interestingly, while PLSCR1 tagged with an N-terminal FLAG tag
217 could rescue, PLSCR1 tagged with a C-terminal FLAG tag could not. The C-terminus of the protein
218 is extracellular, and previous research suggests that this region is important for the protein's
219 scramblase activity and Ca^{2+} binding [113]. It is possible that the addition of this FLAG-tag
220 impaired Ca^{2+} binding, affected PLSCR1's localization at the plasma membrane, or otherwise
221 disrupted the structure of this region, thereby abolishing PLSCR1's antiviral ability. We co-cultured

222 PLSCR1 reconstituted cells and PLSCR1 KO cells in the same well and infected them with SARS-
223 CoV-2. A higher proportion of PLSCR1 KO than PLSCR1 reconstituted cells were positive for SARS-
224 CoV-2 indicating that PLSCR1 acts in a cell autonomous manner (**Fig 4C**). Altogether, these data
225 suggest that intrinsic PLSCR1 contributes to the restriction of SARS-CoV-2, even without IFN.
226

227 ## IFN signaling is unaffected by the loss of PLSCR1 in A549-ACE2 and Huh-7.5 cells.

228 PLSCR1 has been shown to potentiate ISG transcription in IFN-treated Hey1B cells [22].
229 We thus hypothesized PLSCR1 might enhance the type I IFN response in A549-ACE2 and Huh-7.5
230 cells. We investigated PLSCR1's role in the IFN response by infecting Huh-7.5 cells with
231 chikungunya virus (CHIKV), which is unaffected by PLSCR1 KO without IFN (**Fig 5A**). PLSCR1
232 depletion did not functionally affect the antiviral effects of IFN treatment (**Fig 5B**). Furthermore,
233 IFN treatment induced *OAS1* and *IFI6*, two ISGs known to restrict SARS-CoV-2 [10, 12, 17, 91, 92,
234 94, 95], to a similar extent in both WT and PLSCR1 KO cells, indicating that the IFN signaling
235 pathway was unaffected by PLSCR1 depletion (**Fig 5C-J**). Finally, PLSCR1 depletion did not alter
236 basal ISG transcription in the absence of IFN (**Supp Fig 4**).
237 These findings indicate that PLSCR1 limits SARS-CoV-2 infection independently of the IFN
238 signaling pathway in A549-ACE2 and Huh-7.5 cells.
239

240 ## PLSCR1 restricts SARS-CoV-2 entry.

241 We hypothesized that PLSCR1 directly targets and inhibits a specific step of the SARS-CoV-
242 2 life cycle. PLSCR1 primarily localized at the plasma membrane in Huh-7.5 cells (**Fig 6A**).
243 Furthermore, PLSCR1 depletion led to increased SARS-CoV-2 foci formation (**Fig 6B,C**), and PLSCR1
244 KO cells did not show increased susceptibility to a SARS-CoV-2 replicon system that bypasses entry
245 (**Fig 6D**) [114]. In contrast, a single-cycle, replication-defective human immunodeficiency virus
246 type-1 (HIV-1) particles pseudo-typed with SARS-CoV-2 spike showed enhanced entry in PLSCR1
247 depleted cells (**Fig 6E, F**) [115]. This data indicates that PLSCR1 restricts SARS-CoV-2 spike-
248 mediated virion entry. Over-expression of TMPRSS2 lifted the PLSCR1-mediated restriction of
249 authentic SARS-CoV-2 (**Fig 6G-I**) and of SARS-CoV-2 spike pseudo-typed particles (**Fig 6J-M**),
250 indicating that PLSCR1 primarily restricts the endosomal entry route. It is possible that the

251 TMPRSS2-dependent entry near the cell surface provides SARS-CoV-2 with some level of evasion
252 from PLSCR1 restriction, as recently described for the ISG NCOA7 [116].
253 In addition to SARS-CoV-2, we also evaluated the antiviral activity of PLSCR1 against ten
254 viruses that utilize endosomal entry: CHIKV, human parainfluenza virus (hPIV), herpes simplex
255 virus 1 (HSV-1), influenza A virus (IAV), human coronavirus OC43 (hCoV-OC43), human
256 coronavirus NL63 (hCoV-NL63), human coronavirus 229E (hCoV-229E), Sindbis virus (SINV),
257 Venezuelan equine encephalitis virus (VEEV), and vesicular stomatitis virus (VSV). Only SARS-CoV-
258 2 showed a notable susceptibility to PLSCR1's inhibitory effects (**Supp Fig 5**).
259

260 ## Recent variants of SARS-CoV-2 are less restricted by PLSCR1

261 During the COVID-19 pandemic, SARS-CoV-2 variants evolved from the initial strain,
262 showing increased immune evasion and transmissibility [117-119]. To examine if these variants
263 could circumvent the antiviral action of PLSCR1, we infected WT and PLSCR1 KO Huh-7.5 cells with
264 an early strain isolated in July 2020 (NY-RU-NY1) and the Beta (B.1.352), Delta (B.1.617.2),
265 Omicron (BA.5), and Kraken (XBB.1.5) variants **(Fig 7A-E)**. Although PLSCR1 continued to restrict
266 these later variants, the discrepancy in infection rates between WT and PLSCR1 KO cells
267 diminished compared to the original strain, notably with the Omicron and its descendant, Kraken
268 **(Fig 7F)**. We then infected WT and PLSCR1 KO Huh-7.5 cells with the same focus-forming units
269 (FFU) of each virus, as determined in PLSCR1 KO cells, and conducted a focus forming assay. The
270 ratio of foci in WT cells relative to KO cells increased for later variants, especially for the Omicron
271 subvariant Kraken (XBB.1.5) **(Fig 7G)**. Our data suggests a diminished efficacy of PLSCR1 in
272 restricting the newer SARS-CoV-2 variants.
273

274 ## Association between PLSCR1 variants and severe COVID-19

275 PLSCR1 encodes a 318 amino acid protein containing a palmitoylation motif and a
276 transmembrane domain which regulate its plasma membrane localization, and a nuclear
277 localization signal (NLS) and transcriptional activation domain thought to be important for its
278 nuclear functions (**Fig 8A**)[20, 120-125].

279 A recent GWAS has identified an association between PLSCR1 variants and severe COVID-
280 19 outcomes, reporting an odds ratio of approximately 1.2 and a p-value of approximately 10^{-8}
281 (**Table 1**)[23, 24]. In other words, the GWAS suggests that PLSCR1 has a small, but significant effect
282 on severe COVID-19 risks.

283 GWAS typically identify variants associated with increased odds of a disease, but these
284 variants are not necessarily causative. Among the PLSCR1 variants identified in the COVID-19
285 GWAS cited above, only rs343320 results in a protein-coding change, specifically His262Tyr,
286 located in the NLS (**Fig 8A**, **Table 1**). Although we cannot dismiss the possibility that (i) some non-
287 coding variants identified in the GWAS could influence the regulation of *PLSCR1* mRNA,
288 potentially leading to functional outcomes, and (ii) the GWAS might have missed nonsynonymous
289 variants impacting PLSCR1 function, we thought to investigate the functional effects of the
290 His262Tyr variant in cell culture. We ectopically expressed PLSCR1 His262Tyr or PLSCR1 WT in
291 A549-ACE2 cells from a lentiviral vector [126]. PLSCR1 His262Tyr and PLSCR1 WT were expressed
292 at similar levels in this system (**Supp Fig 6**). PLSCR1 His262Tyr did not fully rescue the PLSCR1 KO
293 (**Fig 8B**), indicating that the His262Tyr variant is hypomorphic. Additionally, introducing PLSCR1
294 His262Tyr into cells already expressing PLSCR1 WT increased their susceptibility to SARS-CoV-2
295 infection (**Fig 8B**), suggesting a dominant effect. However, this effect might be attributed to the
296 overexpression of PLSCR1 His262Tyr from the transgene, compared to the natural expression
297 levels of PLSCR1 WT from the endogenous locus. To counter this, we examined patient-derived
298 SV40-immortalized fibroblasts expressing ACE2 that were heterozygous for His262Tyr. These cells
299 were hyper-susceptible to SARS-CoV-2 infection compared to PLSCR1 WT control SV40-fibroblasts
300 (**Fig 8C**), further suggesting that His262Tyr is dominant. We cannot formally rule out that the
301 examined SV40-fibroblasts may carry other mutations influencing SARS-CoV-2 infection.

302 Our data collectively highlight PLSCR1's function in restricting SARS-CoV-2 entry in cell
303 culture, thereby clarifying the association between PLSCR1 variants and severe COVID-19
304 outcomes [23, 24]. Future human genetic studies are crucial for determining if certain PLSCR1
305 variants in the population cause increased risks of severe COVID-19. Our results highlight the
306 variant rs343320 (His262Tyr) as a potential causative candidate, as it caused increased SARS-CoV-
307 2 infection in cell culture.

308 ## Discussion

309 Here, we conducted an unbiased arrayed CRISPR KO screen on Huh-7.5 cells infected with
310 SARS-CoV-2. The screen revealed novel aspects of SARS-CoV-2 and IFN biology while also
311 confirming previously known facets. Pathways related to mRNA transcription and maturation
312 were identified as antiviral. This observation may stem from the conflict between the host cell
313 and SARS-CoV-2, where the host attempts to export mRNAs from the nucleus to facilitate antiviral
314 responses while the virus replicates in the cytoplasm, impeding nuclear export [127-130]. RNA
315 Pol III transcription was specifically essential for the IFN-mediated antiviral response, through
316 mechanisms that are yet to be determined. Interestingly, inborn errors in POLR3A and POLR3C
317 have been previously described in patients with severe varicella zoster virus infections [131].
318 Cellular respiration was identified as a key IFN-independent antiviral pathway. Furthermore,
319 mitophagy was identified as proviral. This may indicate the infected cell's increased demand for
320 energy and ATP to combat the virus. Alternatively, cellular respiration may have other, yet-to-be-
321 identified, IFN-independent antiviral roles. Conversely, translation and cholesterol homeostasis
322 emerged as the foremost proviral pathways. These findings underscore the complex, dualistic
323 nature of the interactions between SARS-CoV-2 and host cells.

324 Our screen notably identified the ISG zinc-finger antiviral protein (*ZC3HAV1*/*ZAP*) as a
325 proviral factor in IFN-treated cells. Initially, ZC3HAV1/ZAP gained attention as an antiviral factor
326 that targets the SARS-CoV-2 RNA genome [111] and prevents programmed ribosomal
327 frameshifting [132]. Yet, a recent study demonstrated that ZC3HAV1/ZAP also promotes the
328 formation of SARS-CoV-2 non-structural proteins 3 and 4-induced double-membrane vesicles,
329 essential for virus replication [68]. SARS-CoV-2 may have adapted to exploit certain ISG products,
330 such as ZC3HAV1/ZAP, within the cellular environment it encounters. It is still unclear if the
331 seemingly contradictory roles of ZC3HAV1/ZAP – both proviral and antiviral – are caused by
332 distinct isoforms.

333 Many other ISG products influenced SARS-CoV-2 infection, PLSCR1 being the most potent
334 restriction factor. PLSCR1 did not influence ISG induction as previously reported [22], but rather
335 inhibited spike-mediated SARS-CoV-2 entry through the endocytic route. Our results corroborate

336 a recent study from Xu et al [18] and provide an explanation for the enrichment for PLSCR1 SNPs
337 observed in a GWAS on severe COVID-19 [23, 24].
338 The molecular mechanisms of PLSCR1-mediated restriction of SARS-CoV-2 entry remain
339 to be elucidated. PLSCR1 could be altering the lipid composition at the contact site between the
340 virus and endosomal membranes, akin to the ISG IFITM3 for influenza A virus [133-136]. PLSCR1
341 was first identified as a Ca^{2+}-dependent phospholipid scramblase [21], but it is unclear whether
342 PLSCR1 depletion affects the bidirectional movement of phospholipids *in vivo* [137-139]. A C-
343 terminal FLAG-tag abolished the antiviral ability of reconstituted PLSCR1, possibly by interfering
344 with the function of the Ca^{2+} binding domain. In contrast, inhibiting PLSCR1's phospholipid
345 scramblase activity did not alleviate SARS-CoV-2 restriction [18].
346 Intriguingly, PLSCR1 specifically restricted SARS-CoV-2 in Huh-7.5 and A549-ACE2 cells but
347 it did not show similar inhibitory effects on other viruses that enter cells via endocytosis. Future
348 studies will investigate the mechanisms behind this specificity. PLSCR1 has been described to
349 inhibit a range of viruses in various cell lines, such as encephalomyocarditis virus, vesicular
350 stomatitis virus, Epstein-Barr virus, hepatitis B virus, hepatitis C virus, human cytomegalovirus,
351 human immunodeficiency virus 1, human T-cell lymphotropic virus type 1, and influenza A virus
352 [22, 140-146]. It has been proposed that PLSCR1 directly binds viral proteins and impairs their
353 functions to restrict the non-coronaviruses cited above, reviewed in [147]. However, it seems
354 unlikely that PLSCR1 has evolved to interact directly with such a diverse set of viral proteins. An
355 alternative explanation is that diverse viral proteins convergently evolved to bind PLSCR1 as a
356 mechanism of immune evasion. Meanwhile, overexpressing PLSCR1 in cell culture could act *like*
357 *a sponge*, absorbing these viral proteins and thereby hindering viral function. We searched for
358 PLSCR1 interactions in ten SARS-CoV-2 proteins interactome studies, relying on ectopic expression
359 of individual viral proteins [96-98, 100-105, 148], and no interaction was reported in two or more
360 independent studies. Two interactions were reported in a single study: (i) PLSCR1-ORF7b [98],
361 and (ii) PLSCR1-ORF8 [101], both by proximity biotinylation, which was less stringent compared
362 to affinity purification-mass spectrometry (AP-MS) and yeast two-hybrid (Y2H) techniques (**Supp**
363 **Fig 7**). To date, there is no strong evidence of a direct interaction between a SARS-CoV-2 protein

364 and PLSCR1, although we cannot rule out that such interactions may occur or even appear in the
365 future as SARS-CoV-2 evolves.

366 Recent SARS-CoV-2 variants, including Omicron (BA.5) and Kraken (XBB.1.5), showed
367 reduced sensitivity to PLSCR1-mediated restriction compared to the New York 2020 strain which
368 served as a reference in our study. Previous research suggests that Omicron, in particular, has
369 developed increased resistance to IFN [149, 150], a trait associated with its highly-mutated spike
370 protein [151]. Omicron's relative resistance to IFN may be due to alternative entry routes that
371 alleviate the restrictions from antiviral ISGs targeting endocytosis, such as PLSCR1 (**Fig 1**). While
372 Omicron favors endocytic entry over TMPRSS-2-dependent entry near the cell-surface [152, 153],
373 recent findings suggest that Omicron can also utilize cellular metalloproteinases for near cell-
374 surface entry, enhancing its infectivity in nasal epithelia [151]. Future research should investigate
375 how SARS-CoV-2 variants evade PLSCR1 and whether this evasion is primarily due to mutations in
376 the spike protein facilitating alternative entry mechanisms or to other factors.

377 Several PLSCR1 variants were enriched in a GWAS on severe COVID-19, with a relatively
378 low odds ratio of approximately 1.2 [23, 24]. Considering the complex redundancies within
379 antiviral defenses, from innate immunity featuring multiple effector ISGs that restrict SARS-CoV-
380 2 [9-14, 17, 18], to adaptive immunity [154], the modest odds ratio associated with a single
381 effector ISG not involved in IFN signaling may not be unexpected. However, for these very reasons,
382 the identification of PLSCR1 in the GWAS remains noteworthy. Of these enriched PLSCR1 variants,
383 only rs343320 resulted in a protein-coding change, His262Tyr. Our findings indicate that His262Tyr
384 exhibits a hypomorphic and dominant effect in cell culture, leading to increased SARS-CoV-2
385 infection. Future research should aim to ascertain whether rs343320, or potentially other PLSCR1
386 variants, are directly responsible for elevated risks of severe COVID-19 in patients. It is also
387 noteworthy to mention the presence of a loss-of-expression/loss-of-function variant in PLSCR1,
388 specifically p.Ile110AsnfsTer6 (rs749938276). This variant exhibits a minor allele frequency (MAF)
389 of 0.0003 in the general population, yet it is notably more prevalent among the Ashkenazi Jewish
390 population, with a maximum MAF (MAFmax) of 0.01. The identification of at least one
391 homozygous individual in the gnomAD database underscores the viability of individuals deficient
392 in PLSCR1 [155]. This suggests a potential enrichment of this variant within specific populations,

393 an aspect that merits further epidemiological and functional exploration to understand its impact
394 on susceptibility to SARS-CoV-2.
395 Our findings show that baseline levels of PLSCR1 are effective in limiting SARS-CoV-2
396 infection. This is in line with other studies where ISGs like *DAXX* and *LY6E* were shown to inhibit
397 SARS-CoV-2 independently of IFN [17, 156, 157]. mRNA-seq analyses of Huh-7.5 cells and primary
398 human hepatocytes, as well as data from the GTEx consortium on various human tissues [35,
399 158], revealed that many ISGs are constitutively expressed, even without IFN stimulation (**Supp**
400 **Fig 8**). This supports the idea that the IFN-induced antiviral state results more from enhanced
401 expression of antiviral genes rather than a binary ON/OFF switch. In future studies, it will be
402 interesting to explore whether intrinsically expressed ISGs also carry out cellular functions beyond
403 pathogen defense.

404 Materials and Methods

405 Plasmids, oligos, and primers

406 The plasmids, gene fragments, and primers used in this study are listed in **Supp Tables**
407 **11, 12, and 13**, respectively.
408

409 Cell Lines

410 Huh-7.5 (human hepatocellular carcinoma) [159], A549-ACE2 (human lung carcinoma,
411 generously provided by the laboratory of Brad R. Rosenberg), Lenti-X 293T (Takara, cat. #632180),
412 Caco2, Vero E6 (*Chlorocebus sabaeus* kidney epithelial cells, ATCC cat. #CRL-1586), BHK-21
413 (hamster kidney) cells, and SV40-Fribroblasts were cultured in Dulbecco's Modified Eagle Medium
414 (DMEM, Fisher Scientific, cat. #11995065) supplemented with 0.1 mM nonessential amino acids
415 (NEAA, Fisher Scientific, cat. #11140076) and 10% fetal bovine serum (FBS, HyClone Laboratories,
416 Lot. #KTH31760) at 37°C and 5% CO2. All cell lines tested negative for mycoplasma.
417

418 Virus stocks

419 **CHIKV-181/25-mKate2:** the infectious clone was a kind gift from Mark Heise (University
420 of North Carolina, USA) [not published yet]. 20 µg of infectious clone DNA was linearized with

421 NotI-HF at 37°C overnight. Complete digestion was confirmed by running a sample of the digested
422 DNA on a 1% agarose gel. After confirmation, linearized DNA was cleaned via phenol-chloroform
423 extraction, and then ethanol precipitated. The precipitated DNA was resuspended in 20 µL of
424 RNase-free H_2O and in vitro transcribed with an SP6 mMessage mMachine In Vitro Transcription
425 Kit (ThermoFisher, cat. AM1340). The generated RNA was electroporated into 1.2 x 10^7 BHK-21
426 cells, and the produced virus was harvested once approximately 80% of the electroporated cells
427 lifted or showed signs of cytopathic effects and 100% of the cells were positive for mKate2 signal.
428 The titer of the virus was 8.5 x 10^6 focus-forming units (FFU) on Huh-7.5 cells.

429 **hCoV-NL63:** was generously provided by Volker Thiel (University of Bern) and amplified at
430 33°C in Huh-7.5 cells as in [29].

431 **hCoV-OC43**: was obtained from ZeptoMetrix (cat. #0810024CF) and amplified at 33°C in
432 Huh-7.5 cells as in [29].

433 **hPIV3-GFP** [160]: stock (based on strain JS) grown in VeroE6 cells as in [161].

434 **HSV-1-GFP**: stock made by passage on VeroE6 cells. 2 x 10^7 cells seeded in a T175 flask
435 were infected at an MOI of 0.01 PFU/ml of HSV-1-GFP virus engineered and provided by Ian Mohr
436 [162]. After a one-hour incubation at 37°C, the inoculum was removed, and 20 ml of DMEM
437 supplemented to contain 10% FBS and NEAA was added. Cells were incubated at 37°C for 24 h or
438 until CPE was evident. Cell supernatant containing progeny virus was harvested and titrated on
439 Vero E6 cells (2.4% avicel, fix 2 dpi) at 2.4 x 10^8 PFU/ml.

440 **IAV WSN (H1N1):** was generated in MDCK cells. Cells were inoculated at MOI 0.01 in
441 DMEM supplemented with NEAA, 0.2% BSA, 0.1% FCS, 50 mM Hepes, and 1 µg/ml TPCK-trypsin.
442 Virus-containing culture supernatant was harvested at 52 h post-infection and cleared by
443 centrifugation.

444 **SARS-CoV-2:** unless otherwise stated, the isolate SARS-CoV-2/human/USA/NY-RU-
445 NY1/2020 was used in this study [163]. The virus was sourced from the saliva of a deidentified
446 patient in New York City, collected on July 28, 2020. Its sequence is publicly accessible (GenBank
447 OM345241). The virus isolate was amplified in Caco-2 cells. The passage 3 stock employed had a
448 titer of 3.4 × 10^6 PFU/ml, as measured on Vero E6 cells using a 1% methylcellulose overlay,
449 according to previously described methods [164]. The Beta (B.1.351), Delta (B.1.617.2), Omicron

450 (BA.5), and Kraken (XBB.1.5) variants were obtained from BEI resources (cat. # NR-54008, NR-
451 55611, NR-58616, and NR-59104, respectively), amplified in Vero E6 cells engineered to stably
452 express TMPRSS2, and titer was determined as described above.

453 **SINV Toto1101** [165]: expressing an nsP3-mScarletI fusion reporter was generated by
454 cloning the sequence encoding mScarletI in frame into a unique SpeI restriction site in the
455 pToto1101 infectious clone plasmid as previously described [166]. *In vitro* transcribed, capped
456 RNA was generated from the pToto1101-nsP3-mScarletI plasmid (Invitrogen mMessage
457 mMachine SP6 kit, AM1340) and electroporated into BHK-J cells, a derivative of BHK-21 cells
458 (ATCC, CCL-10) as previously described [166]. 24 hours post electroporation, centrifuge clarified
459 supernatants were aliquoted and stored at -80C. BHK-J cells were cultured and virus stocks
460 generated in MEM supplemented with 7.5% FBS.

461 **VEEV-dsEGFP** [15, 167]: the infectious clone plasmid was linearized (MluI) and transcribed
462 *in vitro* using an mMessage mMachine SP6 transcription kit (Ambion). BHK-21 cells were
463 electroporated with viral RNA, and supernatant containing progeny virus was harvested after
464 incubation at 37°C for 30 h or until CPE was evident. Virus was titrated by plaque assay on BHK-
465 21 cells (2.4% avicel, fix 2 dpi). BHK-21: 1.45 x 10^9 FPU/ml.

466 **VSV-GFP** [168]: grown in BHK-21 cells as in [161].

467 **YFV 17D:** was generated via transfection of Huh-7.5 with in vitro transcribed RNA from
468 pACNR-FLYF-17D plasmid as described in [161].

469

470 mRNA-seq

471 mRNA-seq on SARS-CoV-2-infected cells

472 **Cell culture and infection:** 75,500 Huh-7.5 cells or 150,000 Calu-3 cells were seeded in
473 each well of a 12-well plate with 1 mL media. Media: DMEM with 5% FBS and 1% NEAA for Huh-
474 7.5 cells or EMEM (ATCC, 30-2003) with 10% FBS for Calu-3 cells. The next day, cells were infected
475 by removing 500 µL of media and adding 500 µL of media with SARS-CoV-2 strain USA-WA1/2020
476 (BEI Resources, NR-52281) at 5,000 PFU/well (virus titer determined in Huh-7.5 cells). After one
477 day, the wells were washed with PBS and cells were harvested in 1 mL TRIzol (Invitrogen, cat.
478 15596-018). N = 3 replicates (separate wells) per sample.

479 **RNA extraction:** 2 ml MaXtract High Density tubes (Qiagen, 129056) were centrifugated
480 at 12,000–16,000 x g for 20-30 second centrifugation. A volume of 750 µL TRIzol-prepared sample
481 was combined with 150 µL chloroform in these tubes and hand-shaken vigorously. Phase
482 separation was accomplished by centrifugation at 1500 x g for 5 min at 4°C. The aqueous phase
483 was then mixed with 400 µL ethanol 95-100% in a separate tube. These preparations were then
484 transferred to Zymo Research RNA clean and concentrator-25 kit columns (Zymo Research, cat.
485 R1018) and subjected to multiple wash and centrifugation steps as recommended by the
486 manufacturer. An in-column DNase I treatment was performed using Qiagen DNase (Qiagen,
487 79254). Finally, RNA was eluted with 50 µL DNase/RNase-Free water and stored at -80°C.
488 **Sequencing:** Poly-A enriched libraries were made using the TruSeq stranded mRNA LT kit
489 (Illumina, Cat# 20020594) and sequenced on a NovaSeq SP with PE150 read length.
490

491 ### mRNA-seq on IFN-treated cells

492 **Cell culture and treatment:** 75,500 Huh-7.5 or 200,000 Calu-3 cells were seeded in each
493 well of a 12-well plate with 1 mL media. Two days later, the media was replaced with 1 mL of
494 DMEM with 5%FBS, 1% NEAA in Huh-7.5 or EMEM (ATCC, cat. 30-2003) with 10% FBS for Calu-3
495 cells with IFN-α2a (PBL, cat. 11101-2) and incubated at 37ºC. 24 h later, cells were harvested in
496 500 µL TRIzol. N = 3 replicates (separate wells) per sample.
497 **RNA extraction** as described above.
498 **Sequencing:** Poly A-enriched libraries were made using the NEBNext Ultra II RNA Library
499 Prep Kit for Illumina (NEB, cat. E7770) and sequenced on a NovaSeq SP with PE150 read length.
500

501 ### mRNA-seq on PLSCR1 KO cells

502 **Cell culture and CRISPR KO:** 30,000 Huh-7.5 cells were seeded in five wells of a 24-well
503 plate with 480 uL media. The cells were reverse transfected with 120 uL of a transfection mixture
504 composed of 250 nM of pooled anti-PLSCR1 or non-targeting Edit-R crRNAs from Horizon
505 Discovery (cat. CM-003729-01-0002, CM-003729-02-0002, CM-003729-03-0002, and CM-
506 003729-04-0002 or U-007501-01-05, U-007502-01-05, U-007503-01-05, and U-007504-01-05,
507 respectively) which had been resuspended with an equimolar amount of Edit-R tracrRNA

508 (Horizon, cat. U-002005-20) and a 1:200 dilution of Dharmafect 4 (Horizon, cat. T-2004-01). The
509 following day, the media was changed, and the cells were progressively scaled up to a 6-well plate
510 over the next 4 days. When the cells were confluent in the 6-well plate, the media was removed
511 from four of the wells. They were then washed with 1x PBS (cat. 14190-144) and lysed with 1 mL
512 TRIzol (Life Technologies, cat. 15596-018) for 5 minutes at room temperature before transferring
513 to an Eppendorf tube and freezing at -80°C to await RNA extraction. The remaining well was lysed
514 with 300 µL of RIPA buffer (Thermo cat. 89900) supplemented with 1x protease inhibitor (Thermo
515 cat. 87786) and 1x EDTA and prepared for western blot as described below, in the "Western Blots"
516 section.
517 **RNA extraction** as described above.
518 **Sequencing:** Poly A-enriched libraries were made using the NEBNext Ultra II RNA Library
519 Prep Kit for Illumina (NEB, cat. E7770) and sequenced on a NovaSeq SP with PE150 read length.
520

521 ### mRNA-seq analysis

522 mRNA-seq reads were first quality-filtered and adapter-trimmed using Trim Galore with
523 parameters -q 20 -e 0.1 --length 20 --paired and Cutadapt. Reads were then mapped to the human
524 genome GRCh38 or to a combined SARS-CoV-2 MN985325.1/human genome GRCh38 using STAR
525 [169] with settings including --runThreadN 8 --outFilterMultimapNmax 1 --twopassMode Basic.
526 Feature counting was performed using the featureCounts function from the Rsubread package
527 [170], with strandness specified depending on the sequencing and other parameters as default.
528 The resulting counts were imported into a DESeqDataSet object using the DESeq2 package [171]
529 with a design formula of ~Group. Size factors were estimated and normalized counts were
530 extracted and saved. Differential expression analysis was performed using DESeq with the created
531 DESeqDataSet object, contrasted by sample groups, cooksCutoff and independentFiltering
532 disabled, and otherwise default parameters.
533

534 ## Unbiased arrayed CRISPR KO screening

535 ### Screen overview

536 The content of each gRNA 384-well plate constituting the whole-genome library (61
537 library plates total) was transfected to 16 assay 384-well plates (976 assay plates total). Positive
538 and negative control gene gRNAs were incorporated into vacant wells of each assay plate as
539 described below. Huh-7.5 cells were subsequently seeded into these assay plates. The 16 assay
540 plates served as replicates for three distinct experimental conditions: 4 replicates for mock
541 treatment followed by mock infection, 5 replicates for IFN-α2a treatment followed by SARS-CoV-
542 2 infection, and 7 replicates for mock treatment followed by SARS-CoV-2 infection. Each day, three
543 library 384-well plates were processed, along with their corresponding 48 assay plates. The full
544 gRNA library, distributed across 61 384-well plates, was completed over a span of 21 days. For
545 each set of plates, cell seeding was conducted on day 0, IFN-α2a treatment on day 4, SARS-CoV-
546 2 infection on day 5, and cell fixation on day 6.

547 ### gRNA library preparation

548 A 0.1 nmol Edit-R Human Whole Genome crRNA Library (Horizon, cat. GP-005005-01)
549 containing four crRNAs per gene and one gene per well (total 0.1 nmol crRNA/well) was
550 resuspended in 80 µL of a 1.25 µM tracrRNA (Horizon, cat. U-002005-1000) 10 mM Tris-HCL pH
551 7.4 solution to create a 1.25 µM gRNA solution. The library was then aliquoted in 10 mM Tris-HCL
552 pH 7.4 in several 96-well plate and 384-well plate copies using a Tecan Freedom EVO liquid
553 handler. A single-use library copy containing a 40 µL/well of a 312.5 nM gRNA solution in the 384-
554 well plate format was used in this study.

555 ### gRNA reverse transfection (day 0)

556 In each well of the 384-well assay plates, 40 µL of a transfection solution was prepared by
557 combining 2% DharmaFect-4 transfection reagent (Horizon, cat. GP-T-2004-07A) in Opti-MEM
558 (Gibco, cat. 31985070). This was added to 40 µL of a 312.5 nM gRNA library using a Thermofisher
559 Multidrop Reagent Dispenser, yielding an 80 µL/well transfection mixture. The mixture was left
560 to incubate at room temperature for 20 minutes. Simultaneously, assay plates were preloaded
561 with 11 µL/well of serum-free media, which was formulated from DMEM, 1X Antibiotic-
562 Antimycotic solution (Gibco, cat. 15240-062), and 1X NEAA, dispensed via a Thermofisher

563 Multidrop Reagent Dispenser. Subsequently, 4 µL/well of the transfection mixture was dispensed
564 into each of the assay plates (16 assay plates per library plate) using a Tecan Freedom EVO liquid
565 handler. During this time, Huh-7.5 cells were prepared in media containing 25% FBS, 1X Antibiotic-
566 Antimycotic solution, and 1X NEAA. A volume of 10 µL cells/well was added to the assay plates,
567 again using a Thermofisher Multidrop Reagent Dispenser. Ultimately, each well contained 1,250
568 cells in a 25 µL final volume, with a composition of 25 nM gRNA, 10% FBS, 0.8X Antibiotic-
569 Antimycotic, and 0.8X NEAA. Plates were then span at 200 g for 5 minutes. To minimize
570 evaporation, plates were sealed with Breathe-Easy sealing membranes (Sigma-Aldrich, cat.
571 Z380059) and placed in humid chambers constructed from a 245 mm x 245 mm dish containing
572 a paper towel moistened with 15 mL of 1X Antibiotic-Antimycotic solution. Four assay plates were
573 placed in each humid chamber and incubated at 37°C.

574 IFN-α2a treatment (day 1)

575 Each well received 5 µL of IFN-α2a (PBL, cat. 11101-2) in media (DMEM, 20% FBS, 1X
576 Antibiotic-Antimycotic solution, 1X NEAA), using a Thermofisher Multidrop Reagent Dispenser,
577 for a final concentration of 1 pM IFN-α2a in a final volume of 30 µL. Plates were then span at 200
578 g for 5 minutes and incubated at 37°C.

579 SARS-CoV-2 infection (day 5)

580 Each well received 212.5 PFU SARS-CoV-2 virus (titer determined on Vero E6 cells, see
581 Virus Stocks section above) diluted in 5 µL of media (DMEM, 20% FBS, 1X Antibiotic-Antimycotic
582 solution, 1X NEAA) for a final volume of 35 µL in the BSL3. Plates were then span at 200 g for 5
583 minutes and incubated at 37°C.

584 Fixing (day 6)

585 Each well received 50 µL of 20% neutral buffered formalin (Azer Scientific, cat. 20NBF-4-
586 G) and plates were incubated overnight. The formalin mixture was then removed and each well
587 received 50 µL of PBS.

588 IF staining

589 For IF staining of SARS-CoV-2 infected cells in the arrayed CRISPR KO screen (**Fig 1E)**, as
590 well as some focused experiments (**Fig 3B**, **Fig 3C**, **Fig 4B,C**, **Fig 8C)**: the following solutions were
591 prepared for both 96-well plate (96-wp) and 384-well plate (384-wp): PBS (Phosphate Buffered

592 Saline), Perm Solution: Comprised of PBS with an added concentration of 0.1% Triton X100,
593 Blocking Solution: PBS was mixed with 1% BSA. This solution was prepared a day in advance and
594 filtered before use, PBST: PBS with 0.1% of Tween 20, Primary Antibody Solution: Genetex anti
595 SARS-CoV-2 N poly rabbit antibody (GTX135357) at a dilution of 1:3000, Secondary Antibody
596 Solution: AF647 anti-rabbit antibodies at a dilution of 1:3000 and Hoechst 33342 (10 mg/ml) at
597 1:10,000. Plates were stained on a Biotek EL406 Microplate Washer Dispenser using the following
598 steps: 1. Priming: The washer was primed with 200 ml of each buffer: PBS, Perm Solution, Blocking
599 Solution, and PBST. 2. First Washing Phase: Contents of the plates were aspirated. Plates were
600 then washed with 50 µL/well (384-wp) or 200 µL/well (96-wp) of Perm Solution, followed by a
601 slow shake for 3 seconds. 3. Permeabilization: A delay of approximately 1 minute was
602 implemented for permeabilization, in addition to the time required to process all the plates
603 (around 1 minute per plate). 4. Second Washing Phase: Plates were washed with 50 µL/well (384-
604 wp) or 200 µL/well (96-wp) of PBS. Subsequently, 50 µL/well (384-wp) or 200 µL/well (96-wp) of
605 Blocking Solution was added to the plates, followed by a slow shake for 3 seconds. 5. Blocking,
606 autoclean, and Primary Antibody Priming: The washer was set to undergo an autoclean cycle with
607 PBS for 30 minutes. Simultaneously, the syringe containing the Primary Antibody Solution was
608 primed with 16 ml. 6. Third Washing Phase and First Antibody Dispensing: After aspirating the
609 contents of the plates, 15 µL/well (384-wp) or 60 µL/well (96-wp) from the Primary Antibody
610 Solution was added, followed by a slow shake for 3 seconds. 7. Primary Antibody Incubation,
611 autoclean, and Secondary Antibody Priming: The washer was subjected to another autoclean
612 cycle using PBS for 2 hours and 5 minutes. The syringe containing the Secondary Antibody
613 Solution was primed with 16 ml during this period. 8. Fourth Washing Phase and Second Antibody
614 Dispensing: Plates were washed with 50 µL/well (384-wp) or 200 µL/well (96-wp) of PBST,
615 followed by a 2-second slow shake and aspiration. Then, 15 µL/well (384-wp) or 60 µL/well (96-
616 wp) from the Secondary Antibody Solution was added, accompanied by a 3-second slow shake.
617 9. Secondary Antibody Incubation and autoclean: An autoclean cycle with PBS was initiated and
618 lasted for 1 hour. 10. Final Washing Phase: Plates were washed with 50 µL/well (384-wp) or 200
619 µL/well (96-wp) of PBST. This was followed by two consecutive washes with 50 µL/well (384-wp)

620 or 200 µL/well (96-wp) of PBS, incorporating a 2-second slow shake in each cycle. Finally, plates
621 were left with 50 µL/well (384-wp) or 200 µL/well (96-wp) of PBS.

622 Imaging

623 Plates were imaged with a ImageXpress micro-XL and analyzed with MetaXpress
624 (Molecular Devices).

625 Analysis

626 Analysis was conducted in R.

627 **Data Omission**: We excluded five library plates, constituting 8% of the total library, due to
628 insufficient infection levels for accurate quantification.

629 **Normalization**: Two variables were subject to normalization—percentage of SARS-CoV-2
630 positive cells and the count of nuclei. The normalization steps were applied separately for the
631 three screening conditions: mock treatment followed by mock infection, IFN-α2a treatment
632 followed by SARS-CoV-2 infection, and mock treatment followed by SARS-CoV-2 infection. Data
633 was first Z-scale normalized within assay plates:

634 $$Scale(x) = \frac{x - mean(x)}{sd(x)}$$

635 And then Z-scale normalized per row and per column to remove any spatial effects.

636 **Statistics:** a robust statistic accounting for technical and biological variability was applied
637 using the below formula within the replicates of each gene**:**

638 $$Stat\ score(x) = \frac{mean(x)}{sd(x)}$$

639 This statistic was further standardized by Z-scaling across all genes to produce our final z-
640 score.

641 **Exclusion of genes influencing cell proliferation:** 224 genes with nuclei count z-score ≥ 2
642 and 388 genes with nuclei count z-score ≤ 2 in the mock treatment followed by mock
643 infection condition were deemed to influence cell proliferation and excluded from
644 subsequent analyses.

645 **Exclusion of genes not expressed in cell lines of interest (A549, Calu-3, Huh-7.5 cells) and**
646 **in human lung cells.** Expression data from cell lines from [33, 34]. Expression data from tissues
647 from [35]. Genes were considered expressed if they had at least one read count within exons.

648

649 ## Gene set enrichment analysis

650 For the pathway analysis, we leveraged the FGSEA package [172] to perform Gene Set
651 Enrichment Analysis (GSEA) using gene sets found in the Molecular Signatures Database (MSigDB)
652 [173]: Reactome [174], KEGG [175], Wikipathways [176], Pathway Interaction Database [177], and
653 Biocarta [178]. The analysis was conducted separately for two conditions: IFN-α pretreated SARS-
654 CoV-2 infection and non-pretreated SARS-CoV-2 infection. We attributed a score to each pathway
655 for both conditions:

656 $$Score = -log10(padj) \times sign(Normalized\ Enrichment\ Score)$$

657 Each pathway was then attributed to one of nine quadrants (as in **Fig 2F**) based on its
658 score in the IFN-α pretreated condition (axis x) versus non-pretreated condition (axis y), using
659 padj ≤ 0.05 as a cutoff.

660

661 ## Compilation of published large-scale omic studies on SARS-CoV-2

662 As a rule, we listed the genes classified as 'hits' by the authors of the respective studies.
663 Below are some exceptions or clarifications:

664 ### Functional genetic screens

665 **Baggen, et al. [76]:** we used the "low stringency adjusted" analysis in Suppl Table 11.
666 Proviral: p_value_neg ≤ 0.05 and log2 FC ≥ 1. Antiviral: p_value_pos ≤ 0.05 and log2 FC ≤ -1. We
667 also used "High stringency" analysis in Suppl Table 7. Proviral: Gene is TMEM106B (log2 FC = 3.8
668 and p_value_neg = 0.08) or p_value_neg ≤ 0.05 and log2 FC ≥ 1 (no gene matched this criteria).
669 Antiviral: p_value_pos ≤ 0.05 and log2 FC ≤ -1 (no gene matched this criteria). **Biering, et al. [75]:**
670 in Supplementary Table 1, in Tab 1: LOF-enriched screen analysis, for proviral genes, we used FDR
671 ≤ 0.05. In Tab 2: GOF-depleted screen analysis, proviral: FDR ≤ 0.05. In Tab 3: GOF-enriched screen
672 analysis, for antiviral genes, we used FDR ≤ 0.05. **Chan, et al. [74]:** in Multimedia component 6,
673 for Vero E6 (T16); UM-UC-4 (T23); HEK293+A+T (T12); HuH-7 (T15) and Calu-3 (T43), we
674 considered gene as hits at FDR < 0.1 (as in Figure 4A). We listed the genes as proviral if differential
675 ≥ 0 or antiviral if differential ≤ 0. **Daniloski, et al. [73]:** we used Table S1. FDR MOI1 ≤ 0.05 or FDR
676 MOI3 ≤ 0.05. **Danziger, et al. [10]:** in S1 Table, we used the genes annotated as proviral or antiviral

677 by the authors. **Gordon, et al. [72]:** for A549 +ACE2 in Table S6 or Caco2 in Table S7, for proviral
678 genes, we used Averaged z-scores ≤ 2 and for antiviral genes, we used Averaged z-scores ≥ 2.
679 **Grodzki, et al. [71]:** for VeroE6 in additional file 4, tab 4, we used FDR <0.25. For HEK293T +Cas9
680 Study 1 in additional file 6, tab17, we used FDR <0.25. For HEK293T +Cas9 Study 1 in additional
681 file 7, tab7, we used FDR <0.25. **Hoffmann, et al. [26]:** for 37°C (Table S1E) and for 33°C (Table
682 S1C), we selected proviral genes if FDR ≤ 0.05 and z-score ≥ 0 and antiviral genes if FDR ≤ 0.05 and
683 z-score ≤ 0. **Hossain, et al. [65]:** in Figure 3E, we selected the top 15 genes in the spike-mNG axis
684 by negative log robust rank aggregation. **Israeli, et al. [70]:** we used Supplementary Data 1. **Kaur,**
685 **et al. [14]:** we used the genes labelled in Figure 1. **Le Pen et al. (this study):** we used z-score ≥ 2
686 for antiviral genes and ≤ 2 for proviral genes, see Unbiased arrayed CRISPR KO Screen analysis
687 section above for more details. **Loo, et al. [69]:** we used the genes labelled in Figure 2. **Mac Kain,**
688 **et al. [17]:** in Electronic Supplementary Material 5, for antiviral genes, we used the filter: pos|rank
689 ≤13, for proviral genes, we used neg|rank ≤13. **Martin-Sancho, et al. [11]:** we used Table S3,
690 "Lentivirus validated hits". **Pahmeier, et al. [68]:** we used the genes labelled in Figure 6.
691 **Rebendenne, et al. [67]:** for Calu3_Gattinara, we used for proviral genes: residual_z-score_avg ≥
692 2.5 and for antiviral genes: residual_z-score_avg ≤ 2.5 (no gene). For VeroE6, proviral: residual_z-
693 score_avg ≥ 2.5, and antiviral: residual_z-score_avg ≤ 2.5. For Caco2, proviral: residual_z-
694 score_avg ≥ 2.5 and antiviral: residual_z-score_avg ≤ 2.5. For Calu3_Calabrese, proviral:
695 residual_z-score_avg ≤ 2 and antiviral: residual_z-score_avg ≥ 2. **Rehfeld, et al. [66]:** In Table S1,
696 we considered genes as hits for PRF-1 top eGFP-mCh or PRF-1 bottom eGFP-mCh if FDR ≤ 0.05.
697 **Schneider, et al. [29]:** for both 37°C (Table_S1A) and 33°C (Table_S1B), we listed the gene as
698 proviral if FDR ≤ 0.05 and z-score ≥ 0 and antiviral if FDR ≤ 0.05 and z-score ≤ 0. **Wang, et al. [63]:**
699 we used Table S1. Proviral: Enrichment score ≤ 10^(-4). **Wei, et al. 2021 [62]:** we used Table S1.
700 For proviral genes, we used Cas9-v1 Avg. ≥ 2.5 & Cas9-v2 Avg. ≥ 2.5. Average between Cas9-v1
701 Avg. and Cas9-v2 Avg. is given in the table. For antiviral genes, we used Cas9-v1 Avg. ≤ -2.5 &
702 Cas9-v2 Avg. ≤ -2.5. Average between Cas9-v1 Avg. and Cas9-v2 Avg. is given in the table. **Wei, et**
703 **al. 2023 [61]:** in Table S1, for Day 7 or Day 14, we used fdr ≤ 0.05 for positive regulators of
704 ribosomal frameshifting or negative regulators of ribosomal frameshifting. **Wickenhagen, et al.**
705 **[12]:** we used the genes labelled in Figure 1B. **Xu, et al. [18]:** in Huh-7.5 or A549-ACE2 cells, in

706 untreated or in IFN-gamma treatment, we used Log10 p-value (mNG-High vs. mNG-Low
707 Enrichment) ≥ 3. **Zhu et al. [60]:** In Supplementary Data 1 , SARS-CoV-2 WT and 2 VOCs tested,
708 for proviral genes, we used pos.score_wt ≤ 0.0005 or pos.score_alpha ≤ 0.0005 or pos.score_beta
709 ≤ 0.0005.

710 ### Human genetic studies

711 **Degenhardt, et al. [86]:** we used Table 2 and added KANSL1 and TAC4, based on new
712 analysis by Pairo-Castineira et al. 2023 [23]. **Kousathanas, et al. [24]:** we used Table 1 from Pairo-
713 Castineira, et al. 2023 [23]. **Pairo-Castineira, et al. 2021 [94]**: we used Table 1 from Pairo-
714 Castineira, et al. 2023 [23]. **Pairo-Castineira, et al. 2023 [23]**: we only considered variants near
715 annotated genes (i.e., we excluded rs1073165). **Roberts, et al. [79]:** we used Supplementary Table
716 4. **Zhou, et al. [91]**: we used Table 1 and the p-values from COVID-19 hospitalization (European
717 ancestry only).

718 ### SARS-CoV-2 protein interactomes

719 **Davies, et al. [105], Laurent, et al. [98], Li, et al. [104], Samavarch-Tehrani, et al. [96], St-**
720 **Germain, et al. [99], Stukalov, et al. [103]:** we used the Supplementay Table 3 from [25]**. Gordon,**
721 **et al. [97]:** we used the genes listed in Table S2. **Liu, et al. [100] and May, et al. [101]:** we used
722 the genes listed in May, et al. [101] Table S5-new. **Zhou, et al. [102]:** we used the genes listed in
723 Table S1. "SARS-CoV-2-human protein-protein interactions identified in this study."

724 ### SARS-CoV-2 RNA interactomes

725 **Flynn, et al. [110], Kamel, et al. [109], Labeau, et al. [108], Lee, et al. [111], Schmidt, et**
726 **al. 2021 [107]:** we used the Supplementay Table 3 from [25]**. Schmidt, et al. 2023 [106]:** we used
727 Table S2, "Huh-7 interactome comparison tab", genes listed in the following categories: "Huh-7
728 gRNA FDR5 HS" and "Huh-7 sgmRNA FDR5 HS".

729 ### Altered phosphorylation states in SARS-CoV-2-infected cells.

730 **Bouhaddou, et al. [112]:** for Vero E6 cells, we used Table S1, tab 1 "PhosphoDataFull" and
731 filtered for adj.pvalue ≤ 0.05 & log2FC ≥ 1 or adj.pvalue ≤ 0.05 & log2FC ≤ -1 in at least three
732 different time points.

733

Generation of PLSCR1 KO cells

CRISPR KO

KO Huh-7.5 and A549-ACE2 cells were generated using two anti-PLSCR1 Edit-R crRNAs from Horizon Discovery (cat. CM-003729-02-0002 and CM-003729-04-0002) or non-targeting controls (cat. U-007501-01-05 and U-007502-01-05) resuspended with an equimolar amount of Edit-R tracrRNA (Horizon, cat. U-002005-20) to form sgRNAs. The sgRNAs were then co-transfected with Cas9-mKate2 mRNA (Horizon, cat. CAS12218) according to the manufacturer's protocol. 24 to 48 hours after transfection, cells were examined for mKate2 signal and FACS sorted into bulk and single cell populations, gating on mKate2 signal. Bulk and single cell populations were then assessed for PLSCR1 expression by western blot to confirm KO.

Amplicon sequencing

Genomic DNA was isolated from a frozen cell pellet using the Qiagen DNeasy kit (Qiagen, cat. 69504) and treated with RNAse A in the optional RNA digestion step. The region of interest was then amplified using Q5 2x mastermix (New England Biolabs, cat. M0492S), 500 ng of template DNA, 0.5 µM of forward and reverse primers, and the following PCR conditions: 98°C for 30 seconds, followed by 98°C for 5 seconds, 64°C for 15 seconds, and 72°C for 20 seconds, repeating those steps 30 times before holding at 72°C for 2 minutes. The primers used when amplifying PLSCR1 genomic DNA from WT and KO Huh-7.5 and A549+ACE2 cells were RU-O-32687 (5' AACATAGAGGTGATTATGATTTCGTCT) and RU-O-32526 (5' GGAGGAGCTTGGATTTCTATCTAC). PCR reactions were run on a 1% agarose gel to confirm amplification. Amplicons were purified with a Zymo DNA clean and concentrator kit (Zymo, cat. D4013) before sending to Genewiz for amplicon sequencing.

Western Blots

Cell pellets were collected and lysed in RIPA buffer (Thermo, catalog number 89900) with 1x Halt protease inhibitor cocktail and 1x EDTA (Thermo, catalog number 87786). Cell lysates were spun down in a refrigerated centrifuge at 15,000 g at 4°C for 15 minutes to pellet any cell debris, and the supernatant was collected and transferred to another tube. The collected samples were quantified by BCA assay (Thermo Scientific, cat. #23225). Before loading into the gel, we added sample buffer (Thermo, catalog number NP0007) with β-mercaptoethanol and heated the sample

763 at 95°C for 10 minutes. Samples were allowed to cool back to room temperature before loading
764 into 12% Bis-Tris 1.0 mm gels (Invitrogen, cat. #NP0321BOX). Proteins were electrophoretically
765 transferred onto nitrocellulose membranes. Membranes were blocked with 5% fat-free milk in 1X
766 TBS (Thermo, catalog number NP00061) and then incubated with primary antibody at 4°C
767 overnight in 5% fat-free milk in 1x TBS with 0.5% Tween-20 (TBST). Primary antibody: rabbit anti-
768 PLSCR1 polyclonal antibody (Proteintech, cat. #11582-1-AP) and mouse anti-β-actin antibody
769 (Millipore Sigma, cat. A5316-100UL) as a loading control. After incubation, membranes were
770 washed three times with 1x TBST and then incubated with fluorescently conjugated secondary
771 antibodies for 2 hours at room temperature. Secondary antibodies: LI-COR IRDye goat anti-rabbit
772 800 and goat anti-mouse 680 (LI-COR cat. 926-32211 and 926-68070, respectively). Membranes
773 were washed three times with 1X TBST, once with 1X TBS, then imaged on an Azure 600. For the
774 western blot in Supplementary Figure 4, this protocol was modified slightly: proteins were
775 electrophoretically transferred onto 0.22 µm polyvinylidene difluoride (PVDF) membranes,
776 incubated with a primary antibody solution of rabbit anti-PLSCR1 polyclonal antibody
777 (Proteintech, cat. #11582-1-AP) and polyclonal rabbit anti-RPS11 antibody (Abcam, cat.
778 ab157101), a secondary antibody solution of goat anti-rabbit HRP (Invitrogen, cat. 31462) and
779 visualized using a SuperSignal West Femto Maximum Sensitivity Substate kit (Thermo, cat.
780 #34096).
781

782 ## Cell viability assay

783 4,000 A549-ACE2 cells/well or 8,000 Huh-7.5 cells/well were seeded on day 0 in 100 µL
784 media (DMEM, 10% FBS, 1X NEAA, 1X Penicillin-Streptomycin) in a 96-well plate. The next day,
785 blasticidin selection was added as indicated in the figure to serve as a control for reduced cell
786 viability. On day 4, cell viability was assessed by resazurin assay (Abcam, cat. ab129732) according
787 to the manufacturer's protocol.
788

789 ## JAK-STAT inhibitor treatment

790 InSolution (Millipore, cat. 420097-500UG) was used according to the manufacturer's
791 instructions.

792

793 ## Titration of IFN-a2a in CHIKV-infected cells

794 6,000 Huh-7.5 cells/well were seeded in 100 µL media (DMEM, 10% FBS, 1X NEAA). The
795 following day, we treated cells with one of twelve concentrations of IFN-a2a (PBL, cat. 11101-2):
796 64 pM, 32 pM, 16 pM, 8 pM, 4 pM, 2 pM, 1 pM, 0.5 pM, 0.25 pM, 0.125 pM, 0.0625 pM, and 0
797 pM. The following day, the cells were infected with 2 µL of CHIKV-181/25-mKate2 (approximately
798 17,000 FFU per well, titer determined on Huh-7.5 cells) and fixed after 12 hours. Plates were
799 stained with a 1:1000 dilution of Hoechst for at least 10 minutes before washing with PBS and
800 imaging for mKate2 signal.

801

802 ## RT-qPCRs on ISGs

803 Huh-7.5 and A549-ACE2 cells were seeded at densities of 36,000 or 18,000 cells/well,
804 respectively, in 500 µL of media (DMEM, 10% FBS, 1X NEAA) in 24-well plates. The following day,
805 a dilution series of IFN-α2a (PBL, cat. 11101-2) or IFN-β (PBL, cat. #11415) was prepared (64 pM,
806 32 pM, 16 pM, 8 pM, 4 pM, 2 pM, 1 pM, 0.5 pM, 0.25 pM, 0.125 pM, 0.0625 pM, and 0 pM) and
807 50 µL of each dilution added to the cells in duplicate. After 24 hours, the media was removed and
808 the cells were washed with 1 mL of ice-cold PBS. 200 µL of RNA Lysis Buffer (Zymo Research, cat.
809 #R1060-1-100) was added to the cells, and the plates were frozen at -20°C before RNA isolation.
810 RNA was extracted using the Zymo Quick RNA 96-kit (Zymo Research, cat. R1052) including
811 DNaseI treatment, followed by cDNA synthesis using the SuperScript™ IV VILO™ Master Mix
812 (Invitrogen, cat. 11756050) according to manufacturers' instructions. qPCRs were conducted on
813 a QuantStudio 3 cycler using the Taqman Fast Advance master mix (Life Technologies Corporation,
814 cat. 4444965) and the following assays: *RPS11* (ThermoFisher 4331182; Hs01574200_gH), *IFI6*
815 (ThermoFisher 4331182; Hs00242571_m1), *OAS1* (ThermoFisher 4331182; Hs00973635_m1).
816 *IFI6* and *OAS1* were normalized to *RPS11* mRNA levels using the deltaCt method [179].

817

818 ## PLSCR1 subcellular localization

819 ### IF staining

820 A549-ACE2 cells were plated onto #1.5, 12mm glass coverslips (Fisher Scientific, cat.
821 #1254581) placed at the bottom of the wells of a 24-well plate. When confluent, the cells were
822 fixed, permeabilized with 1% Triton X-100 for 5 minutes and blocked for 1 hour at room
823 temperature with 1 mL of PBS-BGT (1x PBS with 0.5% bovine serum albumin, 0.1% glycine, 0.05%
824 Tween 20). Afterward, the cells were incubated in a 1:500 dilution of 4D2 mouse anti-PLSCR1
825 antibody (Millipore Sigma, cat. #MABS483) in PBS-BG (1x PBS with 0.5% bovine serum albumin
826 and 0.1% glycine) overnight at 4C with rocking. The cells were then washed twice with PBS-BGT
827 before incubation with a secondary antibody solution of 1:1000 anti-mouse 588 (ThermoFisher,
828 cat. #A-11001) and 1:1000 Hoechst dye (ThermoFisher, cat. #62249) in PBS-BG for two hours at
829 room temperature, followed by three washes with PBS-BGT.

830 ### Imaging

831 The coverslips were mounted onto slides (Fisher Scientific, cat. #1255015) with Invitrogen
832 ProLong Gold Antifade Mountant (Fisher Scientific, cat. # P36930). The slides were allowed to
833 cure for 24 hours before the edges of the coverslips were sealed, and the cells were imaged by
834 confocal microscopy. Confocal images were acquired using Zeiss Zen Blue (v3.5) software on a
835 LSM 980 point scanning confocal microscope (Zeiss) hooked to a Axio Observer.Z1 / 7 stand
836 equipped with C Plan-Apochromat 63X/1.40 oil (RI:1.518 at 23°C) objective lens (Zeiss). CW
837 excitation laser lines 405 nm and 488 nm were used to excite the fluorescence of DAPI and AF488
838 labeled samples. Emitted fluorescence were spectrally grated (410-483 nm for DAPI, 499-552 nm
839 for AF488) to avoid fluorescence bleed through and were detected in MA-PMT (DAPI), and GaAsP-
840 PMT (AF488). The confocal pinhole was set to 1AU for AF488, and the detector master gains were
841 set within the linear range of detection (550-750V). Scanned images were saved as .czi files.

842

843 ## Focus-forming assay on SARS-CoV-2-infected cells

844 In **Fig 6B**, Huh-7.5 and A549-ACE2 cells were cultured in media (DMEM with 5% FBS) and
845 seeded at densities of 2 x 10^5 and 1 x 10^5 cells per well, respectively, in collagen-coated 12-well
846 plates to reach 80-90% confluency by the day of infection. A 1:10 serial dilution of virus stock was

847 made in Opti-MEM in five separate tubes. Media was aspirated from the cells, and the wells were
848 washed with 1 ml of PBS before adding 200 µL of each virus dilution to the cells in triplicate. Plates
849 were incubated at 37°C with 5% CO2 for 1 hour, rocking every 15 minutes for even virus
850 distribution. A 1% methylcellulose overlay medium was prepared and mixed with complete
851 growth media at 37°C; 2 ml of this overlay was added to each well after removing the virus
852 inoculum. Plates were then incubated at 37°C with 5% CO2 for 48 for Huh-7.5 cells or 72 hours
853 for A549-ACE2 cells. Cells were then fixed in final 10% neutral buffered formalin and IF stained as
854 described in the Unbiased Arrayed CRISPR screen section. PLSCR1 KO and WT cells were
855 compared at similar virus dilutions.

856 In **Fig 7G**, the above protocol was followed to titer SARS-CoV-2 strains on Huh-7.5 PLSCR1
857 KO cells. Then, Huh-7.5 WT and KO cells were seeded at 2 x 10^5 cells per well in 1 mL of media
858 (DMEM, 10% FBS, 1X NEAA) in 12-well plates to reach 80-90% confluency the next day. Media
859 was aspirated from the cells, the wells were washed with 1mL of PBS, and then the cells were
860 infected with 50 FFU of SARS-CoV-2 (for each strain) diluted in 200 µL of Opti-MEM. Plates were
861 then incubated, overlayed with methylcellulose, fixed, and stained as described above.

862

863 ## Transfection with SARS-CoV-2 replicon system

864 The SARS-CoV-2 replicon and the method for electroporation has been described
865 previously [114]. Briefly, 6 x 10^6 Huh-7.5 WT and PLSCR1 KO cells were electroporated at 710 V
866 with 2 µg of SARS-CoV-2 N mRNA and 5 µg of replicon RNA. The cells rested for 10 minutes at
867 room temperature before resuspending to a concentration of 300,000 cells/mL and plating 100
868 µL of cells into each well of a 96-well plate. After 24 hours, supernatant was collected from the
869 replicon-transfected cells and assayed for *Renilla* luciferase activity according to kit instructions
870 (Promega, cat. E2810).

871

872 ## Infection with SARS-CoV-2 spike/VSV-G-pseudotyped, single-cycle, replication-defective
873 HIV-1 viruses.

874 ### Virus preparation

875 SARS-CoV-2 spike/VSV-G-pseudotyped, single-cycle, replication-defective HIV-1 viruses
876 (pCCNanoLuc/GFP) were prepared as in [115]. Plasmids were a kind gift of Theodora Hatziioannou
877 and Paul D. Bieniasz (The Rockefeller University, NY, USA) [115]. One day before the transfection,
878 4 x 10^6 293T cells were seeded in a 10 cm dish. One hour prior to transfection, the growth media
879 in the dish was replaced with 9 mL of fresh media containing 2% serum. A 1,000 µL transfection
880 mixture was prepared, comprising the diluent (a 150 mM NaCl solution prepared with sterile cell
881 culture water), 5 µg of HIV GP plasmid, 5 µg of pCLG plasmid, and either 2.5 µg of SARS-CoV-2
882 spike Δ19 or 1 µg of pHCMV.G plasmid, ensuring the total plasmid content did not exceed 12.5
883 µg. After brief vortexing, 50 µL of PEI (1 mg/mL, Polysciences cat. 23966) was added to achieve a
884 1:4 DNA/PEI ratio. The mixture was vortexed for 5 seconds and then allowed to sit for 20 minutes
885 in a hooded environment. Following gentle mixing by pipetting, 1 mL of the transfection mixture
886 was added to the 10 cm dish. Media was changed 12 hours post-transfection, and the supernatant
887 was harvested and filtered through a 0.2-micron filter 48 hours post-transfection, then stored at
888 -80°C.

889 ### Infection of PLSCR1 KO or WT cells

890 Seeded in 96-well plates, 6,000 A549+ACE2 cells per well were cultured in 100 µL of
891 media. After two days, either 10 µL of SARS-CoV-2 spike pseudotyped virus or 0.01 µL of VSV-G
892 pseudotyped virus were diluted in a final volume of 100 µL of media and added to the wells to
893 yield comparable NanoLuc signals. Plates were then spun at 200 g for 5 minutes and incubated at
894 37°C. Two days post-infection, the media was aspirated and replaced with 50 µL of NanoGlo
895 solution, sourced from the Promega Nano-Glo Luciferase Assay kit (Promega, N1110), with a
896 substrate to buffer ratio of 1:100. NanoLuc signal was subsequently quantified using a Fluostar
897 Omega plate reader.

898 ### Infection of siRNA-treated cells

899 Seeded in 96-well plates, 1,600 HEK293T, HEK293T-ACE2, or HEK293T-ACE2-TMPRSS2 cells
900 were cultured in 80 µL of media. The next day, a 20 µL transfection mixture made of Opti-MEM,

901 1% DharmaFECT1 (Horizon, T-2001-03), and 250 nM siRNA, PLSCR1 ON-TARGETplus SMARTpool
902 siRNA (Horizon, cat. L-003729-00-0005) or non-targeting control (Horizon, cat. D-001810-10-05)
903 was added to the cells. The final concentration of siRNAs was 25 nM. After two days, either 2 µL
904 of SARS-CoV-2 spike pseudotyped virus or 0.2 µL of VSV-G pseudotyped virus were diluted in a
905 final volume of 100 µL of media and added to the wells to yield comparable NanoLuc signals.
906 Plates were then span at 200 g for 5 minutes and incubated at 37°C. Two days after infection,
907 NanoLuc signal was quantified as described in the "Infection of PLSCR1 KO or WT cells" section.
908

909 ## Infection of siRNA-treated cells with SARS-CoV-2

910 Seeded in 96-well plates, 1,000 A549, A549-ACE2, or A549-ACE2-TMPRSS2 cells were
911 cultured in 80 µL of media. On the same day, a 20 µL transfection mixture made of Opti-MEM, 1%
912 DharmaFECT1 (Horizon, T-2001-03), and 250 nM siRNA, PLSCR1 ON-TARGETplus SMARTpool
913 siRNA (Horizon, cat. L-003729-00-0005) or non-targeting control (Horizon, cat. D-001810-10-05)
914 was added to the cells. The final concentration of siRNAs was 25 nM. Three days after
915 transfection, the cells were infected by adding 34,000 PFU of SARS-CoV-2 (titer determined on
916 Vero E6 cells) diluted in 10 µL media to each well. Plates were then spun at 200 g for 5 minutes
917 and incubated at 37°C. Staining and readout as described above in the "Unbiased arrayed CRISPR
918 KO screening" section.
919

920 ## Pan-virus infection of PLSCR1 KO cells

921 A549-ACE2 cells were seeded at a density of 6,000 cells/well in 96-well plates in 90 µL
922 media. The following day, 10 µL diluted virus was added to each well. Virus concentrations as
923 follow: CHIKV-mKate, 0.05 µL virus stock per well (titer 8.5 x 10^6 PFU/mL determined in Huh-7.5
924 cells); hCoV-NL63, 10 µL virus stock per well (titer 1.4 x 10^5 PFU/mL); hCoV-OC43, 10 µL virus stock
925 per well (titer 1.06 x 10^7 PFU/mL); hPIV-GFP, 0.05 µL virus stock per well; HSV1-GFP, 0.5 µL virus
926 stock per well (titer 2.4 x 10^8 PFU/mL determined on Vero E6 cells); IAV WSN, 0.5 µL virus stock
927 per well; SARS-CoV-2, 0.5 µL virus stock per well (titer 3.4 x 10^6 PFU/mL determined on Vero E6
928 cells); SINV-Toto1101-mScarletI, 10 µL virus stock per well; VEEV-EGFP, 0.005 µL virus stock per
929 well (titer 1.45 x 10^9 PFU/mL determined on BHK-21); VSV-GFP, 0.05 µL virus stock per well;

930 YFV_17D, 5 µL virus stock per well. The cells were fixed, stained and imaged as described in the
931 *Unbiased arrayed CRISPR KO screen* section. Fluorescent viruses were not stained: the fluorescent
932 signal was used as a reporter. We used the following primary antibodies when applicable: anti-
933 dsRNA (J2) mouse (Nordic MUbio, cat. 10010200) diluted 1:500 was used for hCoV-NL63 and
934 hCoV-OC43, anti-IAV mouse (Millipore, cat. MAB8257) diluted 1:3000, anti-YFV mouse (Santa
935 Cruz Biotechnology, cat# sc-58083) diluted 1:500, anti-SARS2-S rabbit (Genetex, cat. GTX135357)
936 diluted 1:3000.

937 Huh-7.5 cells were transfected with a 1:200 dilution of Dharmafect 4 (Horizon, cat. T-2004-
938 01) and 25 nM ON-TARGETplus SMARTpool siRNAs (Horizon Discovery) in 96-well plates. The cells
939 were infected three days after siRNA transfection with hCoV-NL63 or hCoV-OC43 or four days
940 after siRNA transfection with SARS-CoV-2 or hCoV-229E. IF and imaging as described above.

941

942 Reconstitution of WT and mutant PLSCR1

943 Plasmid cloning

944 N-terminal 3x FLAG-tagged PLSCR1, C-terminal 3x FLAG-tagged PLSCR1, and PLSCR1
945 H262Y were generated by designing and ordering large dsDNA gene blocks of PLSCR1 that
946 contained the desired mutations from IDT. These gene blocks were cloned into the PLSCR1-
947 SCRPSY vector [180] and confirmed by sequencing (see Supplementary Table 12 for sequences).

948 Lentivirus production

949 Lentivirus were generated in Lenti-X 293T cells by transfecting 200 ng VSV-G plasmid, 700
950 ng Gag-Pol plasmid, and 1100 ng plasmid of interest with lipofectamine 2000 in DMEM
951 supplemented with 5% FBS. Media was changed 4-6 hours later, and lentivirus harvested at 24
952 and 48 hours. Lentivirus from both timepoints was pooled, then filtered through a 0.45 µM filter
953 before aliquoting into 2 mL tubes and freezing at -80°C until use.

954 Cell transduction

955 0.3 million cells were transduced in suspension in a 12-well plate. Cells received 8 µg/mL
956 polybrene and 80 mM Hepes in addition to the lentivirus. Cells were then spinoculated at 37°C
957 for 1 hour at 1000 x g. The following day, cells were split into two, 6-well plates, then 24 hours
958 later one of the duplicates was treated with 2 µg/mL puromycin (when using SCRPSY-based

959 lentiviruses) to select for transduced cells. Further experiments were carried out using the cells
960 that had approximately 30% transduction before selection.

961 ### SARS-CoV-2 infection

962 In **Fig 8B**, Huh-7.5 and A549+ACE2 cells were plated at 6,000 cells/well and 3,000
963 cells/well, respectively, in 100 µL of media (DMEM, 10% FBS, 1X NEAA) in 96-well plates. The
964 following day, cells were treated with IFN (10pM for Huh-7.5 cells and 20pM for A549+ACE2 cells).
965 On the third day, the Huh-7.5 cells were infected with 0.1 µL of virus per well and the A549+ACE2
966 cells with 1 µL of virus per well, then spun at 200 g for 5 minutes and incubated at 37°C. Plates
967 were harvested the next day by fixing and staining as described above. For Figure 7A-E, Huh-7.5
968 cells were plated at 7,500 cells/well in 100µL of media (DMEM, 10% FBS, 1X NEAA) in 96-well
969 plates. The next day, cells were infected with quantities of virus that yielded comparable percent
970 infections in the WT cells, then spun at 200 g for 5 minutes and incubated at 33°C. The quantities
971 of virus used were as follows: 0.1 µL/well for parental, 0.05 µL/well for beta, 1 µL/well for delta,
972 0.5 µL/well for omicron, and 0.05 µL/well for kraken. The infected cells were fixed after 24 hours
973 and stained as described previously.

974 ### IF staining and imaging

975 In **Fig 8B**, cells were stained for IF as described in the *Unbiased arrayed CRISPR KO*
976 *screening* section, with different primary and secondary antibody solutions. The primary antibody
977 solution was a 1:3000 dilution of rabbit anti-SARS-CoV-2 nucleocapsid polyclonal antibody
978 (Genetex, cat. #GTX135357) in PBS-BGT, and the secondary antibody solution was 1:1000 goat
979 anti-rabbit 594 (ThermoFisher, cat. #A-11012) or 1:1000 goat anti-rabbit 647 (ThermoFisher, cat.
980 #A-21245), and 1:1000 Hoechst dye (ThermoFisher, cat. #62249) in PBS-BGT.

981

982 ## SARS-CoV-2 infection of human SV40-fibroblasts-ACE2

983 ### Generation of human SV40-fibroblasts ACE2 stable cell lines

984 *ACE2* cDNA was inserted with In-Fusion cloning kit (Takara Bio) and using the XhoI and
985 BamHI restriction sites into linearized pTRIP-SFFV-CD271-P2A in accordance with the
986 manufacturers' instructions. We checked the entire sequence of the *ACE2* cDNA in the plasmid
987 by Sanger sequencing. Then, HEK293T cells were dispensed into a six-well plate at a density of

988 8 x10^5 cells per well. On the next day, cells were transfected with pCMV-VSV-G (0.2 µg), pHXB2-
989 env (0.2 µg; NIH-AIDS Reagent Program; 1069), psPAX2 (1 µg; Addgene plasmid no. 12260) and
990 pTRIP-SFFV-CD271-P2A-ACE2 (1.6 µg) in Opti-MEM (Gibco; 300 µL) containing X-tremeGene-9
991 (Sigma Aldrich; 10 µL) according to the manufacturers' protocol. After transfection for 6 h, the
992 medium was replaced with 3 mL fresh culture medium, and the cells were incubated for a further
993 24 h for the production of lentiviral particles. The viral supernatant was collected and passed
994 through a syringe filter with 0.2 µm pores (Pall) to remove debris. Protamine sulfate (Sigma;
995 10 µg/mL) was added to the supernatant, which was then used immediately or stored at −80 °C
996 until use.

997 For the transduction of SV40-fibroblasts with ACE2, 5 x10^5 cells per well were seeded in
998 six-well plates. Viral supernatant was added (500 µL per well). The cells were then further
999 incubated for 48 h at 37 °C. Cells were keep in culture and after 8 days, transduction efficiency
1000 was evaluated by CD271 surface staining with CD271 AlexaFluor 647, 1:200 dilution (BD
1001 Pharmigen 560326). MACS-sorting was performed with CD271 positive selection beads (Miltenyi
1002 Biotec) if the proportion of CD271-positive cells was below 80% [7, 163].

1003 ### Infection

1004 5,000 cells per well were seeded in a 96-well plate and infected the next day with SARS-
1005 CoV-2 at MOI = 0.05, using a titer determined on Vero E6 cells. Cells were fixed at 2 dpi, stained
1006 and imaged as described in the *Unbiased arrayed CRISPR KO screen* section.

1007

1008 Acknowledgments

1009 We thank Georgia McClain for reading and editing this manuscript. We thank the staff at
1010 the Laboratory of Virology and Infectious Disease: Ellen Castillo, Michela De Santis, Arnella Norris,
1011 Aileen O'Connell, Santa Maria Pecoraro Di Vittorio, Glen Santiago, and Sonia Shirley. Ching-Wen
1012 Chang and Lihong Liu (Columbia University, NY, USA), and Theodora Hatziioannou and Paul D.
1013 Bieniasz (The Rockefeller University, NY, USA) generously provided plasmids and instructions to
1014 generate SARS-CoV-2 spike-pseudotyped, single-cycle, replication-defective HIV-1 viruses [115].
1015 Oded Danziger and Brad R. Rosenberg (Department of Microbiology at the Icahn School of

1016 Medicine at Mount Sinai, NY, USA) kindly provided the A549-ACE2 cells [10] used in this study.
1017 FACS was conducted at the Flow Cytometry Resource Center at Rockefeller University. mRNA-seq
1018 was performed by the Genomics Resource Center at The Rockefeller University and by Novogene.
1019 Confocal microscopy was performed in the Rockefeller University's Bio-Imaging Resource Center,
1020 RRID:SCR_017791. We thank Ankit Patel, Sales Manager at Horizon Discovery.

1021 Trim Galore was developed at The Babraham Institute by @FelixKrueger, now part of Altos
1022 Labs. The Genotype-Tissue Expression (GTEx) Project [35] was supported by the Common Fund of
1023 the Office of the Director of the National Institutes of Health, and by NCI, NHGRI, NHLBI, NIDA,
1024 NIMH, and NINDS. The data used for the analyses described in this manuscript were obtained
1025 from the EMBL-European Bioinformatics Institute portal,
1026 "https://www.ebi.ac.uk/gxa/experiments/E-MTAB-5214/Results", on October 1st, 2020.

1027 Work in the Laboratory of Virology and Infectious Disease was supported by NIH grants
1028 P01AI138398-S1, 2U19AI111825, R01AI091707-10S1, and R01AI161444; a George Mason
1029 University Fast Grant; the G. Harold and Leila Y. Mathers Charitable Foundation; the Meyer
1030 Foundation; the Pilot Project Robertson Therapeutic Development Fund at The Rockefeller
1031 University; and the Bawd Foundation. J.L.P. was supported by the Francois Wallace Monahan
1032 Postdoctoral Fellowship at The Rockefeller University and the European Molecular Biology
1033 Organization Long-Term Fellowship (ALTF 380-2018). G.P. was supported by the James H. Gilliam
1034 Fellowship for Advanced Study from the Howard Hughes Medical Institute and the Graduate
1035 Research Fellowship Program from the National Science Foundation (FAIN 1946429). M.B. was
1036 supported by a Swiss National Science Foundation fellowship (P500PB_203007).

1037 Data and code availability

1038 To be determined.

1039

1040 Tables

1041 Table 1. PLSCR1 variants associated with severe COVID-19 in a GWAS [23, 24]

1042

GWAS p-value	rsID	Genomic Coordinate (GRCh38)	Nucleotide Change	Gene	Functional Consequence
7.52E-07	rs116553931	chr3:146430956	C:T	PLSCR2	intron variant
1.08E-07	rs454645	chr3:146514682	C:T	PLSCR1	Downstream transcript variant
5.43E-08	rs343320	chr3:146517122	G:A	PLSCR1	His262Tyr
8.21E-08	rs343318	chr3:146518204	T:C	PLSCR1	intron variant
1.52E-07	rs343317	chr3:146518374	A:G	PLSCR1	intron variant
1.00E-07	rs186910	chr3:146520241	A:G	PLSCR1	intron variant
1.13E-07	rs173150	chr3:146520256	A:T	PLSCR1	intron variant
1.35E-07	rs71302408	chr3:146520389	T:C	PLSCR1	intron variant
7.06E-08	rs343316	chr3:146521151	A:G	PLSCR1	intron variant
4.64E-08	rs343314	chr3:146522652	C:T	PLSCR1	intron variant
7.46E-08	rs343312	chr3:146522970	G:A	PLSCR1	intron variant

Figure Legends

Figure 1. Known ISGs restricting SARS-CoV-2 entry.

A schematic of SARS-CoV-2 entry and the sites where known ISG entry restriction factors function is shown. CD74 suppresses endolysosomal cathepsins, enzymes that process certain viral glycoproteins to make them fusion-competent [181, 182]. CH25H facilitates the sequestration of accessible cholesterol, which results in decreased virus-cell membrane fusion and viral entry [13, 59]. NCOA7 accelerates the acidification of the lysosome, leading to the degradation of viral antigens [116, 183]. LY6E and PLSCR1 restrict virus-cell membrane fusion at the endosome through unknown mechanisms, see [18, 157] and this study.

1053

1054 Figure 2. Unbiased arrayed CRISPR KO screens reveal IFN-dependent and independent
1055 genes influencing SARS-CoV-2 infection.

1056 A. mRNA-seq comparison between Huh-7.5 and Calu-3 cells, focusing on a subset of 224
1057 ISGs, in response to 24 h SARS-CoV-2 infection MOI 0.03. Red diamond, PLSCR1 RNA level.
1058 Viral RNA levels were comparable in both cell lines (not shown). ****, p<0.0001; two-
1059 tailed t-test.

1060 B. Cells were treated with 0.5 nM IFN-α2a for 24 h. mRNA-seq analysis as in **(A)**.

1061 C. Huh-7.5-Cas9 cells were pretreated with different amounts of IFN-α2a, then infected with
1062 SARS-CoV-2 for 24 h followed by IF staining for SARS-CoV-2 N protein; n = 6; error bars
1063 represent SEM. ****, p<0.0001; two-tailed t-test.

1064 D. Diagram of the arrayed CRISPR KO screen method.

1065 E. The virus level (percentage infected cells was determined by IF staining, then normalized
1066 and z-score was calculated) is plotted for 24 h 0 pM (y axis) or 1 pM (x axis) IFN-α2a
1067 pretreatment followed by 24 h infection (n ≥ 5). The genes were categorized as ISG or
1068 other based on mRNA-seq of IFN-α2a-treated cells as in **(B)**. ISGs were defined by a fold
1069 change ≥ 2 and padj ≤ 0.05 in the IFN-treatment versus untreated pairwise comparison.

1070 F. Gene set enrichment analysis conducted on the arrayed CRISPR KO screens data
1071 represented in **(E)**. Description of the top pathways ranked by p-value for each quadrant.
1072 Databases: [1]Reactome; [2]WikiPathways; [3]Pathway Interaction Database; [4]KEGG; [5]Biocarta.

1073

1074 Figure 3. Human genes significant in human genetics studies on COVID-19 patients and in
1075 functional genetic screens in cell culture

1076

1077 Figure 4. PLSCR1 is a highly effective anti-SARS-CoV-2 effector ISG contributing to intrinsic
1078 immunity in the absence of IFN.

1079 A. Cells were pretreated with a JAK-STAT inhibitor (InSolution 1 μM) for 2 h, followed by IFN-
1080 α2a (10 pM Huh-7.5 or 20 μM A549-ACE2) for 24 h and were infected with SARS-CoV-2 for
1081 24 h followed by IF staining for viral N protein. Huh-7.5 infection using an MOI of 0.5 (titer

1082 determined by focus forming assay on Huh-7.5 WT cells). A549-ACE2 infection using an
1083 MOI of 0.01 (titer determined by focus forming assay on A549-ACE2 WT cells). The
1084 percentage of SARS-CoV-2 positive cells is plotted.
1085 B. Cells were reconstituted with the indicated proteins by stable transduction with
1086 lentiviruses, then infected as in **(A)**.
1087 C. Cells were co-cultured as indicated (50:50 mix), then infected as in **(A)** and the % infection
1088 of each cell type was determined. n = 6; error bars represent sd. ****, p<0.0001; two-
1089 tailed t-test.
1090

1091 ## Figure 5. PLSCR1 is not important for IFN signaling.

1092 A. Huh-7.5 WT and PLSCR1 KO cells were infected with 17,000 FFU of CHIKV 181/25 mKate2
1093 for 12 or 24 hours, then fixed, IF stained for nuclei, and the percentage of positive cells
1094 determined by imaging for mKate2 reporter signal. n = 12 independent infections
1095 (separate wells). Error bars represent sd. ns, non-significant; two-way ANOVA.
1096 B. Huh-7.5 cells, PLSCR1 KO as indicated, were pretreated with different amounts of IFN-
1097 α2a, then infected with 17,000 FFU of CHIKV-mKate for 12 h; n = 7; error bars represent
1098 sd.
1099 C-J. Cells were treated for 24 h by IFN, as indicated, followed by RT-qPCRs on ISGs.
1100

1101 ## Figure 6. PLSCR1 restricts spike-mediated SARS-CoV-2 entry.

1102 A. A549-ACE2 cells were IF stained using an anti-PLSCR1 antibody (white) and Hoechst
1103 33342 nuclear staining (blue) and imaged at 63X magnification on a confocal microscope.
1104 B. Focus forming assays: SARS-CoV-2 N IF (red) and Hoechst 33342 nuclear staining (blue)
1105 on similarly infected WT or PLSCR1 KO Huh-7.5 and A549-ACE2 cells after 2 and 3 d,
1106 respectively.
1107 C. Quantification of **(B)**.
1108 D. Huh-7.5 WT and PLSCR1 KO cells electroporated with SARS-CoV-2 replicon which
1109 produces a secreted luciferase. Luciferase activity assayed 24 hours after electroporation.

1110 n = 36 (separate wells from single electroporation). Error bars represent sd. Ns = non-
1111 significant; two-tailed t-test.
1112 E-F. Transduction of A549-ACE2 cells with an HIV-based replicon expressing the
1113 nanoluciferase pseudotyped with VSV-G or SARS-CoV-2 spike, respectively. n = 5
1114 independent infection (separate wells). Nanoluciferase signal measured 2 dpi. Error bars
1115 represent sd. ns, non-significant, **, p<0.01; two-tailed t-test.
1116 G-I. A549 cells WT, expressing ACE2, or expressing ACE2-TMPRSS2 as indicated were
1117 transfected with PLSCR1 or non-template control (NTC) siRNAs as indicated for 3 d and
1118 infected with SARS-CoV-2 for 1 d. SARS-CoV-2 N was stained by IF and the percentage of
1119 positive cells was determined by imaging. n = 6 independent infection (separate wells).
1120 Error bars represent sd. ns, non-significant, **, p<0.01, ***, p<0.001; two-tailed t-test.
1121 J-M. HEK293T cells expressing ACE2 or ACE2-TMPRSS2, as indicated, were transfected with
1122 siRNA knockdown of PLSCR1 or non-template control (NTC), as indicated, for 3 d and
1123 transduced with an HIV-based replicon expressing the nanoluciferase pseudotyped with
1124 VSV-G or SARS-CoV-2 spike, as indicated for 2 d. n = 3 independent infection (separate
1125 wells). Error bars represent sd. ns, non-significant, **, p<0.01; two-tailed t-test.
1126

1127 ## Figure 7. Newer variants of SARS-CoV-2 are less restricted by PLSCR1

1128 A-E. Infection of Huh-7.5 cells with SARS-CoV-2 (parental) or its descendant variants, Beta,
1129 Delta, Omicron, and Kraken for 24 hours. SARS-CoV-2 N was stained by IF and the
1130 percentage of positive cells determined by imaging. n = 10 independent infection
1131 (separate wells). Error bars represent sd. ****, p < 0.0001; two-tailed t-test.
1132 F. Ratio of WT/KO percent infection from A-E. Error bars represent sd. ns, non-significant.
1133 ***, p<0.001, ****, p<0.0001; one-way ANOVA.
1134 G. Huh-7.5 WT and PLSCR1 KO cells were infected with 50 FFU of virus as titered on PLSCR1
1135 KO cells in a focus-forming assay. Plaques were counted, and then a ratio of WT-to-KO
1136 plotted for each SARS-CoV-2 variant. n = 6 independent infection (separate wells). Error
1137 bars represent sd. **, p<0.01; one-way ANOVA.
1138

1139 Figure 8. PLSCR1 His262Tyr, which associates with severe COVID-19, leads to higher SARS-
1140 CoV-2 infection in cell culture.

1141 A. Protein diagram of PLSCR1. Domain coordinates from UniProt.
1142 B. Huh-7.5 cells, WT and PLSCR1 KO, stably expressing N-terminal FLAG-tagged Firefly
1143 Luciferase (Fluc), N-terminal FLAG-tagged PLSCR1, or N-terminal FLAG-tagged PLSCR1
1144 H262Y mutant and infected with SARS-CoV-2 for 24 hours. SARS-CoV-2 N was stained by
1145 IF and the percentage of positive cells determined by imaging. n = 15 independent
1146 infection (separate wells). Error bars represent sd. ****, p<0.0001; two-tailed t-test.
1147 C. SV40-Fibroblast-ACE2 cells, genotype as indicated, infected for two days with SARS-CoV-
1148 2. N = eight independent infection in separate wells. ns, non-significant, **, p<0.01, ***,
1149 p<0.001; two-tailed t-test.

1150 # Supplementary Figure Legends

1151 ## Supplementary Figure 1.

1152 A. Nuclei count (z-score) in arrayed genetic screen. Examples of VCP (essential gene) and
1153 PLSCR1 (SARS-CoV-2 antiviral hit) are plotted.
1154 B. Volcano plot of Huh-7.5 cells mRNA-seq treated with 0.5 nM IFN-α2a for 24 h as in **Fig 2B**.
1155

1156 ## Supplementary Figure 2

1157 A. Occurrence of human genes interacting with SARS-CoV-2 drawn from a selection of 67
1158 large-scale studies. The occurrence reflects the number of independent studies finding
1159 each gene as significant.
1160 B. Upset plot on data as in **(A)**, showing the overlap in significant genes in large-scale SARS-
1161 CoV-2 studies by category.
1162

1163 ## Supplementary Figure 3.

1164 A. Western blot on PLSCR1 KO cells against PLSCR1 (green) and ß-actin (red).

1165 B. Cells as indicated were seeded at similar density, treated or not with Blasticidin (used here
1166 as a control to decrease cell viability), and cultured for 4 days before resazurin cell viability
1167 assay. n = 4 independent wells.
1168 C. Western blot on PLSCR1 WT and KO A549-ACE2 cells against PLSCR1 (green) and ß-actin
1169 (red).
1170

1171 ## Supplementary Figure 4.

1172 A. Western blot against PLSCR1 and RPS11. Cas-9-expressing Huh-7.5 cells were transfected
1173 with 4-gRNA pools targeting PLSCR1 or non-template control (as indicated) and cells were
1174 in culture for 7 d.
1175 B. Quantification of bands intensity in **(A)**.
1176 C. mRNA-seq on cells as in **(B)**.
1177

1178 ## Supplementary Figure 5.

1179 A-I. Infection of A549-ACE2 cells with viruses as indicated. IF staining was used for IAV WSN,
1180 hCoV-OC43 and SARS-CoV-2, otherwise a fluorescent reporter was used. Percentage of
1181 virus positive cells was determined by imaging. N = six replicates (independent
1182 infections in separate wells), error bars represent SD.
1183 J-M. Infection of Huh-7.5 cells with viruses as indicated. siRNA knockdown of PLSCR1 vs non-
1184 template control (NTC). ****, $p<0.0001$; ns, non-significant; two-tailed t-test.
1185

1186 ## Supplementary Figure 6.

1187 Western Blot against PLSCR1 and β-actin (loading control). Huh-7.5 PLSCR1 KO cells were stably
1188 transduced with FLAG-tagged Fluc, FLAG-tagged PLSCR1, or FLAG-tagged PLSCR1 H262Y.
1189

1190 ## Supplementary Figure 7.

1191 Comparison between selected SARS-CoV-2 protein interactome studies [96-98, 100-105, 148].
1192

1193 ### Supplementary Figure 8.

1194 Comparison between the relative mRNA levels of 97 hallmark IFN-α-stimulated genes and the
1195 remaining transcriptome in cell lines as indicated. Red diamond, *PLSCR1* RNA level. For Huh-7.5
1196 cells mRNA-seq, cells treated with 0.5 nM IFN-α2a for 24 h as in **Fig 2B**. For primary human
1197 hepatocytes, cells were treated with 0.1 nM IFN-α2a for 24 h (full data and methods to be
1198 released elsewhere). For the human tissues, data from [35].

1199

1200 ## Supplementary Material

1201 ### Supplementary Table 1.

1202 mRNA-seq on SARS-CoV-2 infected cells, Normalized reads, related to **Fig 2A**.

1203

1204 ### Supplementary Table 2.

1205 mRNA-seq on SARS-CoV-2 infected cells, Differential Gene Expression.

1206

1207 ### Supplementary Table 3.

1208 mRNA-seq on IFN treated cells, Normalized reads, related to **Fig 2B**, and **Supp Fig 8.**

1209

1210 ### Supplementary Table 4.

1211 mRNA-seq on IFN treated cells, Differential Gene Expression, related to **Fig 2E** and **Supp Fig 1B**.

1212

1213 ### Supplementary Table 5.

1214 Arrayed CRISPR KO screen, raw data.

1215

1216 ### Supplementary Table 6.

1217 Arrayed CRISPR KO screen, analyzed data. Related to **Fig. 2E** and **Supp Fig 1A**.

1218

1219 Supplementary Table 7.

1220 Arrayed CRISPR KO screen, summary table.

1221

1222 Supplementary Table 8.

1223 GSEA on arrayed CRISPR KO screen. Related to **Fig. 2F**.

1224

1225 Supplementary Table 9.

1226 Consolidated list of human genes classified as hits in selected SARS-CoV-2 studies, full table.
1227 Related to **Fig 3** and **Supp Fig 2.**

1228

1229 Supplementary Table 10.

1230 Consolidated list of human genes classified as hits in selected SARS-CoV-2 studies, summary table.
1231 Related to **Fig 3** and **Supp Fig 2.**

1232

1233 Supplementary Table 11.

1234 Plasmids used in this study.

1235

1236 Supplementary Table 12.

1237 Gene fragments used in this study.

1238

1239 Supplementary Table 13.

1240 Primers used in this study.

1241

1242 References

1243 1. Bastard P, Zhang Q, Zhang SY, Jouanguy E, Casanova JL. Type I interferons and SARS-CoV-
1244 2: from cells to organisms. Curr Opin Immunol. 2022;74:172-82. Epub 20220125. doi:

1245 10.1016/j.coi.2022.01.003. PubMed PMID: 35149239; PubMed Central PMCID:
1246 PMCPMC8786610.
1247 2. Bastard P, Gervais A, Le Voyer T, Rosain J, Philippot Q, Manry J, et al. Autoantibodies
1248 neutralizing type I IFNs are present in ~4% of uninfected individuals over 70 years old and
1249 account for ~20% of COVID-19 deaths. Sci Immunol. 2021;6(62). Epub 2021/08/21. doi:
1250 10.1126/sciimmunol.abl4340. PubMed PMID: 34413139.
1251 3. Lopez J, Mommert M, Mouton W, Pizzorno A, Brengel-Pesce K, Mezidi M, et al. Early
1252 nasal type I IFN immunity against SARS-CoV-2 is compromised in patients with autoantibodies
1253 against type I IFNs. J Exp Med. 2021;218(10). Epub 20210806. doi: 10.1084/jem.20211211.
1254 PubMed PMID: 34357402; PubMed Central PMCID: PMCPMC8352718.
1255 4. Asano T, Boisson B, Onodi F, Matuozzo D, Moncada-Velez M, Maglorius Renkilaraj MRL,
1256 et al. X-linked recessive TLR7 deficiency in ~1% of men under 60 years old with life-threatening
1257 COVID-19. Sci Immunol. 2021;6(62). doi: 10.1126/sciimmunol.abl4348. PubMed PMID:
1258 34413140; PubMed Central PMCID: PMCPMC8532080.
1259 5. Zhang Q, Bastard P, Liu Z, Le Pen J, Moncada-Velez M, Chen J, et al. Inborn errors of type
1260 I IFN immunity in patients with life-threatening COVID-19. Science. 2020;370(6515). Epub
1261 20200924. doi: 10.1126/science.abd4570. PubMed PMID: 32972995; PubMed Central PMCID:
1262 PMCPMC7857407.
1263 6. Bastard P, Rosen LB, Zhang Q, Michailidis E, Hoffmann HH, Zhang Y, et al. Autoantibodies
1264 against type I IFNs in patients with life-threatening COVID-19. Science. 2020;370(6515). Epub
1265 20200924. doi: 10.1126/science.abd4585. PubMed PMID: 32972996; PubMed Central PMCID:
1266 PMCPMC7857397.
1267 7. Zhang Q, Matuozzo D, Le Pen J, Lee D, Moens L, Asano T, et al. Recessive inborn errors of
1268 type I IFN immunity in children with COVID-19 pneumonia. J Exp Med. 2022;219(8). Epub
1269 20220616. doi: 10.1084/jem.20220131. PubMed PMID: 35708626; PubMed Central PMCID:
1270 PMCPMC9206114.
1271 8. Zhou P, Yang XL, Wang XG, Hu B, Zhang L, Zhang W, et al. A pneumonia outbreak
1272 associated with a new coronavirus of probable bat origin. Nature. 2020;579(7798):270-3. Epub

1273 20200203. doi: 10.1038/s41586-020-2012-7. PubMed PMID: 32015507; PubMed Central
1274 PMCID: PMCPMC7095418.
1275 9. Savan R, Gale M, Jr. Innate immunity and interferon in SARS-CoV-2 infection outcome.
1276 Immunity. 2023;56(7):1443-50. doi: 10.1016/j.immuni.2023.06.018. PubMed PMID: 37437537;
1277 PubMed Central PMCID: PMCPMC10361255.
1278 10. Danziger O, Patel RS, DeGrace EJ, Rosen MR, Rosenberg BR. Inducible CRISPR activation
1279 screen for interferon-stimulated genes identifies OAS1 as a SARS-CoV-2 restriction factor. PLoS
1280 Pathog. 2022;18(4):e1010464. Epub 20220414. doi: 10.1371/journal.ppat.1010464. PubMed
1281 PMID: 35421191; PubMed Central PMCID: PMCPMC9041830.
1282 11. Martin-Sancho L, Lewinski MK, Pache L, Stoneham CA, Yin X, Becker ME, et al. Functional
1283 landscape of SARS-CoV-2 cellular restriction. Mol Cell. 2021;81(12):2656-68 e8. Epub 20210413.
1284 doi: 10.1016/j.molcel.2021.04.008. PubMed PMID: 33930332; PubMed Central PMCID:
1285 PMCPMC8043580.
1286 12. Wickenhagen A, Sugrue E, Lytras S, Kuchi S, Noerenberg M, Turnbull ML, et al. A
1287 prenylated dsRNA sensor protects against severe COVID-19. Science. 2021;374(6567):eabj3624.
1288 Epub 20211029. doi: 10.1126/science.abj3624. PubMed PMID: 34581622.
1289 13. Zang R, Case JB, Yutuc E, Ma X, Shen S, Gomez Castro MF, et al. Cholesterol 25-
1290 hydroxylase suppresses SARS-CoV-2 replication by blocking membrane fusion. Proc Natl Acad Sci
1291 U S A. 2020;117(50):32105-13. Epub 20201125. doi: 10.1073/pnas.2012197117. PubMed PMID:
1292 33239446; PubMed Central PMCID: PMCPMC7749331.
1293 14. Kaur R, Tada T, Landau NR. Restriction of SARS-CoV-2 replication by receptor transporter
1294 protein 4 (RTP4). mBio. 2023;14(4):e0109023. Epub 20230629. doi: 10.1128/mbio.01090-23.
1295 PubMed PMID: 37382452; PubMed Central PMCID: PMCPMC10470548.
1296 15. Schoggins JW, Wilson SJ, Panis M, Murphy MY, Jones CT, Bieniasz P, et al. A diverse range
1297 of gene products are effectors of the type I interferon antiviral response. Nature.
1298 2011;472(7344):481-5. Epub 20110410. doi: 10.1038/nature09907. PubMed PMID: 21478870;
1299 PubMed Central PMCID: PMCPMC3409588.

1300 16. Schoggins JW. Interferon-Stimulated Genes: What Do They All Do? Annu Rev Virol.
1301 2019;6(1):567-84. Epub 2019/07/10. doi: 10.1146/annurev-virology-092818-015756. PubMed
1302 PMID: 31283436.
1303 17. Mac Kain A, Maarifi G, Aicher SM, Arhel N, Baidaliuk A, Munier S, et al. Identification of
1304 DAXX as a restriction factor of SARS-CoV-2 through a CRISPR/Cas9 screen. Nat Commun.
1305 2022;13(1):2442. Epub 20220504. doi: 10.1038/s41467-022-30134-9. PubMed PMID:
1306 35508460; PubMed Central PMCID: PMCPMC9068693.
1307 18. Xu D, Jiang W, Wu L, Gaudet RG, Park ES, Su M, et al. PLSCR1 is a cell-autonomous
1308 defence factor against SARS-CoV-2 infection. Nature. 2023;619(7971):819-27. Epub 20230712.
1309 doi: 10.1038/s41586-023-06322-y. PubMed PMID: 37438530; PubMed Central PMCID:
1310 PMCPMC10371867.
1311 19. Kim HS, Lee K, Kim SJ, Cho S, Shin HJ, Kim C, et al. Arrayed CRISPR screen with image-
1312 based assay reliably uncovers host genes required for coxsackievirus infection. Genome Res.
1313 2018;28(6):859-68. Epub 20180430. doi: 10.1101/gr.230250.117. PubMed PMID: 29712754;
1314 PubMed Central PMCID: PMCPMC5991512.
1315 20. Kodigepalli KM, Bowers K, Sharp A, Nanjundan M. Roles and regulation of phospholipid
1316 scramblases. FEBS Lett. 2015;589(1):3-14. Epub 20141203. doi: 10.1016/j.febslet.2014.11.036.
1317 PubMed PMID: 25479087.
1318 21. Zhou Q, Zhao J, Stout JG, Luhm RA, Wiedmer T, Sims PJ. Molecular cloning of human
1319 plasma membrane phospholipid scramblase. A protein mediating transbilayer movement of
1320 plasma membrane phospholipids. J Biol Chem. 1997;272(29):18240-4. doi:
1321 10.1074/jbc.272.29.18240. PubMed PMID: 9218461.
1322 22. Dong B, Zhou Q, Zhao J, Zhou A, Harty RN, Bose S, et al. Phospholipid scramblase 1
1323 potentiates the antiviral activity of interferon. J Virol. 2004;78(17):8983-93. doi:
1324 10.1128/JVI.78.17.8983-8993.2004. PubMed PMID: 15308695; PubMed Central PMCID:
1325 PMCPMC506946.
1326 23. Pairo-Castineira E, Rawlik K, Bretherick AD, Qi T, Wu Y, Nassiri I, et al. GWAS and meta-
1327 analysis identifies 49 genetic variants underlying critical COVID-19. Nature. 2023;617(7962):764-

1328 8. Epub 20230517. doi: 10.1038/s41586-023-06034-3. PubMed PMID: 37198478; PubMed
1329 Central PMCID: PMCPMC10208981.
1330 24. Kousathanas A, Pairo-Castineira E, Rawlik K, Stuckey A, Odhams CA, Walker S, et al.
1331 Whole-genome sequencing reveals host factors underlying critical COVID-19. Nature.
1332 2022;607(7917):97-103. Epub 20220307. doi: 10.1038/s41586-022-04576-6. PubMed PMID:
1333 35255492; PubMed Central PMCID: PMCPMC9259496.
1334 25. Baggen J, Vanstreels E, Jansen S, Daelemans D. Cellular host factors for SARS-CoV-2
1335 infection. Nat Microbiol. 2021;6(10):1219-32. Epub 20210901. doi: 10.1038/s41564-021-00958-
1336 0. PubMed PMID: 34471255.
1337 26. Hoffmann HH, Sanchez-Rivera FJ, Schneider WM, Luna JM, Soto-Feliciano YM, Ashbrook
1338 AW, et al. Functional interrogation of a SARS-CoV-2 host protein interactome identifies unique
1339 and shared coronavirus host factors. Cell Host Microbe. 2021;29(2):267-80 e5. Epub 20201216.
1340 doi: 10.1016/j.chom.2020.12.009. PubMed PMID: 33357464; PubMed Central PMCID:
1341 PMCPMC7833927.
1342 27. Li Q, Wu J, Nie J, Zhang L, Hao H, Liu S, et al. The Impact of Mutations in SARS-CoV-2
1343 Spike on Viral Infectivity and Antigenicity. Cell. 2020;182(5):1284-94 e9. Epub 20200717. doi:
1344 10.1016/j.cell.2020.07.012. PubMed PMID: 32730807; PubMed Central PMCID:
1345 PMCPMC7366990.
1346 28. Riva L, Yuan S, Yin X, Martin-Sancho L, Matsunaga N, Pache L, et al. Discovery of SARS-
1347 CoV-2 antiviral drugs through large-scale compound repurposing. Nature. 2020;586(7827):113-
1348 9. Epub 20200724. doi: 10.1038/s41586-020-2577-1. PubMed PMID: 32707573; PubMed
1349 Central PMCID: PMCPMC7603405.
1350 29. Schneider WM, Luna JM, Hoffmann HH, Sanchez-Rivera FJ, Leal AA, Ashbrook AW, et al.
1351 Genome-Scale Identification of SARS-CoV-2 and Pan-coronavirus Host Factor Networks. Cell.
1352 2021;184(1):120-32 e14. Epub 20201209. doi: 10.1016/j.cell.2020.12.006. PubMed PMID:
1353 33382968; PubMed Central PMCID: PMCPMC7796900.
1354 30. Xia S, Lan Q, Su S, Wang X, Xu W, Liu Z, et al. The role of furin cleavage site in SARS-CoV-2
1355 spike protein-mediated membrane fusion in the presence or absence of trypsin. Signal

1356 Transduct Target Ther. 2020;5(1):92. Epub 20200612. doi: 10.1038/s41392-020-0184-0. PubMed
1357 PMID: 32532959; PubMed Central PMCID: PMCPMC7289711.
1358 31. Xia S, Liu M, Wang C, Xu W, Lan Q, Feng S, et al. Inhibition of SARS-CoV-2 (previously
1359 2019-nCoV) infection by a highly potent pan-coronavirus fusion inhibitor targeting its spike
1360 protein that harbors a high capacity to mediate membrane fusion. Cell Res. 2020;30(4):343-55.
1361 Epub 20200330. doi: 10.1038/s41422-020-0305-x. PubMed PMID: 32231345; PubMed Central
1362 PMCID: PMCPMC7104723.
1363 32. Yan Y, Chang L, Wang L. Laboratory testing of SARS-CoV, MERS-CoV, and SARS-CoV-2
1364 (2019-nCoV): Current status, challenges, and countermeasures. Rev Med Virol.
1365 2020;30(3):e2106. Epub 20200417. doi: 10.1002/rmv.2106. PubMed PMID: 32302058; PubMed
1366 Central PMCID: PMCPMC7235496.
1367 33. Barretina J, Caponigro G, Stransky N, Venkatesan K, Margolin AA, Kim S, et al. The Cancer
1368 Cell Line Encyclopedia enables predictive modelling of anticancer drug sensitivity. Nature.
1369 2012;483(7391):603-7. Epub 20120328. doi: 10.1038/nature11003. PubMed PMID: 22460905;
1370 PubMed Central PMCID: PMCPMC3320027.
1371 34. Klijn C, Durinck S, Stawiski EW, Haverty PM, Jiang Z, Liu H, et al. A comprehensive
1372 transcriptional portrait of human cancer cell lines. Nat Biotechnol. 2015;33(3):306-12. Epub
1373 20141208. doi: 10.1038/nbt.3080. PubMed PMID: 25485619.
1374 35. Consortium GT. Human genomics. The Genotype-Tissue Expression (GTEx) pilot analysis:
1375 multitissue gene regulation in humans. Science. 2015;348(6235):648-60. Epub 20150507. doi:
1376 10.1126/science.1262110. PubMed PMID: 25954001; PubMed Central PMCID:
1377 PMCPMC4547484.
1378 36. de Weerd NA, Samarajiwa SA, Hertzog PJ. Type I interferon receptors: biochemistry and
1379 biological functions. J Biol Chem. 2007;282(28):20053-7. Epub 20070514. doi:
1380 10.1074/jbc.R700006200. PubMed PMID: 17502368.
1381 37. de Weerd NA, Nguyen T. The interferons and their receptors--distribution and regulation.
1382 Immunol Cell Biol. 2012;90(5):483-91. Epub 20120313. doi: 10.1038/icb.2012.9. PubMed PMID:
1383 22410872; PubMed Central PMCID: PMCPMC7165917.

1384 38. Uze G, Schreiber G, Piehler J, Pellegrini S. The receptor of the type I interferon family.
1385 Curr Top Microbiol Immunol. 2007;316:71-95. doi: 10.1007/978-3-540-71329-6_5. PubMed
1386 PMID: 17969444.
1387 39. Horvath CM, Stark GR, Kerr IM, Darnell JE, Jr. Interactions between STAT and non-STAT
1388 proteins in the interferon-stimulated gene factor 3 transcription complex. Mol Cell Biol.
1389 1996;16(12):6957-64. doi: 10.1128/MCB.16.12.6957. PubMed PMID: 8943351; PubMed Central
1390 PMCID: PMCPMC231699.
1391 40. Veals SA, Schindler C, Leonard D, Fu XY, Aebersold R, Darnell JE, Jr., et al. Subunit of an
1392 alpha-interferon-responsive transcription factor is related to interferon regulatory factor and
1393 Myb families of DNA-binding proteins. Mol Cell Biol. 1992;12(8):3315-24. doi:
1394 10.1128/mcb.12.8.3315-3324.1992. PubMed PMID: 1630447; PubMed Central PMCID:
1395 PMCPMC364572.
1396 41. Darnell JE, Jr., Kerr IM, Stark GR. Jak-STAT pathways and transcriptional activation in
1397 response to IFNs and other extracellular signaling proteins. Science. 1994;264(5164):1415-21.
1398 doi: 10.1126/science.8197455. PubMed PMID: 8197455.
1399 42. Schindler C, Strehlow I. Cytokines and STAT signaling. Adv Pharmacol. 2000;47:113-74.
1400 doi: 10.1016/s1054-3589(08)60111-8. PubMed PMID: 10582086.
1401 43. Levy DE, Darnell JE, Jr. Stats: transcriptional control and biological impact. Nat Rev Mol
1402 Cell Biol. 2002;3(9):651-62. doi: 10.1038/nrm909. PubMed PMID: 12209125.
1403 44. Perng YC, Lenschow DJ. ISG15 in antiviral immunity and beyond. Nat Rev Microbiol.
1404 2018;16(7):423-39. doi: 10.1038/s41579-018-0020-5. PubMed PMID: 29769653; PubMed
1405 Central PMCID: PMCPMC7097117.
1406 45. Speer SD, Li Z, Buta S, Payelle-Brogard B, Qian L, Vigant F, et al. ISG15 deficiency and
1407 increased viral resistance in humans but not mice. Nat Commun. 2016;7:11496. Epub
1408 20160519. doi: 10.1038/ncomms11496. PubMed PMID: 27193971; PubMed Central PMCID:
1409 PMCPMC4873964.
1410 46. Zhang X, Bogunovic D, Payelle-Brogard B, Francois-Newton V, Speer SD, Yuan C, et al.
1411 Human intracellular ISG15 prevents interferon-alpha/beta over-amplification and auto-

1412 inflammation. Nature. 2015;517(7532):89-93. Epub 20141012. doi: 10.1038/nature13801.
1413 PubMed PMID: 25307056; PubMed Central PMCID: PMCPMC4303590.
1414 47. Naka T, Narazaki M, Hirata M, Matsumoto T, Minamoto S, Aono A, et al. Structure and
1415 function of a new STAT-induced STAT inhibitor. Nature. 1997;387(6636):924-9. doi:
1416 10.1038/43219. PubMed PMID: 9202127.
1417 48. Malakhova OA, Kim KI, Luo JK, Zou W, Kumar KG, Fuchs SY, et al. UBP43 is a novel
1418 regulator of interferon signaling independent of its ISG15 isopeptidase activity. EMBO J.
1419 2006;25(11):2358-67. Epub 20060518. doi: 10.1038/sj.emboj.7601149. PubMed PMID:
1420 16710296; PubMed Central PMCID: PMCPMC1478183.
1421 49. Francois-Newton V, Magno de Freitas Almeida G, Payelle-Brogard B, Monneron D,
1422 Pichard-Garcia L, Piehler J, et al. USP18-based negative feedback control is induced by type I and
1423 type III interferons and specifically inactivates interferon alpha response. PLoS One.
1424 2011;6(7):e22200. Epub 20110714. doi: 10.1371/journal.pone.0022200. PubMed PMID:
1425 21779393; PubMed Central PMCID: PMCPMC3136508.
1426 50. Ziegler CGK, Allon SJ, Nyquist SK, Mbano IM, Miao VN, Tzouanas CN, et al. SARS-CoV-2
1427 Receptor ACE2 Is an Interferon-Stimulated Gene in Human Airway Epithelial Cells and Is
1428 Detected in Specific Cell Subsets across Tissues. Cell. 2020;181(5):1016-35 e19. Epub 20200427.
1429 doi: 10.1016/j.cell.2020.04.035. PubMed PMID: 32413319; PubMed Central PMCID:
1430 PMCPMC7252096.
1431 51. Onabajo OO, Banday AR, Stanifer ML, Yan W, Obajemu A, Santer DM, et al. Interferons
1432 and viruses induce a novel truncated ACE2 isoform and not the full-length SARS-CoV-2 receptor.
1433 Nat Genet. 2020;52(12):1283-93. Epub 20201019. doi: 10.1038/s41588-020-00731-9. PubMed
1434 PMID: 33077916; PubMed Central PMCID: PMCPMC9377523.
1435 52. Zhao MM, Yang WL, Yang FY, Zhang L, Huang WJ, Hou W, et al. Cathepsin L plays a key
1436 role in SARS-CoV-2 infection in humans and humanized mice and is a promising target for new
1437 drug development. Signal Transduct Target Ther. 2021;6(1):134. Epub 20210327. doi:
1438 10.1038/s41392-021-00558-8. PubMed PMID: 33774649; PubMed Central PMCID:
1439 PMCPMC7997800.

1440 53. Shang J, Wan Y, Luo C, Ye G, Geng Q, Auerbach A, et al. Cell entry mechanisms of SARS-
1441 CoV-2. Proc Natl Acad Sci U S A. 2020;117(21):11727-34. Epub 20200506. doi:
1442 10.1073/pnas.2003138117. PubMed PMID: 32376634; PubMed Central PMCID:
1443 PMCPMC7260975.
1444 54. Liu T, Luo S, Libby P, Shi GP. Cathepsin L-selective inhibitors: A potentially promising
1445 treatment for COVID-19 patients. Pharmacol Ther. 2020;213:107587. Epub 20200526. doi:
1446 10.1016/j.pharmthera.2020.107587. PubMed PMID: 32470470; PubMed Central PMCID:
1447 PMCPMC7255230.
1448 55. Hoffmann M, Kleine-Weber H, Schroeder S, Kruger N, Herrler T, Erichsen S, et al. SARS-
1449 CoV-2 Cell Entry Depends on ACE2 and TMPRSS2 and Is Blocked by a Clinically Proven Protease
1450 Inhibitor. Cell. 2020;181(2):271-80 e8. Epub 20200305. doi: 10.1016/j.cell.2020.02.052. PubMed
1451 PMID: 32142651; PubMed Central PMCID: PMCPMC7102627.
1452 56. Jackson CB, Farzan M, Chen B, Choe H. Mechanisms of SARS-CoV-2 entry into cells. Nat
1453 Rev Mol Cell Biol. 2022;23(1):3-20. Epub 20211005. doi: 10.1038/s41580-021-00418-x. PubMed
1454 PMID: 34611326; PubMed Central PMCID: PMCPMC8491763.
1455 57. Pellegrini S, John J, Shearer M, Kerr IM, Stark GR. Use of a selectable marker regulated
1456 by alpha interferon to obtain mutations in the signaling pathway. Mol Cell Biol.
1457 1989;9(11):4605-12. doi: 10.1128/mcb.9.11.4605-4612.1989. PubMed PMID: 2513475;
1458 PubMed Central PMCID: PMCPMC363606.
1459 58. Velazquez L, Fellous M, Stark GR, Pellegrini S. A protein tyrosine kinase in the interferon
1460 alpha/beta signaling pathway. Cell. 1992;70(2):313-22. doi: 10.1016/0092-8674(92)90105-l.
1461 PubMed PMID: 1386289.
1462 59. Wang S, Li W, Hui H, Tiwari SK, Zhang Q, Croker BA, et al. Cholesterol 25-Hydroxylase
1463 inhibits SARS-CoV-2 and other coronaviruses by depleting membrane cholesterol. EMBO J.
1464 2020;39(21):e106057. Epub 20201005. doi: 10.15252/embj.2020106057. PubMed PMID:
1465 32944968; PubMed Central PMCID: PMCPMC7537045.
1466 60. Zhu Y, Feng F, Hu G, Wang Y, Yu Y, Zhu Y, et al. A genome-wide CRISPR screen identifies
1467 host factors that regulate SARS-CoV-2 entry. Nat Commun. 2021;12(1):961. Epub 20210211. doi:

1468 10.1038/s41467-021-21213-4. PubMed PMID: 33574281; PubMed Central PMCID:
1469 PMCPMC7878750.
1470 61. Wei LH, Sun Y, Guo JU. Genome-wide CRISPR screens identify noncanonical translation
1471 factor eIF2A as an enhancer of SARS-CoV-2 programmed -1 ribosomal frameshifting. Cell Rep.
1472 2023;42(8):112987. Epub 20230814. doi: 10.1016/j.celrep.2023.112987. PubMed PMID:
1473 37581984.
1474 62. Wei J, Alfajaro MM, DeWeirdt PC, Hanna RE, Lu-Culligan WJ, Cai WL, et al. Genome-wide
1475 CRISPR Screens Reveal Host Factors Critical for SARS-CoV-2 Infection. Cell. 2021;184(1):76-91
1476 e13. Epub 20201020. doi: 10.1016/j.cell.2020.10.028. PubMed PMID: 33147444; PubMed
1477 Central PMCID: PMCPMC7574718.
1478 63. Wang R, Simoneau CR, Kulsuptrakul J, Bouhaddou M, Travisano KA, Hayashi JM, et al.
1479 Genetic Screens Identify Host Factors for SARS-CoV-2 and Common Cold Coronaviruses. Cell.
1480 2021;184(1):106-19 e14. Epub 20201209. doi: 10.1016/j.cell.2020.12.004. PubMed PMID:
1481 33333024; PubMed Central PMCID: PMCPMC7723770.
1482 64. Song J, Chow RD, Pena-Hernandez MA, Zhang L, Loeb SA, So EY, et al. LRRC15 inhibits
1483 SARS-CoV-2 cellular entry in trans. PLoS Biol. 2022;20(10):e3001805. Epub 20221013. doi:
1484 10.1371/journal.pbio.3001805. PubMed PMID: 36228039; PubMed Central PMCID:
1485 PMCPMC9595563.
1486 65. Hossain MS, Kerkvliet JG, Hoppe AD. Whole genome CRISPR screening strategy to
1487 identify genes contributing to SARS-CoV-2 spike and VSV-G mediated entry. J Med Virol.
1488 2023;95(9):e29087. doi: 10.1002/jmv.29087. PubMed PMID: 37707319.
1489 66. Rehfeld F, Eitson JL, Ohlson MB, Chang TC, Schoggins JW, Mendell JT. CRISPR screening
1490 reveals a dependency on ribosome recycling for efficient SARS-CoV-2 programmed ribosomal
1491 frameshifting and viral replication. Cell Rep. 2023;42(2):112076. Epub 20230130. doi:
1492 10.1016/j.celrep.2023.112076. PubMed PMID: 36753415; PubMed Central PMCID:
1493 PMCPMC9884621.
1494 67. Rebendenne A, Roy P, Bonaventure B, Chaves VAL, Desmarets L, Rouille Y, et al.
1495 Bidirectional genome-wide CRISPR screens reveal host factors regulating SARS-CoV-2, MERS-CoV

1496 and seasonal HCoVs. Res Sq. 2021. Epub 20210527. doi: 10.21203/rs.3.rs-555275/v1. PubMed
1497 PMID: 34075371; PubMed Central PMCID: PMCPMC8168385.
1498 68. Pahmeier F, Lavacca TM, Goellner S, Neufeldt CJ, Prasad V, Cerikan B, et al. Identification
1499 of host dependency factors involved in SARS-CoV-2 replication organelle formation through
1500 proteomics and ultrastructural analysis. J Virol. 2023:e0087823. Epub 20231031. doi:
1501 10.1128/jvi.00878-23. PubMed PMID: 37905840.
1502 69. Loo L, Waller MA, Moreno CL, Cole AJ, Stella AO, Pop OT, et al. Fibroblast-expressed
1503 LRRC15 is a receptor for SARS-CoV-2 spike and controls antiviral and antifibrotic transcriptional
1504 programs. PLoS Biol. 2023;21(2):e3001967. Epub 20230209. doi: 10.1371/journal.pbio.3001967.
1505 PubMed PMID: 36757924; PubMed Central PMCID: PMCPMC9910744.
1506 70. Israeli M, Finkel Y, Yahalom-Ronen Y, Paran N, Chitlaru T, Israeli O, et al. Genome-wide
1507 CRISPR screens identify GATA6 as a proviral host factor for SARS-CoV-2 via modulation of ACE2.
1508 Nat Commun. 2022;13(1):2237. Epub 20220425. doi: 10.1038/s41467-022-29896-z. PubMed
1509 PMID: 35469023; PubMed Central PMCID: PMCPMC9039069.
1510 71. Grodzki M, Bluhm AP, Schaefer M, Tagmount A, Russo M, Sobh A, et al. Genome-scale
1511 CRISPR screens identify host factors that promote human coronavirus infection. Genome Med.
1512 2022;14(1):10. Epub 20220127. doi: 10.1186/s13073-022-01013-1. PubMed PMID: 35086559;
1513 PubMed Central PMCID: PMCPMC8792531.
1514 72. Gordon DE, Hiatt J, Bouhaddou M, Rezelj VV, Ulferts S, Braberg H, et al. Comparative
1515 host-coronavirus protein interaction networks reveal pan-viral disease mechanisms. Science.
1516 2020;370(6521). Epub 20201015. doi: 10.1126/science.abe9403. PubMed PMID: 33060197;
1517 PubMed Central PMCID: PMCPMC7808408.
1518 73. Daniloski Z, Jordan TX, Wessels HH, Hoagland DA, Kasela S, Legut M, et al. Identification
1519 of Required Host Factors for SARS-CoV-2 Infection in Human Cells. Cell. 2021;184(1):92-105 e16.
1520 Epub 20201024. doi: 10.1016/j.cell.2020.10.030. PubMed PMID: 33147445; PubMed Central
1521 PMCID: PMCPMC7584921.
1522 74. Chan K, Farias AG, Lee H, Guvenc F, Mero P, Brown KR, et al. Survival-based CRISPR
1523 genetic screens across a panel of permissive cell lines identify common and cell-specific SARS-
1524 CoV-2 host factors. Heliyon. 2023;9(1):e12744. Epub 20221230. doi:

1525 10.1016/j.heliyon.2022.e12744. PubMed PMID: 36597481; PubMed Central PMCID:
1526 PMCPMC9800021.
1527 75. Biering SB, Sarnik SA, Wang E, Zengel JR, Leist SR, Schafer A, et al. Genome-wide
1528 bidirectional CRISPR screens identify mucins as host factors modulating SARS-CoV-2 infection.
1529 Nat Genet. 2022;54(8):1078-89. Epub 20220725. doi: 10.1038/s41588-022-01131-x. PubMed
1530 PMID: 35879412; PubMed Central PMCID: PMCPMC9355872.
1531 76. Baggen J, Persoons L, Vanstreels E, Jansen S, Van Looveren D, Boeckx B, et al. Genome-
1532 wide CRISPR screening identifies TMEM106B as a proviral host factor for SARS-CoV-2. Nat
1533 Genet. 2021;53(4):435-44. Epub 20210308. doi: 10.1038/s41588-021-00805-2. PubMed PMID:
1534 33686287.
1535 77. van der Made CI, Simons A, Schuurs-Hoeijmakers J, van den Heuvel G, Mantere T,
1536 Kersten S, et al. Presence of Genetic Variants Among Young Men With Severe COVID-19. JAMA.
1537 2020;324(7):663-73. doi: 10.1001/jama.2020.13719. PubMed PMID: 32706371; PubMed
1538 Central PMCID: PMCPMC7382021.
1539 78. Shelton JF, Shastri AJ, Ye C, Weldon CH, Filshtein-Sonmez T, Coker D, et al. Trans-ancestry
1540 analysis reveals genetic and nongenetic associations with COVID-19 susceptibility and severity.
1541 Nat Genet. 2021;53(6):801-8. Epub 20210422. doi: 10.1038/s41588-021-00854-7. PubMed
1542 PMID: 33888907.
1543 79. Roberts GHL, Partha R, Rhead B, Knight SC, Park DS, Coignet MV, et al. Expanded COVID-
1544 19 phenotype definitions reveal distinct patterns of genetic association and protective effects.
1545 Nat Genet. 2022;54(4):374-81. Epub 20220411. doi: 10.1038/s41588-022-01042-x. PubMed
1546 PMID: 35410379.
1547 80. Pietzner M, Chua RL, Wheeler E, Jechow K, Willett JDS, Radbruch H, et al. ELF5 is a
1548 potential respiratory epithelial cell-specific risk gene for severe COVID-19. Nat Commun.
1549 2022;13(1):4484. Epub 20220815. doi: 10.1038/s41467-022-31999-6. PubMed PMID:
1550 35970849; PubMed Central PMCID: PMCPMC9378714.
1551 81. Latini A, Agolini E, Novelli A, Borgiani P, Giannini R, Gravina P, et al. COVID-19 and
1552 Genetic Variants of Protein Involved in the SARS-CoV-2 Entry into the Host Cells. Genes (Basel).

1553 2020;11(9). Epub 20200827. doi: 10.3390/genes11091010. PubMed PMID: 32867305; PubMed
1554 Central PMCID: PMCPMC7565048.
1555 82. Horowitz JE, Kosmicki JA, Damask A, Sharma D, Roberts GHL, Justice AE, et al. Genome-
1556 wide analysis provides genetic evidence that ACE2 influences COVID-19 risk and yields risk
1557 scores associated with severe disease. Nat Genet. 2022;54(4):382-92. Epub 20220303. doi:
1558 10.1038/s41588-021-01006-7. PubMed PMID: 35241825; PubMed Central PMCID:
1559 PMCPMC9005345.
1560 83. Garcia-Garcia A, Perez de Diego R, Flores C, Rinchai D, Sole-Violan J, Deya-Martinez A, et
1561 al. Humans with inherited MyD88 and IRAK-4 deficiencies are predisposed to hypoxemic COVID-
1562 19 pneumonia. J Exp Med. 2023;220(5). Epub 20230303. doi: 10.1084/jem.20220170. PubMed
1563 PMID: 36880831; PubMed Central PMCID: PMCPMC9998661.
1564 84. Fallerini C, Daga S, Mantovani S, Benetti E, Picchiotti N, Francisci D, et al. Association of
1565 Toll-like receptor 7 variants with life-threatening COVID-19 disease in males: findings from a
1566 nested case-control study. Elife. 2021;10. Epub 20210302. doi: 10.7554/eLife.67569. PubMed
1567 PMID: 33650967; PubMed Central PMCID: PMCPMC7987337.
1568 85. Severe Covid GG, Ellinghaus D, Degenhardt F, Bujanda L, Buti M, Albillos A, et al.
1569 Genomewide Association Study of Severe Covid-19 with Respiratory Failure. N Engl J Med.
1570 2020;383(16):1522-34. Epub 20200617. doi: 10.1056/NEJMoa2020283. PubMed PMID:
1571 32558485; PubMed Central PMCID: PMCPMC7315890.
1572 86. Degenhardt F, Ellinghaus D, Juzenas S, Lerga-Jaso J, Wendorff M, Maya-Miles D, et al.
1573 Detailed stratified GWAS analysis for severe COVID-19 in four European populations. Hum Mol
1574 Genet. 2022;31(23):3945-66. doi: 10.1093/hmg/ddac158. PubMed PMID: 35848942; PubMed
1575 Central PMCID: PMCPMC9703941.
1576 87. D'Antonio M, Nguyen JP, Arthur TD, Matsui H, Initiative C-HG, D'Antonio-Chronowska A,
1577 et al. SARS-CoV-2 susceptibility and COVID-19 disease severity are associated with genetic
1578 variants affecting gene expression in a variety of tissues. Cell Rep. 2021;37(7):110020. Epub
1579 20211103. doi: 10.1016/j.celrep.2021.110020. PubMed PMID: 34762851; PubMed Central
1580 PMCID: PMCPMC8563343.

1581 88. Cruz R, Diz-de Almeida S, Lopez de Heredia M, Quintela I, Ceballos FC, Pita G, et al. Novel
1582 genes and sex differences in COVID-19 severity. Hum Mol Genet. 2022;31(22):3789-806. doi:
1583 10.1093/hmg/ddac132. PubMed PMID: 35708486; PubMed Central PMCID: PMCPMC9652109.
1584 89. Initiative C-HG. A first update on mapping the human genetic architecture of COVID-19.
1585 Nature. 2022;608(7921):E1-E10. Epub 20220803. doi: 10.1038/s41586-022-04826-7. PubMed
1586 PMID: 35922517; PubMed Central PMCID: PMCPMC9352569.
1587 90. Andolfo I, Russo R, Lasorsa VA, Cantalupo S, Rosato BE, Bonfiglio F, et al. Common
1588 variants at 21q22.3 locus influence MX1 and TMPRSS2 gene expression and susceptibility to
1589 severe COVID-19. iScience. 2021;24(4):102322. Epub 20210317. doi:
1590 10.1016/j.isci.2021.102322. PubMed PMID: 33748697; PubMed Central PMCID:
1591 PMCPMC7968217.
1592 91. Zhou S, Butler-Laporte G, Nakanishi T, Morrison DR, Afilalo J, Afilalo M, et al. A
1593 Neanderthal OAS1 isoform protects individuals of European ancestry against COVID-19
1594 susceptibility and severity. Nat Med. 2021;27(4):659-67. Epub 20210225. doi: 10.1038/s41591-
1595 021-01281-1. PubMed PMID: 33633408.
1596 92. Huffman JE, Butler-Laporte G, Khan A, Pairo-Castineira E, Drivas TG, Peloso GM, et al.
1597 Multi-ancestry fine mapping implicates OAS1 splicing in risk of severe COVID-19. Nat Genet.
1598 2022;54(2):125-7. Epub 20220113. doi: 10.1038/s41588-021-00996-8. PubMed PMID:
1599 35027740; PubMed Central PMCID: PMCPMC8837537.
1600 93. Initiative C-HG. Mapping the human genetic architecture of COVID-19. Nature.
1601 2021;600(7889):472-7. Epub 20210708. doi: 10.1038/s41586-021-03767-x. PubMed PMID:
1602 34237774; PubMed Central PMCID: PMCPMC8674144.
1603 94. Pairo-Castineira E, Clohisey S, Klaric L, Bretherick AD, Rawlik K, Pasko D, et al. Genetic
1604 mechanisms of critical illness in COVID-19. Nature. 2021;591(7848):92-8. Epub 20201211. doi:
1605 10.1038/s41586-020-03065-y. PubMed PMID: 33307546.
1606 95. Banday AR, Stanifer ML, Florez-Vargas O, Onabajo OO, Papenberg BW, Zahoor MA, et al.
1607 Genetic regulation of OAS1 nonsense-mediated decay underlies association with COVID-19
1608 hospitalization in patients of European and African ancestries. Nat Genet. 2022;54(8):1103-16.

1609 Epub 20220714. doi: 10.1038/s41588-022-01113-z. PubMed PMID: 35835913; PubMed Central
1610 PMCID: PMCPMC9355882.
1611 96. Payman S-T, Hala A, James DRK, Audrey A, Reuben S, Zhen-Yuan L, et al. A SARS-CoV-2 –
1612 host proximity interactome. bioRxiv. 2020:2020.09.03.282103. doi:
1613 10.1101/2020.09.03.282103.
1614 97. Gordon DE, Jang GM, Bouhaddou M, Xu J, Obernier K, White KM, et al. A SARS-CoV-2
1615 protein interaction map reveals targets for drug repurposing. Nature. 2020;583(7816):459-68.
1616 Epub 20200430. doi: 10.1038/s41586-020-2286-9. PubMed PMID: 32353859; PubMed Central
1617 PMCID: PMCPMC7431030.
1618 98. Estelle MNL, Yorgos S, Anastassia K, Jean-Pascal G, Payman Samavarchi T, Dae-Kyum K, et
1619 al. Global BioID-based SARS-CoV-2 proteins proximal interactome unveils novel ties between
1620 viral polypeptides and host factors involved in multiple COVID19-associated mechanisms.
1621 bioRxiv. 2020:2020.08.28.272955. doi: 10.1101/2020.08.28.272955.
1622 99. St-Germain JR, Astori A, Samavarchi-Tehrani P, Abdouni H, Macwan V, Kim D-K, et al. A
1623 SARS-CoV-2 BioID-based virus-host membrane protein interactome and virus peptide
1624 compendium: new proteomics resources for COVID-19 research. bioRxiv.
1625 2020:2020.08.28.269175. doi: 10.1101/2020.08.28.269175.
1626 100. Liu X, Huuskonen S, Laitinen T, Redchuk T, Bogacheva M, Salokas K, et al. SARS-CoV-2-
1627 host proteome interactions for antiviral drug discovery. Mol Syst Biol. 2021;17(11):e10396. doi:
1628 10.15252/msb.202110396. PubMed PMID: 34709727; PubMed Central PMCID:
1629 PMCPMC8552907.
1630 101. May DG, Martin-Sancho L, Anschau V, Liu S, Chrisopulos RJ, Scott KL, et al. A BioID-
1631 Derived Proximity Interactome for SARS-CoV-2 Proteins. Viruses. 2022;14(3). Epub 20220315.
1632 doi: 10.3390/v14030611. PubMed PMID: 35337019; PubMed Central PMCID:
1633 PMCPMC8951556.
1634 102. Zhou Y, Liu Y, Gupta S, Paramo MI, Hou Y, Mao C, et al. A comprehensive SARS-CoV-2-
1635 human protein-protein interactome reveals COVID-19 pathobiology and potential host
1636 therapeutic targets. Nat Biotechnol. 2023;41(1):128-39. Epub 20221010. doi: 10.1038/s41587-
1637 022-01474-0. PubMed PMID: 36217030; PubMed Central PMCID: PMCPMC9851973.

1638 103. Stukalov A, Girault V, Grass V, Karayel O, Bergant V, Urban C, et al. Multilevel proteomics
1639 reveals host perturbations by SARS-CoV-2 and SARS-CoV. Nature. 2021;594(7862):246-52. Epub
1640 20210412. doi: 10.1038/s41586-021-03493-4. PubMed PMID: 33845483.
1641 104. Li J, Guo M, Tian X, Wang X, Yang X, Wu P, et al. Virus-Host Interactome and Proteomic
1642 Survey Reveal Potential Virulence Factors Influencing SARS-CoV-2 Pathogenesis. Med.
1643 2021;2(1):99-112 e7. Epub 20200721. doi: 10.1016/j.medj.2020.07.002. PubMed PMID:
1644 32838362; PubMed Central PMCID: PMCPMC7373048.
1645 105. Davies JP, Almasy KM, McDonald EF, Plate L. Comparative Multiplexed Interactomics of
1646 SARS-CoV-2 and Homologous Coronavirus Nonstructural Proteins Identifies Unique and Shared
1647 Host-Cell Dependencies. ACS Infect Dis. 2020;6(12):3174-89. Epub 20201202. doi:
1648 10.1021/acsinfecdis.0c00500. PubMed PMID: 33263384; PubMed Central PMCID:
1649 PMCPMC7724760.
1650 106. Schmidt N, Ganskih S, Wei Y, Gabel A, Zielinski S, Keshishian H, et al. SND1 binds SARS-
1651 CoV-2 negative-sense RNA and promotes viral RNA synthesis through NSP9. Cell.
1652 2023;186(22):4834-50 e23. Epub 20231003. doi: 10.1016/j.cell.2023.09.002. PubMed PMID:
1653 37794589; PubMed Central PMCID: PMCPMC10617981.
1654 107. Schmidt N, Lareau CA, Keshishian H, Ganskih S, Schneider C, Hennig T, et al. The SARS-
1655 CoV-2 RNA-protein interactome in infected human cells. Nat Microbiol. 2021;6(3):339-53. Epub
1656 20201221. doi: 10.1038/s41564-020-00846-z. PubMed PMID: 33349665; PubMed Central
1657 PMCID: PMCPMC7906908.
1658 108. Labeau A, Fery-Simonian L, Lefevre-Utile A, Pourcelot M, Bonnet-Madin L, Soumelis V, et
1659 al. Characterization and functional interrogation of the SARS-CoV-2 RNA interactome. Cell Rep.
1660 2022;39(4):110744. doi: 10.1016/j.celrep.2022.110744. PubMed PMID: 35477000; PubMed
1661 Central PMCID: PMCPMC9040432.
1662 109. Kamel W, Noerenberg M, Cerikan B, Chen H, Jarvelin AI, Kammoun M, et al. Global
1663 analysis of protein-RNA interactions in SARS-CoV-2-infected cells reveals key regulators of
1664 infection. Mol Cell. 2021;81(13):2851-67 e7. Epub 20210524. doi:
1665 10.1016/j.molcel.2021.05.023. PubMed PMID: 34118193; PubMed Central PMCID:
1666 PMCPMC8142890.

1667 110. Flynn RA, Belk JA, Qi Y, Yasumoto Y, Wei J, Alfajaro MM, et al. Discovery and functional
1668 interrogation of SARS-CoV-2 RNA-host protein interactions. Cell. 2021;184(9):2394-411 e16.
1669 Epub 20210311. doi: 10.1016/j.cell.2021.03.012. PubMed PMID: 33743211; PubMed Central
1670 PMCID: PMCPMC7951565.
1671 111. Lee S, Lee YS, Choi Y, Son A, Park Y, Lee KM, et al. The SARS-CoV-2 RNA interactome. Mol
1672 Cell. 2021;81(13):2838-50 e6. Epub 20210427. doi: 10.1016/j.molcel.2021.04.022. PubMed
1673 PMID: 33989516; PubMed Central PMCID: PMCPMC8075806.
1674 112. Bouhaddou M, Memon D, Meyer B, White KM, Rezelj VV, Correa Marrero M, et al. The
1675 Global Phosphorylation Landscape of SARS-CoV-2 Infection. Cell. 2020;182(3):685-712 e19.
1676 Epub 20200628. doi: 10.1016/j.cell.2020.06.034. PubMed PMID: 32645325; PubMed Central
1677 PMCID: PMCPMC7321036.
1678 113. Sanchez-Magraner L, Posada IM, Andraka N, Contreras FX, Viguera AR, Guerin DM, et al.
1679 The C-terminal transmembrane domain of human phospholipid scramblase 1 is essential for the
1680 protein flip-flop activity and Ca(2)(+)-binding. J Membr Biol. 2014;247(2):155-65. Epub
1681 20131217. doi: 10.1007/s00232-013-9619-7. PubMed PMID: 24343571.
1682 114. Ricardo-Lax I, Luna JM, Thao TTN, Le Pen J, Yu Y, Hoffmann HH, et al. Replication and
1683 single-cycle delivery of SARS-CoV-2 replicons. Science. 2021;374(6571):1099-106. Epub
1684 20211014. doi: 10.1126/science.abj8430. PubMed PMID: 34648371; PubMed Central PMCID:
1685 PMCPMC9007107.
1686 115. Schmidt F, Weisblum Y, Muecksch F, Hoffmann HH, Michailidis E, Lorenzi JCC, et al.
1687 Measuring SARS-CoV-2 neutralizing antibody activity using pseudotyped and chimeric viruses. J
1688 Exp Med. 2020;217(11). doi: 10.1084/jem.20201181. PubMed PMID: 32692348; PubMed
1689 Central PMCID: PMCPMC7372514.
1690 116. Khan H, Winstone H, Jimenez-Guardeno JM, Graham C, Doores KJ, Goujon C, et al.
1691 TMPRSS2 promotes SARS-CoV-2 evasion from NCOA7-mediated restriction. PLoS Pathog.
1692 2021;17(11):e1009820. Epub 20211122. doi: 10.1371/journal.ppat.1009820. PubMed PMID:
1693 34807954; PubMed Central PMCID: PMCPMC8648102.
1694 117. Thorne LG, Bouhaddou M, Reuschl AK, Zuliani-Alvarez L, Polacco B, Pelin A, et al.
1695 Evolution of enhanced innate immune evasion by SARS-CoV-2. Nature. 2022;602(7897):487-95.

1696 Epub 20211223. doi: 10.1038/s41586-021-04352-y. PubMed PMID: 34942634; PubMed Central
1697 PMCID: PMCPMC8850198.
1698 118. Markov PV, Ghafari M, Beer M, Lythgoe K, Simmonds P, Stilianakis NI, et al. The evolution
1699 of SARS-CoV-2. Nature Reviews Microbiology. 2023;21(6):361-79. doi: 10.1038/s41579-023-
1700 00878-2.
1701 119. Carabelli AM, Peacock TP, Thorne LG, Harvey WT, Hughes J, de Silva TI, et al. SARS-CoV-2
1702 variant biology: immune escape, transmission and fitness. Nature Reviews Microbiology.
1703 2023;21(3):162-77. doi: 10.1038/s41579-022-00841-7.
1704 120. Huang P, Liao R, Chen X, Wu X, Li X, Wang Y, et al. Nuclear translocation of PLSCR1
1705 activates STAT1 signaling in basal-like breast cancer. Theranostics. 2020;10(10):4644-58. Epub
1706 20200325. doi: 10.7150/thno.43150. PubMed PMID: 32292520; PubMed Central PMCID:
1707 PMCPMC7150476.
1708 121. Nanjundan M, Sun J, Zhao J, Zhou Q, Sims PJ, Wiedmer T. Plasma membrane
1709 phospholipid scramblase 1 promotes EGF-dependent activation of c-Src through the epidermal
1710 growth factor receptor. J Biol Chem. 2003;278(39):37413-8. Epub 20030718. doi:
1711 10.1074/jbc.M306182200. PubMed PMID: 12871937.
1712 122. Ben-Efraim I, Zhou Q, Wiedmer T, Gerace L, Sims PJ. Phospholipid scramblase 1 is
1713 imported into the nucleus by a receptor-mediated pathway and interacts with DNA.
1714 Biochemistry. 2004;43(12):3518-26. doi: 10.1021/bi0356911. PubMed PMID: 15035622.
1715 123. Chen MH, Ben-Efraim I, Mitrousis G, Walker-Kopp N, Sims PJ, Cingolani G. Phospholipid
1716 scramblase 1 contains a nonclassical nuclear localization signal with unique binding site in
1717 importin alpha. J Biol Chem. 2005;280(11):10599-606. Epub 20041217. doi:
1718 10.1074/jbc.M413194200. PubMed PMID: 15611084.
1719 124. Wiedmer T, Zhao J, Nanjundan M, Sims PJ. Palmitoylation of phospholipid scramblase 1
1720 controls its distribution between nucleus and plasma membrane. Biochemistry.
1721 2003;42(5):1227-33. doi: 10.1021/bi026679w. PubMed PMID: 12564925.
1722 125. Zhao J, Zhou Q, Wiedmer T, Sims PJ. Palmitoylation of phospholipid scramblase is
1723 required for normal function in promoting Ca2+-activated transbilayer movement of membrane

1724 phospholipids. Biochemistry. 1998;37(18):6361-6. doi: 10.1021/bi980218m. PubMed PMID:
1725 9572851.
1726 126. Dittmann M, Hoffmann HH, Scull MA, Gilmore RH, Bell KL, Ciancanelli M, et al. A serpin
1727 shapes the extracellular environment to prevent influenza A virus maturation. Cell.
1728 2015;160(4):631-43. doi: 10.1016/j.cell.2015.01.040. PubMed PMID: 25679759; PubMed
1729 Central PMCID: PMCPMC4328142.
1730 127. Burke JM, St Clair LA, Perera R, Parker R. SARS-CoV-2 infection triggers widespread host
1731 mRNA decay leading to an mRNA export block. RNA. 2021;27(11):1318-29. Epub 20210727. doi:
1732 10.1261/rna.078923.121. PubMed PMID: 34315815; PubMed Central PMCID:
1733 PMCPMC8522697.
1734 128. Zhang K, Miorin L, Makio T, Dehghan I, Gao S, Xie Y, et al. Nsp1 protein of SARS-CoV-2
1735 disrupts the mRNA export machinery to inhibit host gene expression. Sci Adv. 2021;7(6). Epub
1736 20210205. doi: 10.1126/sciadv.abe7386. PubMed PMID: 33547084; PubMed Central PMCID:
1737 PMCPMC7864571.
1738 129. Kimura I, Konno Y, Uriu K, Hopfensperger K, Sauter D, Nakagawa S, et al. Sarbecovirus
1739 ORF6 proteins hamper induction of interferon signaling. Cell Rep. 2021;34(13):108916. Epub
1740 20210312. doi: 10.1016/j.celrep.2021.108916. PubMed PMID: 33765414; PubMed Central
1741 PMCID: PMCPMC7953434.
1742 130. Setaro AC, Gaglia MM. All hands on deck: SARS-CoV-2 proteins that block early anti-viral
1743 interferon responses. Curr Res Virol Sci. 2021;2:100015. Epub 20211112. doi:
1744 10.1016/j.crviro.2021.100015. PubMed PMID: 34786565; PubMed Central PMCID:
1745 PMCPMC8588586.
1746 131. Ogunjimi B, Zhang SY, Sorensen KB, Skipper KA, Carter-Timofte M, Kerner G, et al. Inborn
1747 errors in RNA polymerase III underlie severe varicella zoster virus infections. J Clin Invest.
1748 2017;127(9):3543-56. Epub 20170807. doi: 10.1172/JCI92280. PubMed PMID: 28783042;
1749 PubMed Central PMCID: PMCPMC5669568.
1750 132. Zimmer MM, Kibe A, Rand U, Pekarek L, Ye L, Buck S, et al. The short isoform of the host
1751 antiviral protein ZAP acts as an inhibitor of SARS-CoV-2 programmed ribosomal frameshifting.

1752 Nat Commun. 2021;12(1):7193. Epub 20211210. doi: 10.1038/s41467-021-27431-0. PubMed
1753 PMID: 34893599; PubMed Central PMCID: PMCPMC8664833.
1754 133. Klein S, Golani G, Lolicato F, Lahr C, Beyer D, Herrmann A, et al. IFITM3 blocks influenza
1755 virus entry by sorting lipids and stabilizing hemifusion. Cell Host Microbe. 2023. Epub 20230329.
1756 doi: 10.1016/j.chom.2023.03.005. PubMed PMID: 37003257.
1757 134. Guo X, Steinkuhler J, Marin M, Li X, Lu W, Dimova R, et al. Interferon-Induced
1758 Transmembrane Protein 3 Blocks Fusion of Diverse Enveloped Viruses by Altering Mechanical
1759 Properties of Cell Membranes. ACS Nano. 2021;15(5):8155-70. Epub 20210303. doi:
1760 10.1021/acsnano.0c10567. PubMed PMID: 33656312; PubMed Central PMCID:
1761 PMCPMC8159881.
1762 135. Suddala KC, Lee CC, Meraner P, Marin M, Markosyan RM, Desai TM, et al. Interferon-
1763 induced transmembrane protein 3 blocks fusion of sensitive but not resistant viruses by
1764 partitioning into virus-carrying endosomes. PLoS Pathog. 2019;15(1):e1007532. Epub 20190114.
1765 doi: 10.1371/journal.ppat.1007532. PubMed PMID: 30640957; PubMed Central PMCID:
1766 PMCPMC6347298.
1767 136. Desai TM, Marin M, Chin CR, Savidis G, Brass AL, Melikyan GB. IFITM3 restricts influenza
1768 A virus entry by blocking the formation of fusion pores following virus-endosome hemifusion.
1769 PLoS Pathog. 2014;10(4):e1004048. Epub 20140403. doi: 10.1371/journal.ppat.1004048.
1770 PubMed PMID: 24699674; PubMed Central PMCID: PMCPMC3974867.
1771 137. Fadeel B, Gleiss B, Hogstrand K, Chandra J, Wiedmer T, Sims PJ, et al. Phosphatidylserine
1772 exposure during apoptosis is a cell-type-specific event and does not correlate with plasma
1773 membrane phospholipid scramblase expression. Biochem Biophys Res Commun.
1774 1999;266(2):504-11. doi: 10.1006/bbrc.1999.1820. PubMed PMID: 10600532.
1775 138. Zhou Q, Zhao J, Al-Zoghaibi F, Zhou A, Wiedmer T, Silverman RH, et al. Transcriptional
1776 control of the human plasma membrane phospholipid scramblase 1 gene is mediated by
1777 interferon-alpha. Blood. 2000;95(8):2593-9. PubMed PMID: 10753839.
1778 139. Zhou Q, Zhao J, Wiedmer T, Sims PJ. Normal hemostasis but defective hematopoietic
1779 response to growth factors in mice deficient in phospholipid scramblase 1. Blood.
1780 2002;99(11):4030-8. doi: 10.1182/blood-2001-12-0271. PubMed PMID: 12010804.

1781 140. Kusano S, Eizuru Y. Human phospholipid scramblase 1 interacts with and regulates
1782 transactivation of HTLV-1 Tax. Virology. 2012;432(2):343-52. Epub 20120711. doi:
1783 10.1016/j.virol.2012.06.019. PubMed PMID: 22789739.
1784 141. Kusano S, Eizuru Y. Interaction of the phospholipid scramblase 1 with HIV-1 Tat results in
1785 the repression of Tat-dependent transcription. Biochem Biophys Res Commun. 2013;433(4):438-
1786 44. Epub 20130315. doi: 10.1016/j.bbrc.2013.02.098. PubMed PMID: 23501106.
1787 142. Sadanari H, Takemoto M, Ishida T, Otagiri H, Daikoku T, Murayama T, et al. The
1788 Interferon-Inducible Human PLSCR1 Protein Is a Restriction Factor of Human Cytomegalovirus.
1789 Microbiol Spectr. 2022;10(1):e0134221. Epub 2022/02/10. doi: 10.1128/spectrum.01342-21.
1790 PubMed PMID: 35138119; PubMed Central PMCID: PMCPMC8826943.
1791 143. Metz P, Dazert E, Ruggieri A, Mazur J, Kaderali L, Kaul A, et al. Identification of type I and
1792 type II interferon-induced effectors controlling hepatitis C virus replication. Hepatology.
1793 2012;56(6):2082-93. Epub 20121014. doi: 10.1002/hep.25908. PubMed PMID: 22711689.
1794 144. Yang J, Zhu X, Liu J, Ding X, Han M, Hu W, et al. Inhibition of Hepatitis B virus replication
1795 by phospholipid scramblase 1 in vitro and in vivo. Antiviral Res. 2012;94(1):9-17. Epub
1796 20120209. doi: 10.1016/j.antiviral.2012.01.010. PubMed PMID: 22342889.
1797 145. Kusano S, Ikeda M. Interaction of phospholipid scramblase 1 with the Epstein-Barr virus
1798 protein BZLF1 represses BZLF1-mediated lytic gene transcription. J Biol Chem.
1799 2019;294(41):15104-16. Epub 2019/08/23. doi: 10.1074/jbc.RA119.008193. PubMed PMID:
1800 31434743; PubMed Central PMCID: PMCPMC6791327.
1801 146. Luo W, Zhang J, Liang L, Wang G, Li Q, Zhu P, et al. Phospholipid scramblase 1 interacts
1802 with influenza A virus NP, impairing its nuclear import and thereby suppressing virus replication.
1803 PLoS Pathog. 2018;14(1):e1006851. Epub 20180119. doi: 10.1371/journal.ppat.1006851.
1804 PubMed PMID: 29352288; PubMed Central PMCID: PMCPMC5792031.
1805 147. Dal Col J, Lamberti MJ, Nigro A, Casolaro V, Fratta E, Steffan A, et al. Phospholipid
1806 scramblase 1: a protein with multiple functions via multiple molecular interactors. Cell Commun
1807 Signal. 2022;20(1):78. Epub 2022/06/02. doi: 10.1186/s12964-022-00895-3. PubMed PMID:
1808 35650588.

1809 148. Jonathan RS-G, Audrey A, Payman S-T, Hala A, Vinitha M, Dae-Kyum K, et al. A SARS-CoV-
1810 2 BioID-based virus-host membrane protein interactome and virus peptide compendium: new
1811 proteomics resources for COVID-19 research. bioRxiv. 2020:2020.08.28.269175. doi:
1812 10.1101/2020.08.28.269175.
1813 149. Guo K, Barrett BS, Morrison JH, Mickens KL, Vladar EK, Hasenkrug KJ, et al. Interferon
1814 resistance of emerging SARS-CoV-2 variants. Proc Natl Acad Sci U S A.
1815 2022;119(32):e2203760119. Epub 20220722. doi: 10.1073/pnas.2203760119. PubMed PMID:
1816 35867811; PubMed Central PMCID: PMCPMC9371743.
1817 150. Shalamova L, Felgenhauer U, Wilhelm J, Schaubmar AR, Buttner K, Schoen A, et al.
1818 Omicron variant of SARS-CoV-2 exhibits an increased resilience to the antiviral type I interferon
1819 response. PNAS Nexus. 2022;1(2):pgac067. Epub 20220523. doi: 10.1093/pnasnexus/pgac067.
1820 PubMed PMID: 36713328; PubMed Central PMCID: PMCPMC9802332.
1821 151. Shi G, Li T, Lai KK, Johnson RF, Yewdell JW, Compton AA. Omicron Spike confers enhanced
1822 infectivity and interferon resistance to SARS-CoV-2 in human nasal tissue. Nat Commun.
1823 2024;15(1):889. Epub 20240130. doi: 10.1038/s41467-024-45075-8. PubMed PMID: 38291024;
1824 PubMed Central PMCID: PMCPMC10828397.
1825 152. Willett BJ, Grove J, MacLean OA, Wilkie C, De Lorenzo G, Furnon W, et al. SARS-CoV-2
1826 Omicron is an immune escape variant with an altered cell entry pathway. Nat Microbiol.
1827 2022;7(8):1161-79. Epub 20220707. doi: 10.1038/s41564-022-01143-7. PubMed PMID:
1828 35798890; PubMed Central PMCID: PMCPMC9352574.
1829 153. Peacock TP, Brown JC, Zhou J, Thakur N, Sukhova K, Newman J, et al. The altered entry
1830 pathway and antigenic distance of the SARS-CoV-2 Omicron variant map to separate domains of
1831 spike protein. bioRxiv. 2022:2021.12.31.474653. doi: 10.1101/2021.12.31.474653.
1832 154. Sette A, Crotty S. Adaptive immunity to SARS-CoV-2 and COVID-19. Cell.
1833 2021;184(4):861-80. Epub 20210112. doi: 10.1016/j.cell.2021.01.007. PubMed PMID:
1834 33497610; PubMed Central PMCID: PMCPMC7803150.
1835 155. Chen S, Francioli LC, Goodrich JK, Collins RL, Kanai M, Wang Q, et al. A genomic
1836 mutational constraint map using variation in 76,156 human genomes. Nature.
1837 2024;625(7993):92-100. doi: 10.1038/s41586-023-06045-0.

1838 156. Mar KB, Van Dyke MC, Lopez AH, Eitson JL, Fan W, Hanners NW, et al. LY6E protects mice
1839 from pathogenic effects of murine coronavirus and SARS-CoV-2. bioRxiv. 2023. Epub 20230126.
1840 doi: 10.1101/2023.01.25.525551. PubMed PMID: 36747632; PubMed Central PMCID:
1841 PMCPMC9900800.
1842 157. Pfaender S, Mar KB, Michailidis E, Kratzel A, Boys IN, V'Kovski P, et al. LY6E impairs
1843 coronavirus fusion and confers immune control of viral disease. Nat Microbiol. 2020;5(11):1330-
1844 9. Epub 20200723. doi: 10.1038/s41564-020-0769-y. PubMed PMID: 32704094; PubMed
1845 Central PMCID: PMCPMC7916999.
1846 158. Consortium GT. The Genotype-Tissue Expression (GTEx) project. Nat Genet.
1847 2013;45(6):580-5. doi: 10.1038/ng.2653. PubMed PMID: 23715323; PubMed Central PMCID:
1848 PMCPMC4010069.
1849 159. Blight KJ, McKeating JA, Rice CM. Highly permissive cell lines for subgenomic and
1850 genomic hepatitis C virus RNA replication. J Virol. 2002;76(24):13001-14. doi:
1851 10.1128/jvi.76.24.13001-13014.2002. PubMed PMID: 12438626; PubMed Central PMCID:
1852 PMCPMC136668.
1853 160. Zhang L, Bukreyev A, Thompson CI, Watson B, Peeples ME, Collins PL, et al. Infection of
1854 ciliated cells by human parainfluenza virus type 3 in an in vitro model of human airway
1855 epithelium. J Virol. 2005;79(2):1113-24. doi: 10.1128/JVI.79.2.1113-1124.2005. PubMed PMID:
1856 15613339; PubMed Central PMCID: PMCPMC538579.
1857 161. Hoffmann HH, Schneider WM, Rozen-Gagnon K, Miles LA, Schuster F, Razooky B, et al.
1858 TMEM41B Is a Pan-flavivirus Host Factor. Cell. 2021;184(1):133-48 e20. Epub 20201209. doi:
1859 10.1016/j.cell.2020.12.005. PubMed PMID: 33338421; PubMed Central PMCID:
1860 PMCPMC7954666.
1861 162. Benboudjema L, Mulvey M, Gao Y, Pimplikar SW, Mohr I. Association of the herpes
1862 simplex virus type 1 Us11 gene product with the cellular kinesin light-chain-related protein PAT1
1863 results in the redistribution of both polypeptides. J Virol. 2003;77(17):9192-203. doi:
1864 10.1128/jvi.77.17.9192-9203.2003. PubMed PMID: 12915535; PubMed Central PMCID:
1865 PMCPMC187382.

1866 163. Lee D, Le Pen J, Yatim A, Dong B, Aquino Y, Ogishi M, et al. Inborn errors of OAS-RNase L
1867 in SARS-CoV-2-related multisystem inflammatory syndrome in children. Science.
1868 2023;379(6632):eabo3627. Epub 20230210. doi: 10.1126/science.abo3627. PubMed PMID:
1869 36538032.
1870 164. Mendoza EJ, Manguiat K, Wood H, Drebot M. Two Detailed Plaque Assay Protocols for
1871 the Quantification of Infectious SARS-CoV-2. Curr Protoc Microbiol. 2020;57(1):ecpmc105. doi:
1872 10.1002/cpmc.105. PubMed PMID: 32475066; PubMed Central PMCID: PMCPMC7300432.
1873 165. Polo JM, Davis NL, Rice CM, Huang HV, Johnston RE. Molecular analysis of Sindbis virus
1874 pathogenesis in neonatal mice by using virus recombinants constructed in vitro. J Virol.
1875 1988;62(6):2124-33. doi: 10.1128/JVI.62.6.2124-2133.1988. PubMed PMID: 2835514; PubMed
1876 Central PMCID: PMCPMC253309.
1877 166. Bick MJ, Carroll JW, Gao G, Goff SP, Rice CM, MacDonald MR. Expression of the zinc-
1878 finger antiviral protein inhibits alphavirus replication. J Virol. 2003;77(21):11555-62. doi:
1879 10.1128/jvi.77.21.11555-11562.2003. PubMed PMID: 14557641; PubMed Central PMCID:
1880 PMCPMC229374.
1881 167. Atasheva S, Kim DY, Akhrymuk M, Morgan DG, Frolova EI, Frolov I. Pseudoinfectious
1882 Venezuelan equine encephalitis virus: a new means of alphavirus attenuation. J Virol.
1883 2013;87(4):2023-35. Epub 20121205. doi: 10.1128/JVI.02881-12. PubMed PMID: 23221545;
1884 PubMed Central PMCID: PMCPMC3571482.
1885 168. Dalton KP, Rose JK. Vesicular stomatitis virus glycoprotein containing the entire green
1886 fluorescent protein on its cytoplasmic domain is incorporated efficiently into virus particles.
1887 Virology. 2001;279(2):414-21. doi: 10.1006/viro.2000.0736. PubMed PMID: 11162797.
1888 169. Dobin A, Davis CA, Schlesinger F, Drenkow J, Zaleski C, Jha S, et al. STAR: ultrafast
1889 universal RNA-seq aligner. Bioinformatics. 2013;29(1):15-21. Epub 20121025. doi:
1890 10.1093/bioinformatics/bts635. PubMed PMID: 23104886; PubMed Central PMCID:
1891 PMCPMC3530905.
1892 170. Liao Y, Smyth GK, Shi W. The R package Rsubread is easier, faster, cheaper and better for
1893 alignment and quantification of RNA sequencing reads. Nucleic Acids Res. 2019;47(8):e47. doi:
1894 10.1093/nar/gkz114. PubMed PMID: 30783653; PubMed Central PMCID: PMCPMC6486549.

171. Love MI, Huber W, Anders S. Moderated estimation of fold change and dispersion for RNA-seq data with DESeq2. Genome Biol. 2014;15(12):550. doi: 10.1186/s13059-014-0550-8. PubMed PMID: 25516281; PubMed Central PMCID: PMCPMC4302049.

172. Korotkevich G, Sukhov V, Budin N, Shpak B, Artyomov MN, Sergushichev A. Fast gene set enrichment analysis. bioRxiv. 2021:060012. doi: 10.1101/060012.

173. Liberzon A, Subramanian A, Pinchback R, Thorvaldsdottir H, Tamayo P, Mesirov JP. Molecular signatures database (MSigDB) 3.0. Bioinformatics. 2011;27(12):1739-40. Epub 20110505. doi: 10.1093/bioinformatics/btr260. PubMed PMID: 21546393; PubMed Central PMCID: PMCPMC3106198.

174. Fabregat A, Jupe S, Matthews L, Sidiropoulos K, Gillespie M, Garapati P, et al. The Reactome Pathway Knowledgebase. Nucleic Acids Res. 2018;46(D1):D649-D55. doi: 10.1093/nar/gkx1132. PubMed PMID: 29145629; PubMed Central PMCID: PMCPMC5753187.

175. Kanehisa M, Goto S. KEGG: kyoto encyclopedia of genes and genomes. Nucleic Acids Res. 2000;28(1):27-30. doi: 10.1093/nar/28.1.27. PubMed PMID: 10592173; PubMed Central PMCID: PMCPMC102409.

176. Agrawal A, Balci H, Hanspers K, Coort SL, Martens M, Slenter DN, et al. WikiPathways 2024: next generation pathway database. Nucleic Acids Res. 2024;52(D1):D679-D89. doi: 10.1093/nar/gkad960. PubMed PMID: 37941138; PubMed Central PMCID: PMCPMC10767877.

177. Schaefer CF, Anthony K, Krupa S, Buchoff J, Day M, Hannay T, et al. PID: the Pathway Interaction Database. Nucleic Acids Res. 2009;37(Database issue):D674-9. Epub 20081002. doi: 10.1093/nar/gkn653. PubMed PMID: 18832364; PubMed Central PMCID: PMCPMC2686461.

178. Nishimura D. BioCarta. Biotech Software & Internet Report: The Computer Software Journal for Scient. 2001;2(3):117-20.

179. Schmittgen TD, Livak KJ. Analyzing real-time PCR data by the comparative C(T) method. Nat Protoc. 2008;3(6):1101-8. doi: 10.1038/nprot.2008.73. PubMed PMID: 18546601.

180. Dittmann M, Hoffmann HH, Scull MA, Gilmore RH, Bell KL, Ciancanelli M, et al. A serpin shapes the extracellular environment to prevent influenza A virus maturation. Cell. 2015;160(4):631-43. doi: 10.1016/j.cell.2015.01.040. PubMed PMID: 25679759; PubMed Central PMCID: PMC4328142.

1924 181. Majdoul S, Compton AA. Lessons in self-defence: inhibition of virus entry by intrinsic
1925 immunity. Nat Rev Immunol. 2022;22(6):339-52. Epub 20211013. doi: 10.1038/s41577-021-
1926 00626-8. PubMed PMID: 34646033; PubMed Central PMCID: PMCPMC8511856.
1927 182. Bruchez A, Sha K, Johnson J, Chen L, Stefani C, McConnell H, et al. MHC class II
1928 transactivator CIITA induces cell resistance to Ebola virus and SARS-like coronaviruses. Science.
1929 2020;370(6513):241-7. Epub 20200827. doi: 10.1126/science.abb3753. PubMed PMID:
1930 32855215; PubMed Central PMCID: PMCPMC7665841.
1931 183. Doyle T, Moncorge O, Bonaventure B, Pollpeter D, Lussignol M, Tauziet M, et al. The
1932 interferon-inducible isoform of NCOA7 inhibits endosome-mediated viral entry. Nat Microbiol.
1933 2018;3(12):1369-76. Epub 20181126. doi: 10.1038/s41564-018-0273-9. PubMed PMID:
1934 30478388; PubMed Central PMCID: PMCPMC6329445.
1935

Figure 1

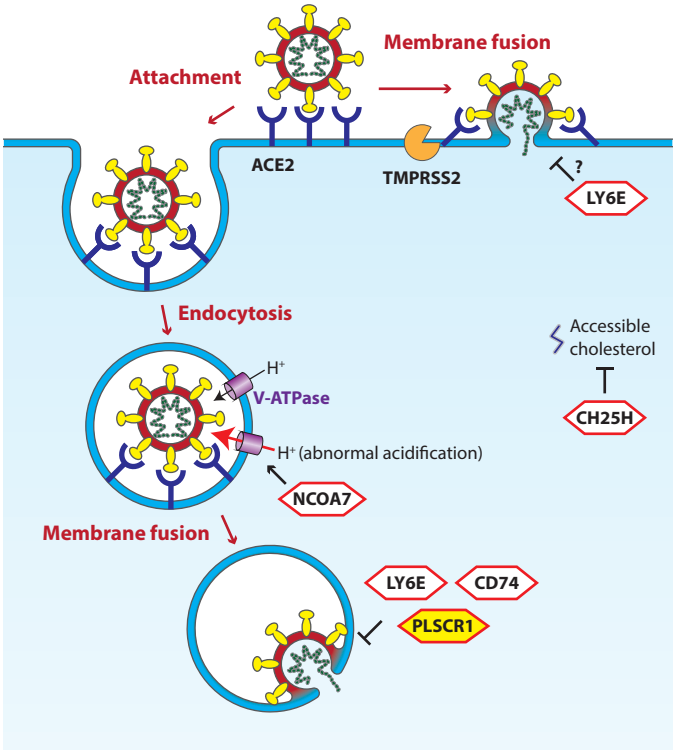
Attachment
Membrane fusion
ACE2
TMPRSS2
?
LY6E
Endocytosis
Accessible cholesterol
H+
V-ATPase
CH25H
H+ (abnormal acidification)
NCOA7
Membrane fusion
LY6E
CD74
PLSCR1

Figure 2

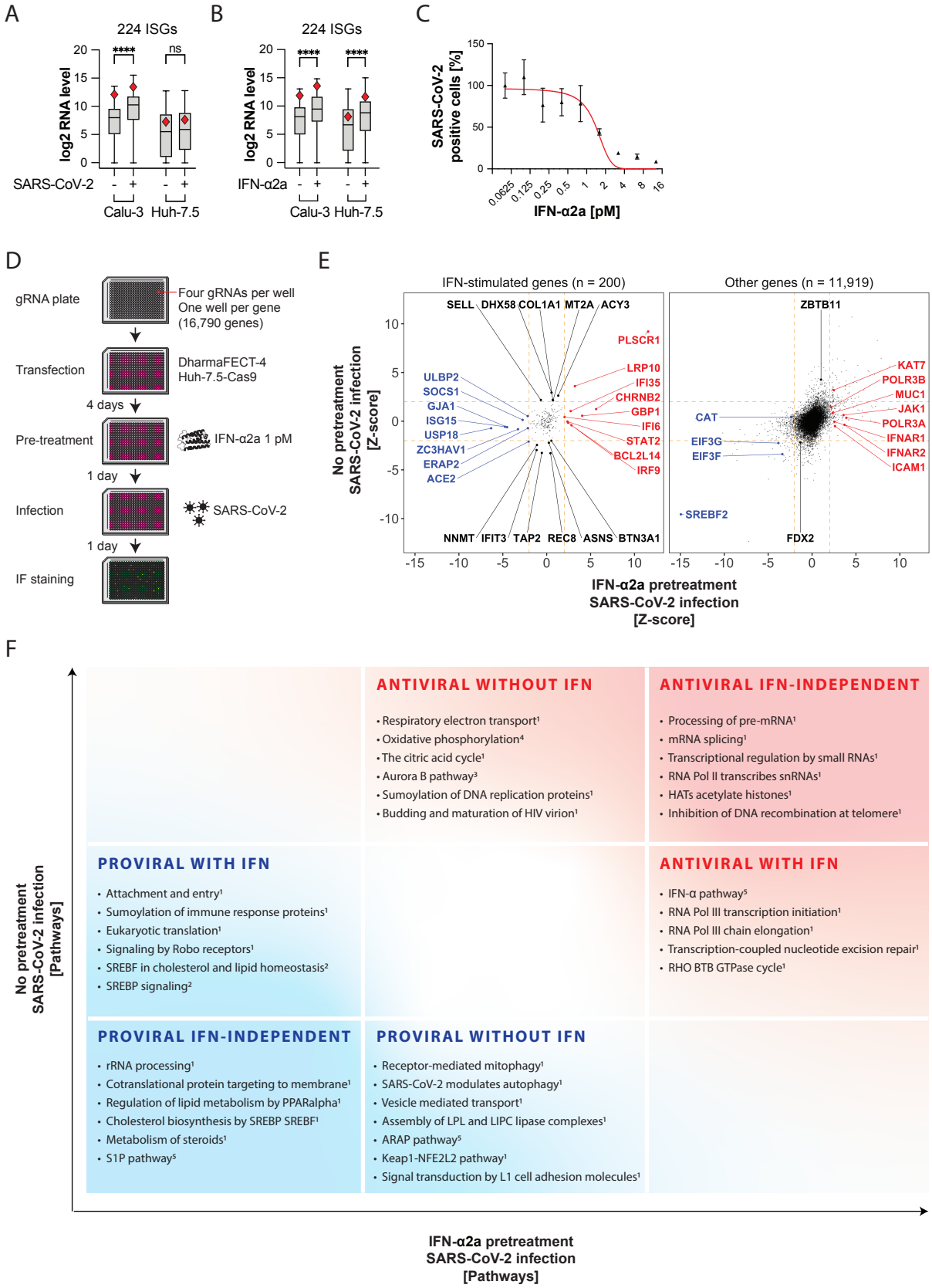
A
224 ISGs
log2 RNA level
****
ns
SARS-CoV-2
Calu-3
Huh-7.5
B
224 ISGs
log2 RNA level
****
****
IFN-α2a
Calu-3
Huh-7.5
C
SARS-CoV-2 positive cells [%]
IFN-α2a [pM]
D
gRNA plate
Four gRNAs per well
One well per gene
(16,790 genes)
Transfection
DharmaFECT-4
Huh-7.5-Cas9
4 days
Pre-treatment
IFN-α2a 1 pM
1 day
Infection
SARS-CoV-2
1 day
IF staining
E
IFN-stimulated genes (n = 200)
Other genes (n = 11,919)
No pretreatment SARS-CoV-2 infection [Z-score]
IFN-α2a pretreatment SARS-CoV-2 infection [Z-score]
SELL
DHX58
COL1A1
MT2A
ACY3
PLSCR1
LRP10
IFI35
CHRNB2
GBP1
IFI6
STAT2
BCL2L14
IRF9
ULBP2
SOCS1
GJA1
ISG15
USP18
ZC3HAV1
ERAP2
ACE2
NNMT
IFIT3
TAP2
REC8
ASNS
BTN3A1
ZBTB11
KAT7
POLR3B
MUC1
JAK1
POLR3A
IFNAR1
IFNAR2
ICAM1
CAT
EIF3G
EIF3F
SREBF2
FDX2
F
ANTIVIRAL WITHOUT IFN
• Respiratory electron transport¹
• Oxidative phosphorylation⁴
• The citric acid cycle¹
• Aurora B pathway³
• Sumoylation of DNA replication proteins¹
• Budding and maturation of HIV virion¹
ANTIVIRAL IFN-INDEPENDENT
• Processing of pre-mRNA¹
• mRNA splicing¹
• Transcriptional regulation by small RNAs¹
• RNA Pol II transcribes snRNAs¹
• HATs acetylate histones¹
• Inhibition of DNA recombination at telomere¹
PROVIRAL WITH IFN
• Attachment and entry¹
• Sumoylation of immune response proteins¹
• Eukaryotic translation¹
• Signaling by Robo receptors¹
• SREBF in cholesterol and lipid homeostasis²
• SREBP signaling²
ANTIVIRAL WITH IFN
• IFN-α pathway⁵
• RNA Pol III transcription initiation¹
• RNA Pol III chain elongation¹
• Transcription-coupled nucleotide excision repair¹
• RHO BTB GTPase cycle¹
PROVIRAL IFN-INDEPENDENT
• rRNA processing¹
• Cotranslational protein targeting to membrane¹
• Regulation of lipid metabolism by PPARalpha¹
• Cholesterol biosynthesis by SREBP SREBF¹
• Metabolism of steroids¹
• S1P pathway⁵
PROVIRAL WITHOUT IFN
• Receptor-mediated mitophagy¹
• SARS-CoV-2 modulates autophagy¹
• Vesicle mediated transport¹
• Assembly of LPL and LIPC lipase complexes¹
• ARAP pathway⁵
• Keap1-NFE2L2 pathway¹
• Signal transduction by L1 cell adhesion molecules¹
No pretreatment SARS-CoV-2 infection [Pathways]
IFN-α2a pretreatment SARS-CoV-2 infection [Pathways]

Figure 3

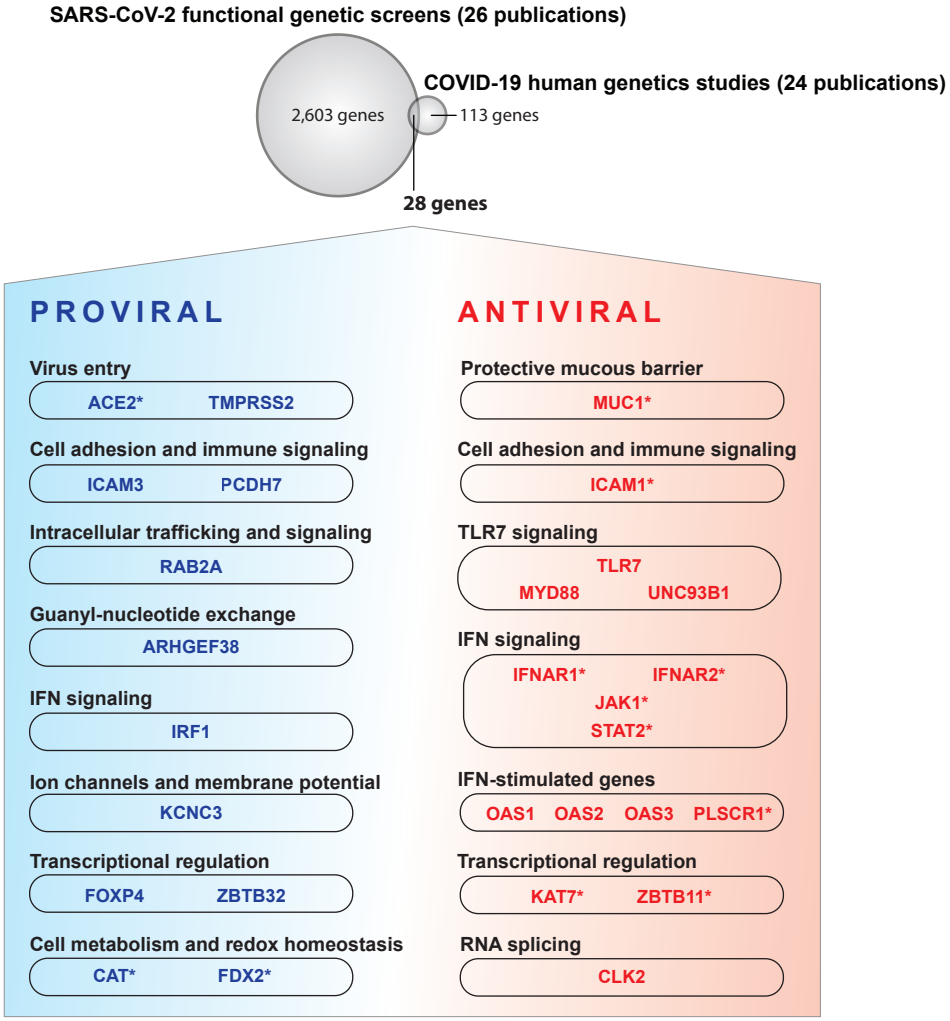

* Hit in arrayed CRISPR KO screen.

Figure 4

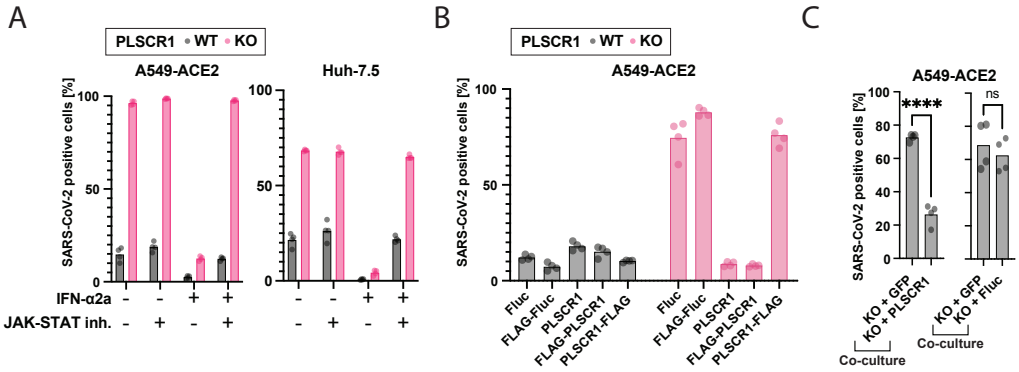
A
PLSCR1 WT KO
A549-ACE2
Huh-7.5
SARS-CoV-2 positive cells [%]
100
50
0
IFN-α2a - - + +
JAK-STAT inh. - + - +
B
PLSCR1 WT KO
A549-ACE2
Fluc
FLAG-Fluc
PLSCR1
FLAG-PLSCR1
PLSCR1-FLAG
C
A549-ACE2
****
ns
KO + GFP
KO + PLSCR1
KO + Fluc
Co-culture

Figure 5

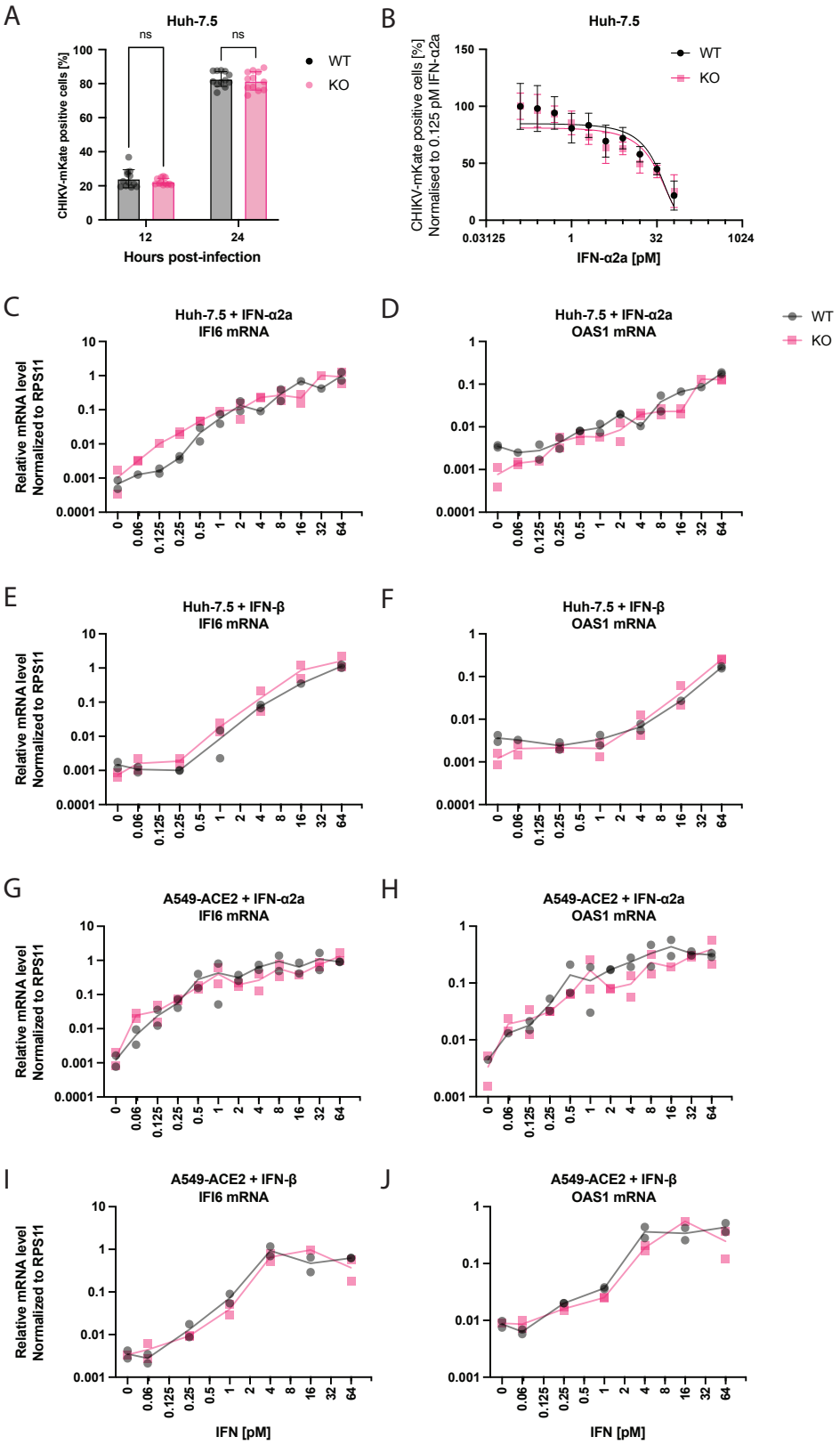
A
Huh-7.5
ns
ns
CHIKV-mKate positive cells [%]
Hours post-infection
WT
KO
B
Huh-7.5
CHIKV-mKate positive cells [%]
Normalised to 0.125 pM IFN-α2a
IFN-α2a [pM]
WT
KO
C
Huh-7.5 + IFN-α2a
IFI6 mRNA
Relative mRNA level
Normalized to RPS11
D
Huh-7.5 + IFN-α2a
OAS1 mRNA
WT
KO
E
Huh-7.5 + IFN-β
IFI6 mRNA
F
Huh-7.5 + IFN-β
OAS1 mRNA
G
A549-ACE2 + IFN-α2a
IFI6 mRNA
H
A549-ACE2 + IFN-α2a
OAS1 mRNA
I
A549-ACE2 + IFN-β
IFI6 mRNA
J
A549-ACE2 + IFN-β
OAS1 mRNA
IFN [pM]

Figure 6

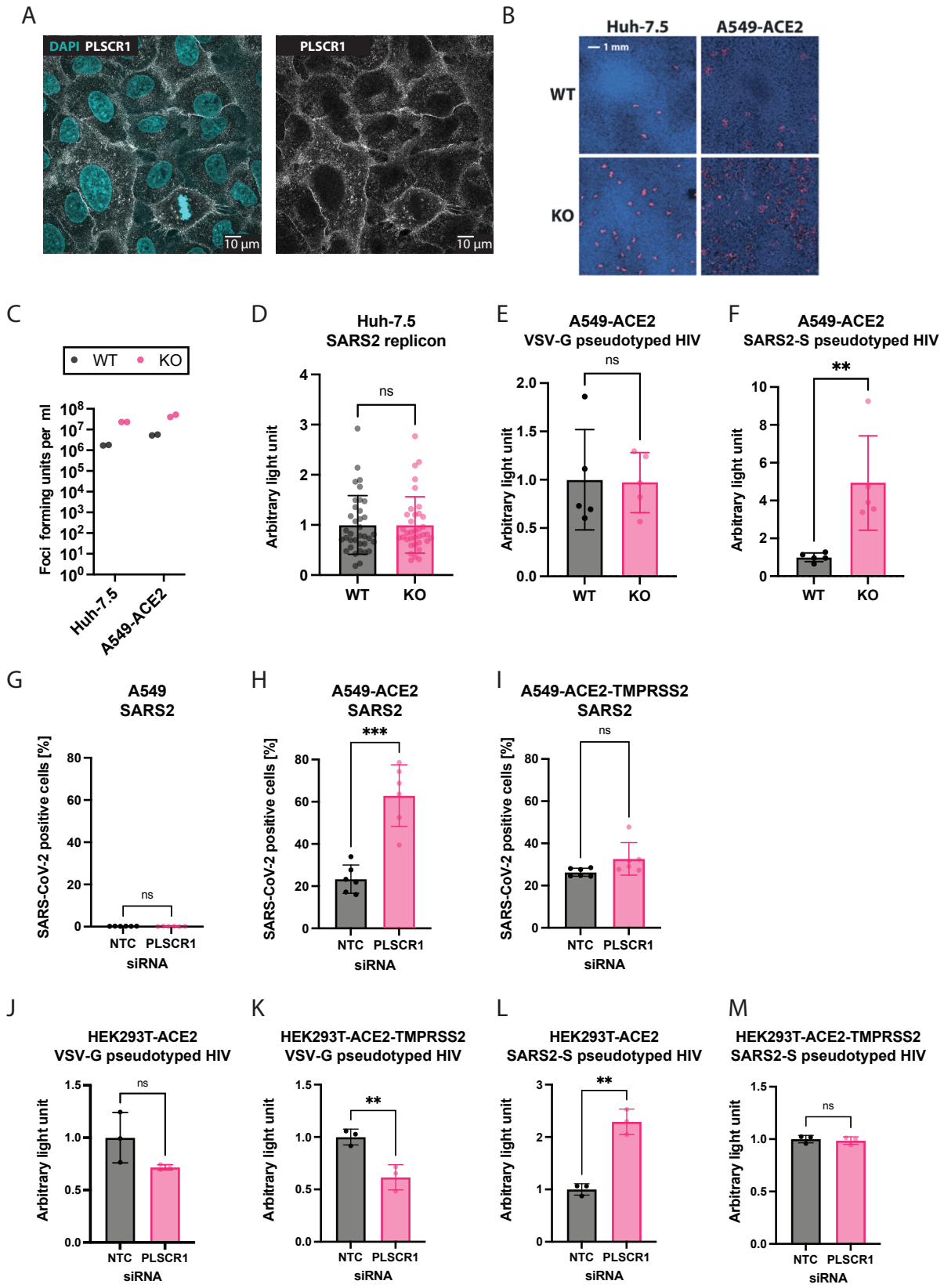
A
DAPI PLSCR1
10 µm
PLSCR1
10 µm
B
Huh-7.5
A549-ACE2
1 mm
WT
KO
C
WT
KO
Foci forming units per ml
Huh-7.5
A549-ACE2
D
Huh-7.5
SARS2 replicon
Arbitrary light unit
ns
WT
KO
E
A549-ACE2
VSV-G pseudotyped HIV
ns
F
A549-ACE2
SARS2-S pseudotyped HIV
**
G
A549
SARS2
SARS-CoV-2 positive cells [%]
ns
NTC
PLSCR1
siRNA
H
A549-ACE2
SARS2
***
I
A549-ACE2-TMPRSS2
SARS2
J
HEK293T-ACE2
VSV-G pseudotyped HIV
K
HEK293T-ACE2-TMPRSS2
VSV-G pseudotyped HIV
L
HEK293T-ACE2
SARS2-S pseudotyped HIV
M
HEK293T-ACE2-TMPRSS2
SARS2-S pseudotyped HIV

Figure 7

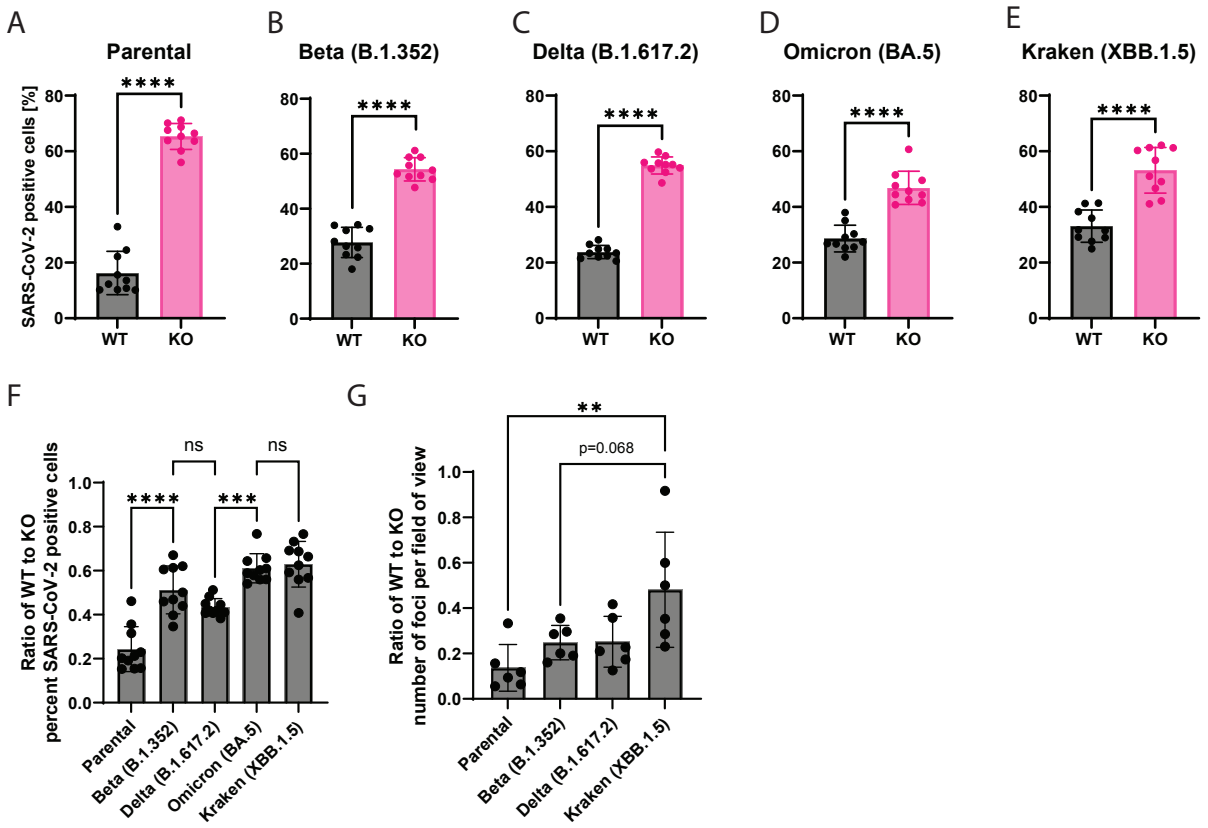
A
Parental
B
Beta (B.1.352)
C
Delta (B.1.617.2)
D
Omicron (BA.5)
E
Kraken (XBB.1.5)
SARS-CoV-2 positive cells [%]
****
WT
KO
F
Ratio of WT to KO
percent SARS-CoV-2 positive cells
****
***
ns
ns
Parental
Beta (B.1.352)
Delta (B.1.617.2)
Omicron (BA.5)
Kraken (XBB.1.5)
G
Ratio of WT to KO
number of foci per field of view
**
p=0.068

Figure 8

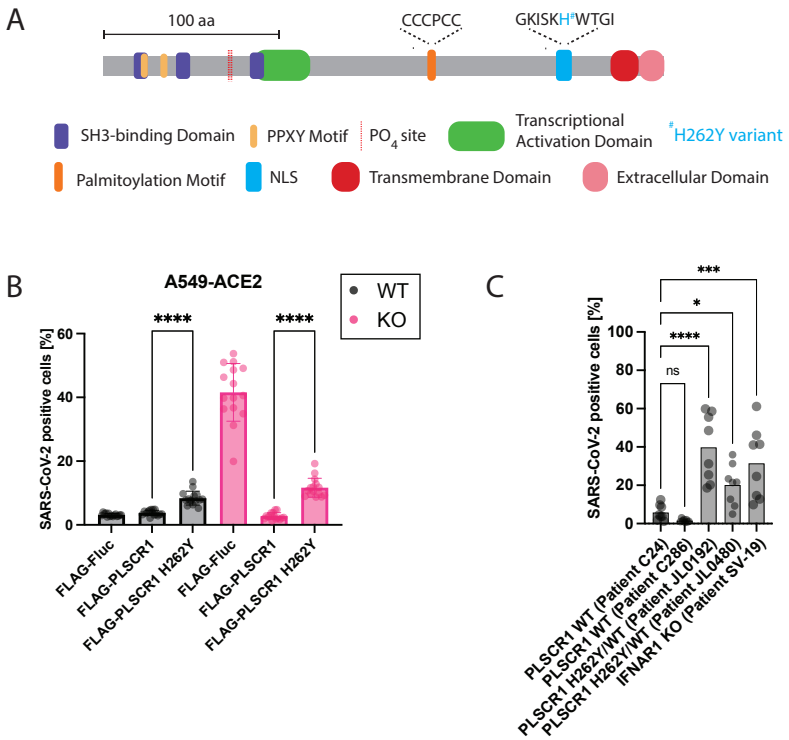
A
100 aa
CCCPCC
GKISKH#WTGI
SH3-binding Domain
PPXY Motif
PO4 site
Transcriptional Activation Domain
#H262Y variant
Palmitoylation Motif
NLS
Transmembrane Domain
Extracellular Domain
B
A549-ACE2
WT
KO
SARS-CoV-2 positive cells [%]
****
****
FLAG-Fluc
FLAG-PLSCR1
FLAG-PLSCR1 H262Y
FLAG-Fluc
FLAG-PLSCR1
FLAG-PLSCR1 H262Y
C
SARS-CoV-2 positive cells [%]
***
*
****
ns
PLSCR1 WT (Patient C24)
PLSCR1 WT (Patient C286)
PLSCR1 H262Y/WT (Patient JL0192)
PLSCR1 H262Y/WT (Patient JL0430)
IFNAR1 KO (Patient SV-19)

Supplementary figure 1

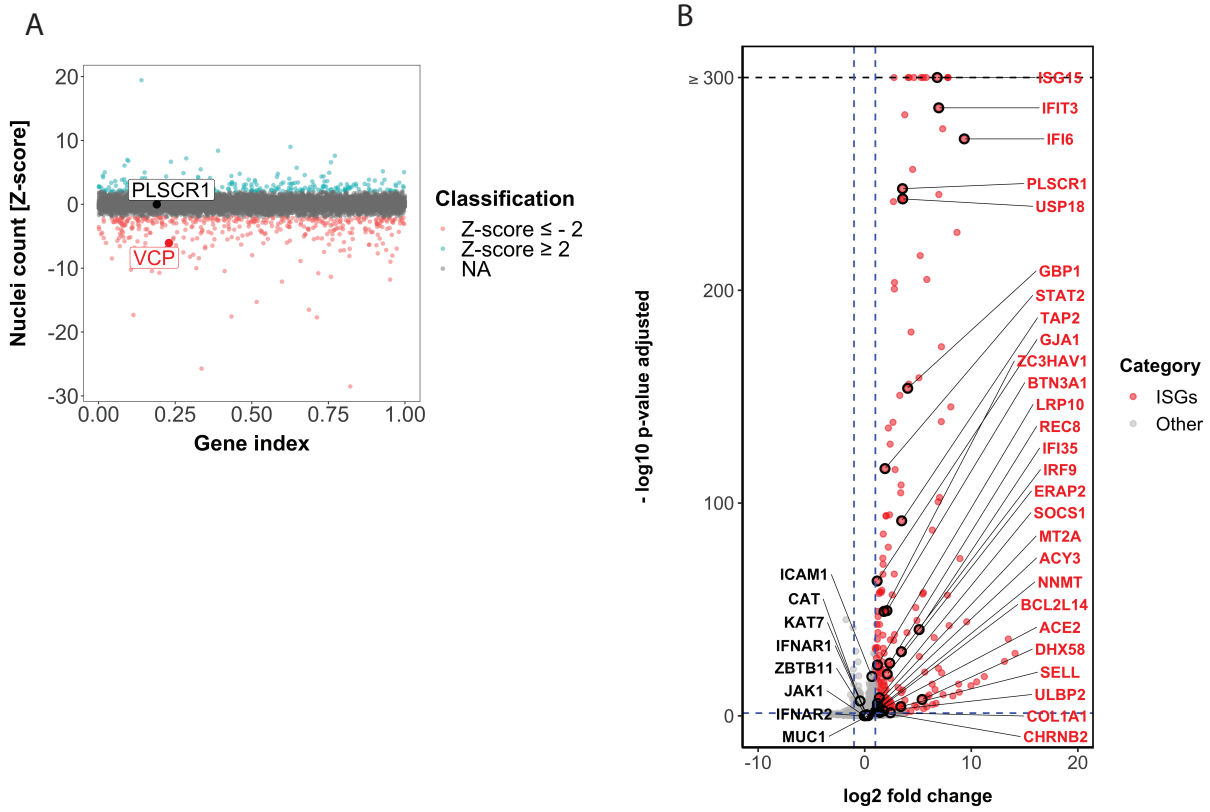

Supplementary figure 2

A

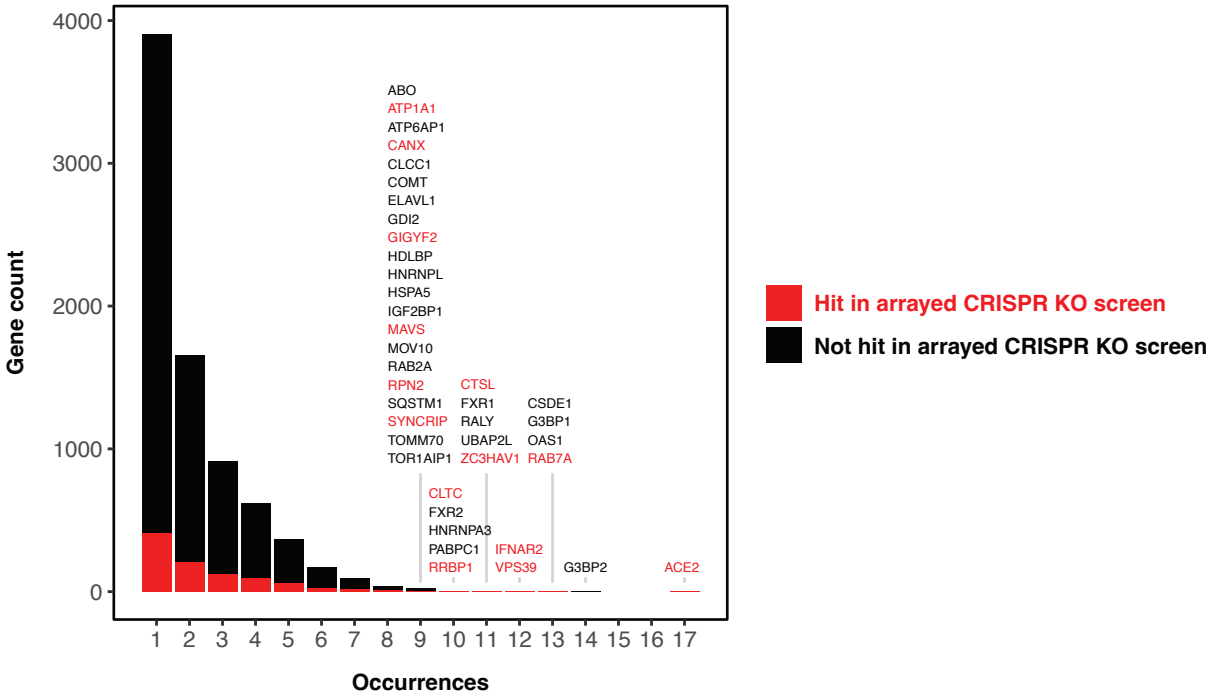

B

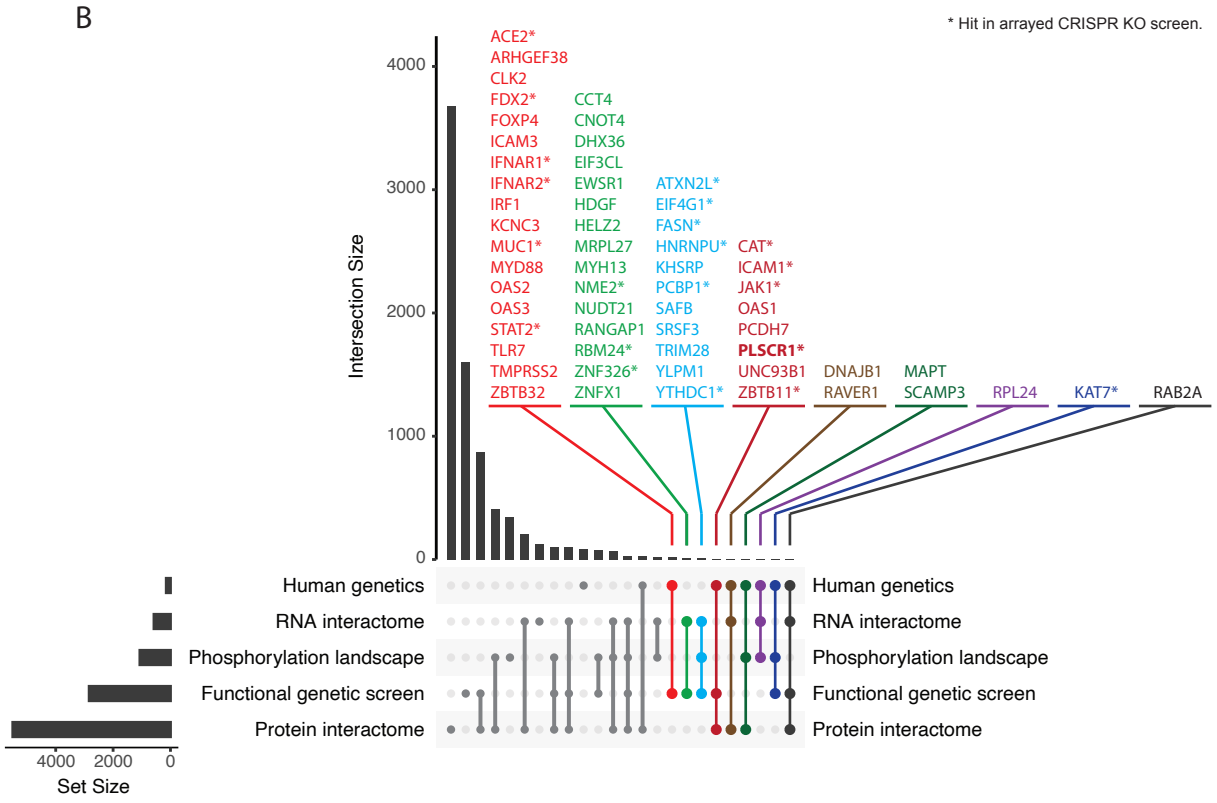

Supplementary figure 3

A

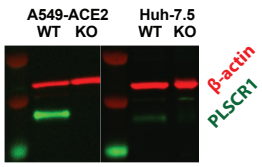

B

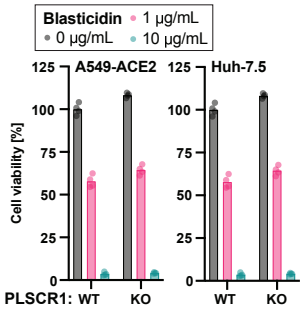

C

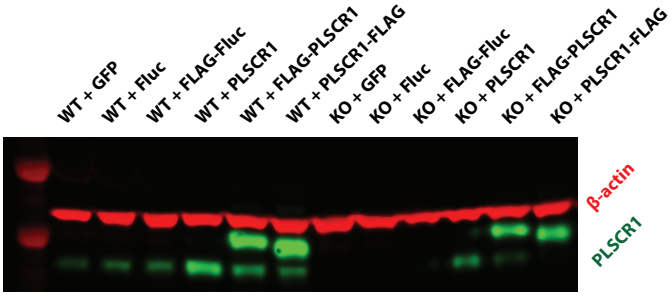

Supplementary figure 4

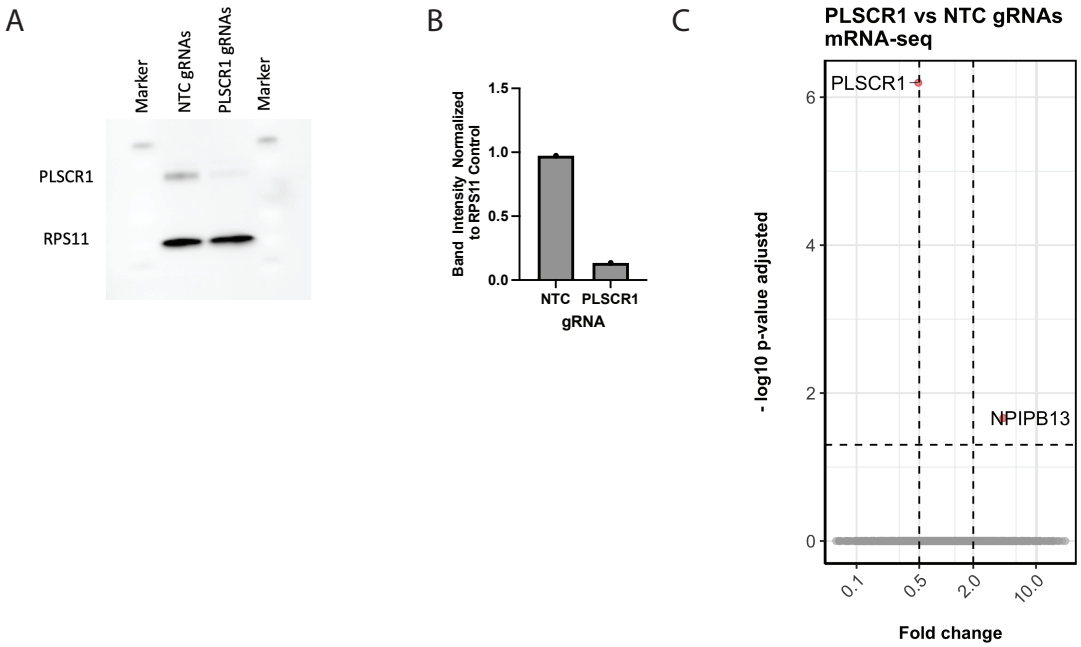

Supplementary figure 5

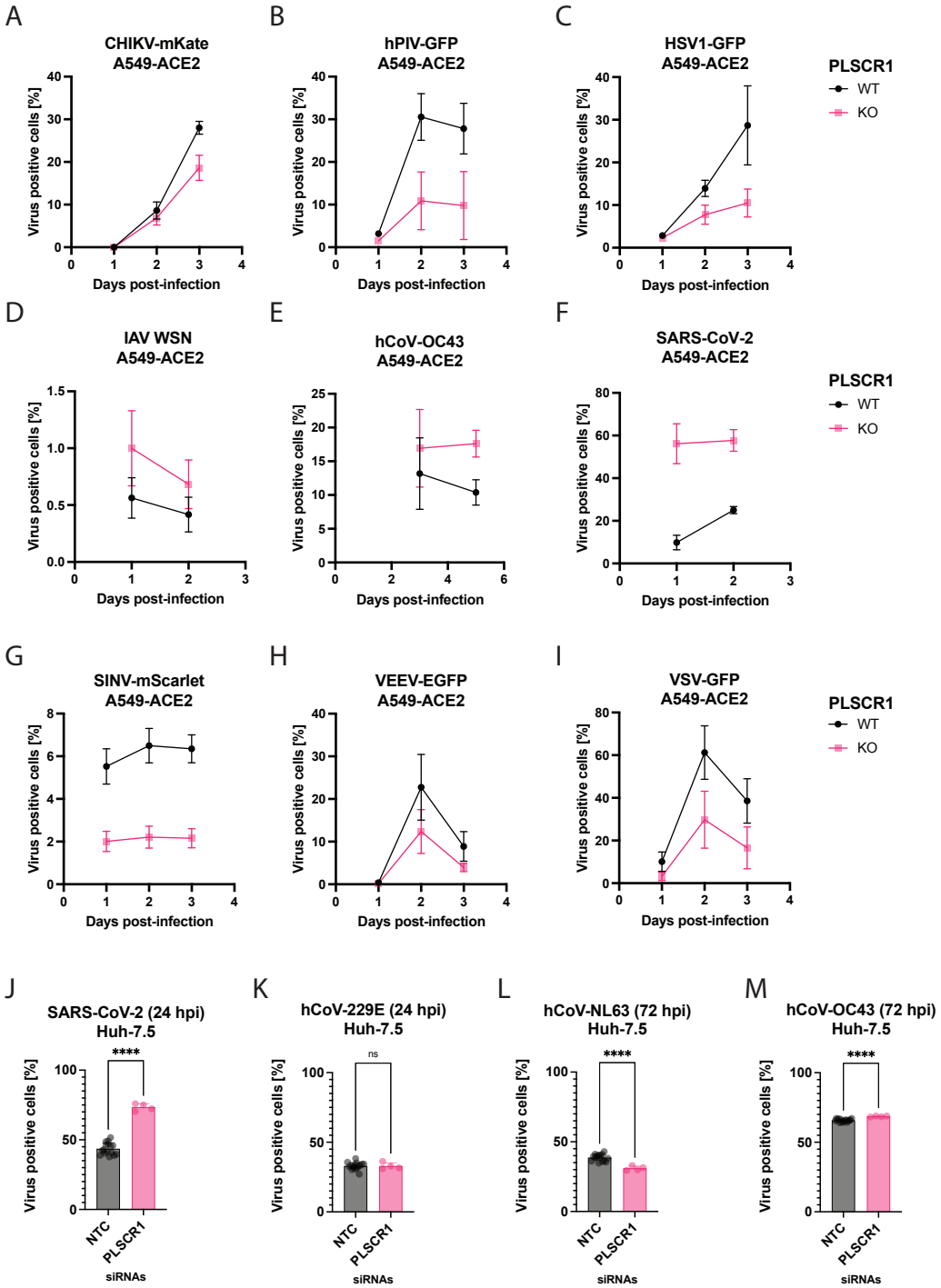

Supplementary figure 6

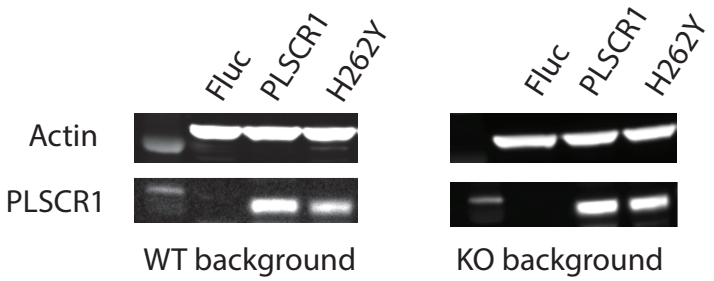

Supplementary figure 7

A

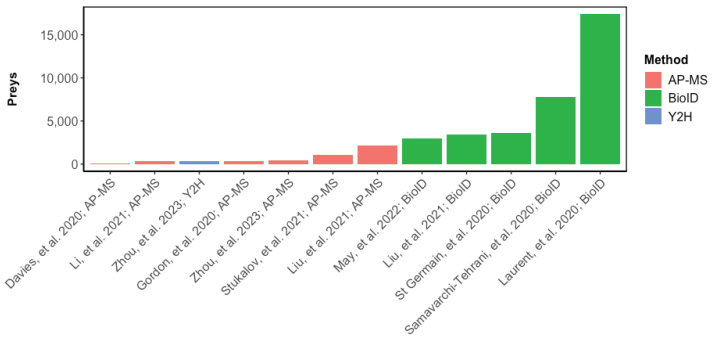

B

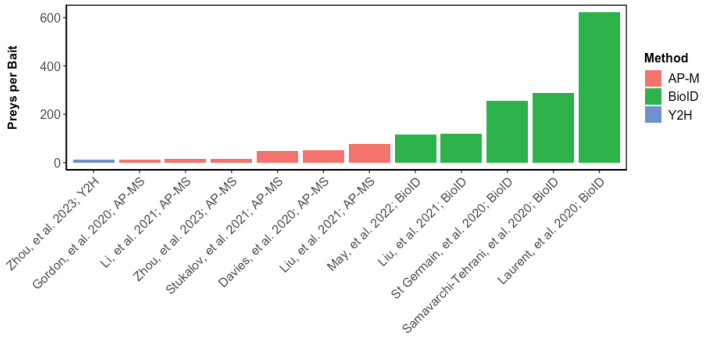
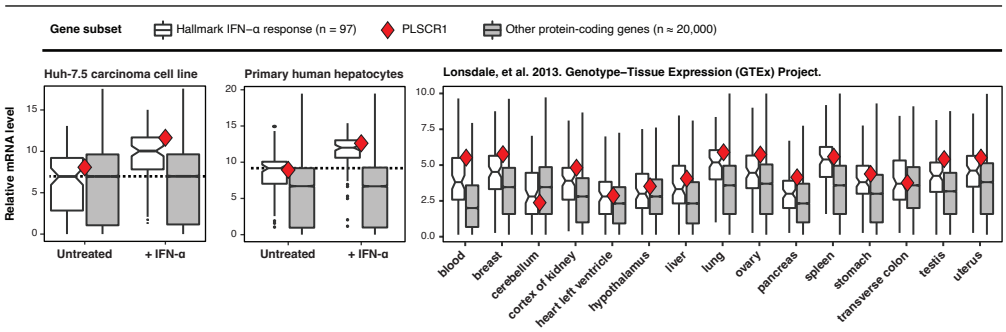
Supplementary figure 8